Spring 2021

Qunatum Transport Phenomena and Non-Trivial Spin Structures

Domenico Andreoli
University of New Hampshire, Durham

Quantum Transport Phenomena and Non-Trivial Spin Structures

By

Domenico Andreoli Jr
Bachelor of Science, Edinboro University of Pennsylvania, 2016

DISSERTATION

Submitted to the University of New Hampshire
in Partial Fulfillment of
the Requirements for the Degree of

Doctor of Philosophy
In
Physics

May 2021

This thesis/dissertation was examined and approved in partial fulfillment of the requirements for the degree of Doctor of Philosophy in Physics by:

Thesis/Dissertation Director,Jiadong Zang, Associate Professor of Physics

Karsten Pohl, Professor of Physics

Shawna Hollen, Assistant Professor of Physics

Chanda Prescod-Weinstein, Assistant Professor of Physics

Joseph R. Dwyer, Professor of Physics

On May 5th, 2021

Approval signatures are on file with the University of New Hampshire Graduate School.

ACKNOWLEDGMENT

I would like to acknowledge my advisor Jiadong Zang for all the guidance and support on all of these works, also, the Department of Energy for giving the funding on these projects. Our collaborators Jian-Xiao Yang and Chao-Xing Liu for their guidance on the theoretical calculations throughout this thesis. The committee for their time and effort. I would like to say thank you to my group members past and present, Sergey, Shihua, Yibo, Tan, Chris, Alex, Wentao, Jie-Xiang, and Morgan. Special thanks to John Gianforte for being a wonderful mentor and friend as my time working as Observatory Manager. I also want to thank the following friends for making graduate school a wonderful experience; Steve, Tierney, Adam, Ben, Jason, Jake, Alex, Alissa, Salman, and Zelda.

Dedication

To my loving mother, sister, brother, and sister-in-law.

TABLE OF CONTENTS

LIST OF FIGURES

ABSTRACT

Quantum Transport is an important part of condensed matter physics. With the discovery of non-trivial spin textures new transport phenomena have given rise to possible alternatives to conventional electronic devices. Studying how these phenomena occur is of utmost importance to the success of these new devices. A theoretical understanding is developed through out this thesis with focus on 2-D spin textures known as Skyrmions. The main topic discussed through-out these works will be how the condensed matter community at large thinks the Skyrmion is directly responsible for what is known as the Topological Hall Effect. It will be argued that the Skyrmion is not the only non-trivial spin structure to giving rise to this phenomena. Two of the works in this thesis are dedicated to show this to be true. It is the purpose of these works to change the communities mind of the Topological Hall Effect.

Chapter One

Introduction

In 1930 Lars Onsager wrote a paper describing irreversible processes, in it he gave a phenomenological relation between the electromotive forces X_1, X_2 and current densities J_1 and J_2 [1],

$$\begin{aligned} X_1 =& R_{11}J_1 + R_{12}J_2 \\ X_2 =& R_{21}J_1 + R_{22}J_2 \end{aligned} \tag{1.1}$$

where $R_{\alpha\beta}$ are the resistivities before Onsager, Lord Kelvin, using thermodynamic reasoning claimed[1],

$$R_{12} = R_{21}. \tag{1.2}$$

In his paper, Onsager found a generalization of this relationship by recognizing the role of time reversal symmetry (TRS)[1, 2]. This generalization is formulated by the Kubo formula, which gives a relationship of the linear response of an observable quantity due to a time-dependent perturbation. Onsager's extension of Lord Kelvin's work is known today as Onsager's theorem. Throughout this work the linear response will mostly be considered. However, there will be mention to nonlinear responses where another symmetry, inversion symmetry, is the main cause for the response.

Onsager's theorem is part of a larger subject known as non-reciprocity. It is known as

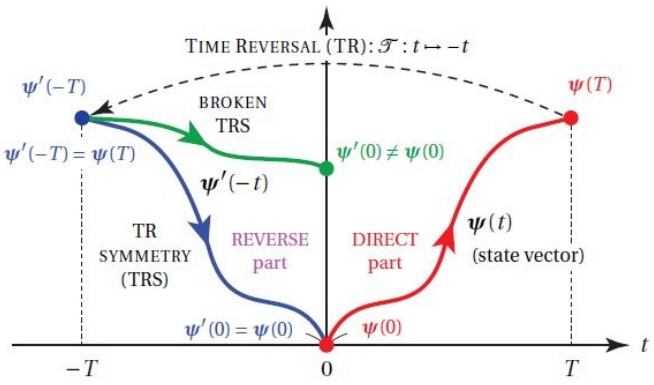

Figure 1.1 Time-reversal symmetry (TRS) (red and blue curves) and broken time-reversal symmetry (red and green curves) or time reversal asymmetry [3]

the absence of "reciprocity"[3]. The adjective reciprocal itself comes from the Latin word "reciprocus", built on the prefixes re-(backward) and pro-(forward), that combine in the phrase reque proque with the meaning of "going backward as forward"[3]. Thus, "reciprocal" means going the same way backward as forward"[3]. An example of this is breaking time reversal symmetry. Starting with a wave function $\psi(0)$ and time evolving it to $\psi(T)$ as shown in figure 1 (red path). Time reversal is then applied (dashed line) and ends up at $\psi'(-T)$. Then, two paths can be taken, the TRS path (blue line) which ends back at the same wave function, $\psi'(0) = \psi(0)$. The other path, which can happen in the case of an applied magnetic field, drives the wave function to a different path (green line) resulting in $\psi'(0) \neq \psi(0)$.

Another important aspect of non-reciprocity is that of inversion symmetry. The inversion operation $\hat{I}$ can be expressed in terms of the product of the mirror transformation and the 180-degree rotation C_2 around the axis perpendicular to the mirror plane. When a material preserves $\hat{I}$ it is known as centrosymmetric while materials that break it are non-centrosymmetric. A simple example of preserving $\hat{I}$ is to take a vector in the x-y plane. This plane will be mirror plane and the z-axis is used to perform the C_2 rotation since it is perpendicular to the plane. Therefore the vector $\mathbf{r} = (x, y)$ will become $\mathbf{r}' = (-x, -y)$ under

the mirror operation. Then, a 180 degree rotation about z gives just the same vector $\mathbf{r}$. Thus inversion symmetry is preserved. If a 3-D vector is used and the mirror plane and rotation axis remain the same we find that the inversion is broken. This is because, $\mathbf{r} = (x, y, z)$ will become $\mathbf{r}' = (-x, -y, -z)$ under mirror then under rotation, $\mathbf{r}'' = (x, y, -z)$. Therefore in this case the Inversion is broken.

This inversion symmetry and asymmetry can be seen in real materials. Take, for example, an ABX_3 perovskite structure shown in figure 2. It can be shown that (a) is centrosymmetric because the inversion center is the same location as B. Performing the mirror and rotation will leave (a) the same. In (b) and (c), B has been moved away from the inversion center by means of an external stimulus, such as, an electric field, E, the temperature T, photon energy, $h\nu$, or by stress, σ. So, what are the fundamental importance of TRS

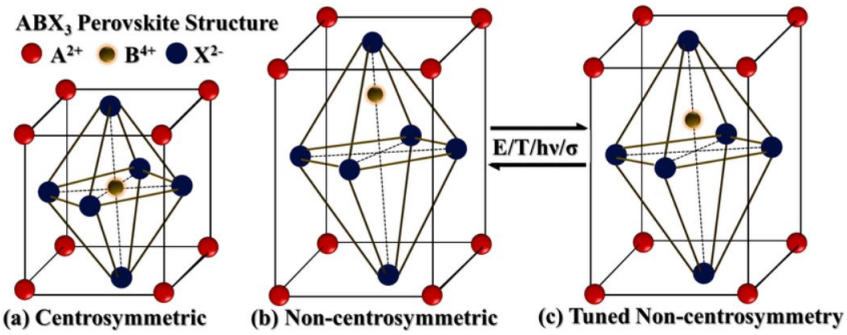

Figure 1.2 Centrosymmetric vs. Noncentrosymmetric materials [4]

and inversion symmetry to quantum transport? In 1879 Edwin H. Hall observed that when an electric current passed through a gold film under a magnetic field, a transverse voltage developed. This effect, known as the Hall effect, forms the basis of fundamental research and practical applications, such as magnetic field measurements and motion detectors[5]. In contrast to the classical Hall effect, whereby the Lorentz force bend the trajectories of charge carriers, quantum mechanics describes the bending via the intrinsic geometry of the quantum electron wave functions under TRS breaking[5]. This breaking led to the discoveries of Berry Curvature and topological Chern numbers, both of which have become essential in modern condensed matter physics[5]. A simple analogy of the Berry Curvature is that one

may think of it as a "magnetic field" except this is induced by the geometrical nature of the electron wave function,

$$\Omega = \nabla \times \mathbf{A}. \tag{1.3}$$

Ω is the Berry cuvature and $\mathbf{A}$ is the Berry connection given by $\mathbf{A} = i\langle u_{nk}|\nabla_k|u_{nk}\rangle$ where $|u_{nk}\rangle$ is an eigenstate of the Hamiltonian of the system. A topological Chern number represents a topological invariant, which means that if an object undergoes a continuous transformation the Chern number does not change. An example of this is the Hall conductivity formulated by the Kubo formula at zero temperature,

$$\sigma_{xy} = -\frac{1}{8\pi^2}\int\int_{FBZ} dk_x dk_y \mathbf{d}(\mathbf{k}) \cdot (\partial_x \mathbf{d}(\mathbf{k}) \times \partial_y \mathbf{d}(\mathbf{k})) \tag{1.4}$$

which is a topological invariant defined on the first Brillouin zone (FBZ) and $\partial_i \equiv \frac{\partial}{\partial_{k_i}}$[6]. The vector $\mathbf{d}(\mathbf{k})$ is determined by the Hamiltonian of the form $H(\mathbf{k}) = \mathbf{d}(\mathbf{k}) \cdot \boldsymbol{\sigma}$. It will also be shown that the Berry curvature is related to the integrand of the conductivity. The reason why equation (1.4) is a topological invariant is because $\mathbf{d}$ is a mapping from the Brillouin zone to the unit sphere and the integrand is the Jacobian of this mapping[6]. Therefore, integrating over it yields the total area, 4π. Previous studies have shown that

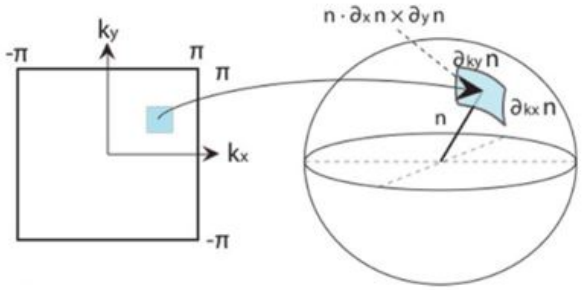

Figure 1.3 The mapping from Billouin zone to unit sphere. [7]

the Hall effect generally has three conditions, a non-vanishing Hall conductivity that arises from the momentum-integrated Berry curvature, a Hall voltage that is linearly proportional

to the external electric field, and a Hall conductivity that is a fraction of the longitudinal conductivity. The non-vanishing Hall conductivity requires TRS breaking and is realized in magnets or by application of a magnetic field[5]. In cases where the conductivity is proportional to the square of the electric field is when Inversion symmetry is broken.

The main focus of the works below are about the Hall effect that is caused by Skyrmions. A Skyrmion can be thought of as a swirling vortex of spin. It has an overall magnetization that gives rise to an effective magnetic field that is large enough to deflect electrons of it giving rise to what is known as the Topological Hall Effect (THE). The Skyrmion itself is a topological invariant, thus continuous transformations do not effect it. This can be seen in what is known as the Skyrmion number given by,

$$N = \frac{1}{4\pi} \int d\mathbf{r}\mathbf{n}(\mathbf{r}) \cdot (\partial_x \mathbf{n}(\mathbf{r}) \times \partial_y \mathbf{n}(\mathbf{r})). \tag{1.5}$$

Here, $\mathbf{n}$ is the magnetization and you will see that it is related to equation (1.4). Except, in this case the magnetization is in the real space instead of the momentum space. In fact one of the questions in one of the works below is to determine the interplay between the real space Skyrmion and the momentum space Berry connection. The number N gives the number of times a Skyrmion can wrap around a unit sphere. As is mentioned before the integrands of (1.4) and (1.5) map to a unit sphere.

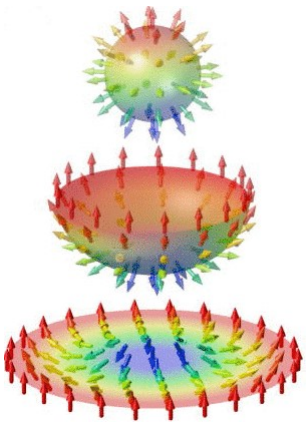

Figure 1.4 Mapping a Skyrmion onto unit Sphere. [8]

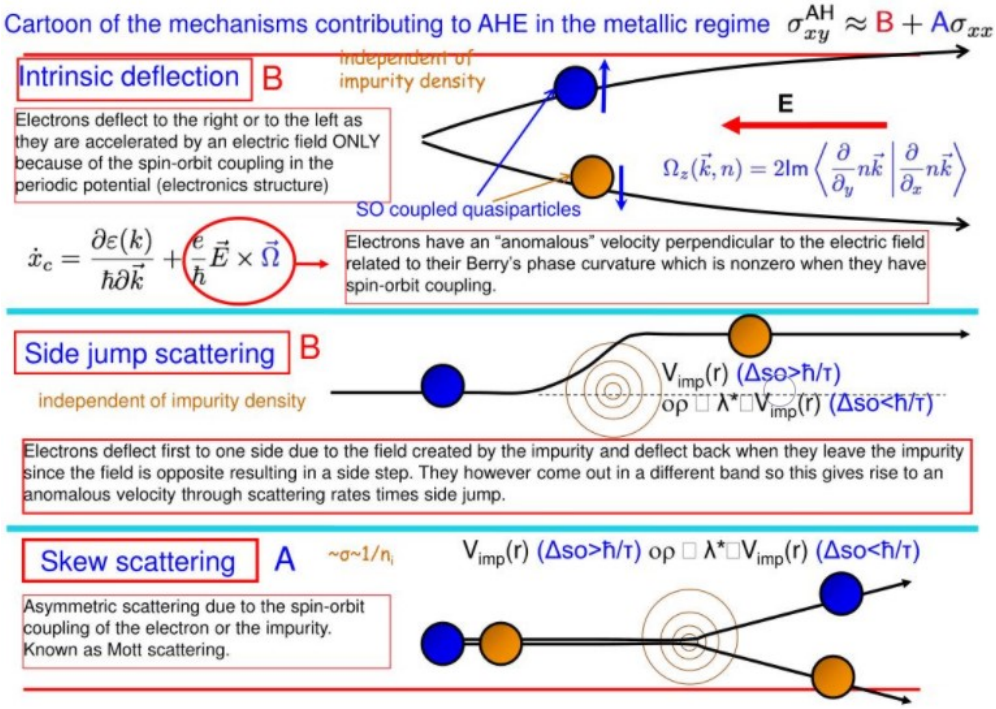

Figure 1.5 Intrinsic and Extrinsic contributions to AHE. [11]

Since the Skyrmion itself is a topological invariant it makes a good candidate as an information carrier. Therefore, there is potential for magnetic nonvolatile memories with ultrahigh density[9]. Since the THE was first observed back in 2009[10] it has been identified as an additional component to the resistivity,

$$\rho_{xy} = \rho_{xy}^{O} + \rho_{xy}^{A} + \rho_{xy}^{THE} \tag{1.6}$$

with ρ_{xy}^{O} involving the ordinary Hall effect(OHE), ρ_{xy}^{A} is the anomalous Hall effect(AHE),and ρ_{xy}^{THE} is the contribution from the Topological Hall effect. The first term is caused by an applied magnetic field that deflects the electron via the Lorentz force. The second term arises from what are known as intrinsic and extrinsic terms. The intrinsic part is due to the momentum space Berry connection that is mentioned above. This gives rise to an effective magnetic field that acts as a Lorentz type force on the electron. The extrinsic parts are directly due to impurities in the sample.

The THE arises due to an incoming electron scattering off the Skyrmion. More precisely, the electron will interact with three non-coplanar spins giving rise to asymmetric scattering. This scattering happens because of a non-zero N which means that the spin chirality density is non-zero, $n_1 \cdot (n_2 \times n_3)$. This is similar to the integrand given in 1.5 except it is the case of discrete spins.

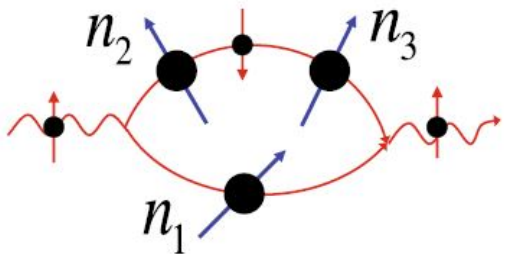

Figure 1.6 Electron Scattering off three non-coplanar spins. Asymmetric scattering arises due to non-zero spin chirality $n_1 \cdot (n_2 \times n_3)$ [12]

Theoretical applicability of the THE is challenging because one must understand the regime to work in. The adiabatic regime occurs when the exchange interaction and the Skyrmion radius are large. The exchange quantifies the interaction between the electron's spin and the magnetization of the Skyrmion. While in the non-adiabatic region there is weak exchange with small radius. One must take care when considering each region. For example, as will be shown below perturbation in the adiabatic regime can be done but must be addressed carefully. When in the non-adiabatic regime one can use the exchange interaction as the perturbation. Not only is the theory different in these two different regimes but the physics of the transport phenomena vary greatly. Take the adiabatic regime. It is seen that for spin up/down electrons that scatter off the Skyrmion they scatter in opposite directions. Thus, charge builds up on opposite sides of the material with different spins. This is what is known as a spin Hall current. In the non-adiabatic regime electrons with opposite spins will be deflected in the same direction giving rise to a Hall current. These regions are also determined by what is known as the adiabatic parameter. The parameter is defined as $\lambda_a = \omega_{ex}\tau$, where ω_{ex} is the spin splitting energy due to the exchange interaction. τ is the

time of flight of the electron through the Skyrmion. In particular one of the works below will go into greater detail of the adiabatic region and why one must take care if perturbation techniques want to be employed. All the works on the THE have been in regards to the Skyrmion, which is a 2-D object. However, there are other works, two of which will be discussed later that either make no mention of a Skyrmion or take the case of 3 dimensions where the Hopfion is considered. In both works a THE is still found. This means that the THE is not solely due to Skyrmions and the goal of these works is to highlight that the THE needs further work to be understood theoretically.

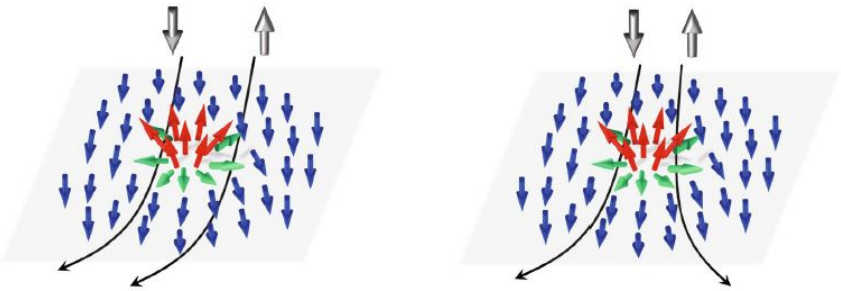

Figure 1.7 THE in the weak and strong coupling regime, respectively. [12]

Skyrmions are known to be stable in materials with broken inversion symmetry. The interplay between the Spins that align parallel/anti-parallel to each other start to become frustrated which can lead this swirling vortex of spins known as a Skyrmion. Therefore, most THE measurements have been performed in these type of materials. For example, B20 materials such as FeGe or MnSi. These are well known materials that can exhibit the THE because at certain temperatures and magnetic fields these materials host a Skyrmion lattice (SkX)[9, 10, 13]. However, it has been found that other materials can also host this transport phenomena. Some of these materials are even centrosymmetric and not able to host Skyrmions. For example, one of the works below shows that a Topological Insulator (TI), which is an Insulator in the bulk and conductor on the surface was able to measure this THE. The theory to reproduce the results will be shown later but the argument for why this THE exists is due to domain walls that form in the material as the magnitude of the

field applied to it changed. Since this work demonstrates that the THE does not require Skyrmions it is a goal of this work to make this clear to the community and to find a broader more general definition to the THE.

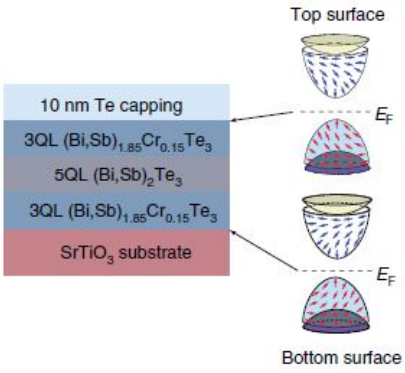

Figure 1.8 Topological Insulator used to show THE with no Skyrmion. [14]

Fig. 1.8 overall shows no Inversion symmetry breaking due to how it is layered and then capped off by a magnetic layer Te and the substrate on the bottom. However, when an external magnetic field is applied and the resistivity is measured the Hysteresis loop reveals two distinct bumps. This is a tell-tale sign of the THE.

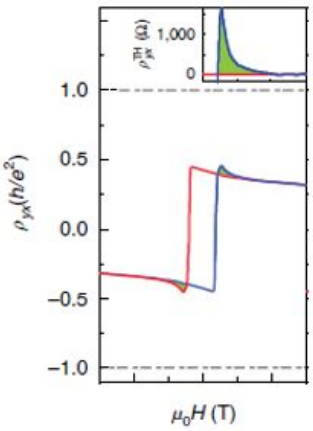

Figure 1.9 Hysteresis loop showing evidence of THE.[14]

As of now there is not much discussion of THE in 3 dimensional spin textures. This gave motivation to investigate if a Hopfion can yield the THE. The Hopfion can be thought of as two different Skyrmions joined together. One will have its center spin pointing while

the other has its spin pointing down. This actually yields a net zero spin chirality density. Since the Hopfion is also a topological invariant it to has what is known as a Hopfion number which is defined as,

$$N_H = \frac{1}{(2\pi)^2} \int d^3r \mathbf{B} \cdot \mathbf{A}. \tag{1.7}$$

Here, $\vec{B}$ is the magnetic field produced by the Hopfion and $\vec{A}$ is the vector potential. Since $\int d^3r B_z = 0$ for a Hopfion one might expect that there will be no interesting transport phenomena associated with it. Since we expect that the THE is not necessarily caused by Skyrmions and work has demonstrated that centrosymmetric materials can host it, calculating the conductivity for the Hopfion is worth considering.

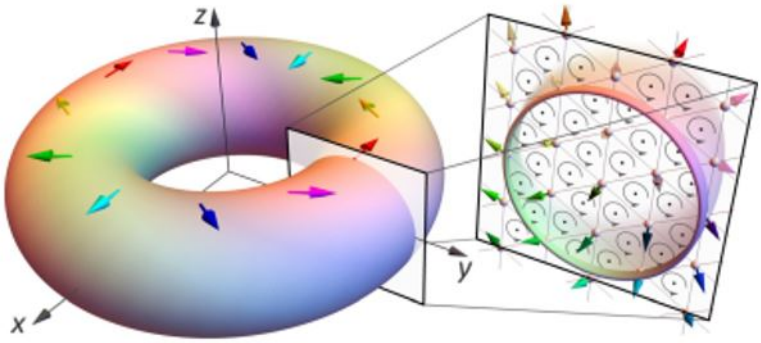

Figure 1.10 Hopfion with $N_H = 1$. [15]

So, what is the motivation to want to understand the THE? The answer lies in spintronics, which is the study of the intrinsic spin of the electron and its associated magnetic moment, in addition to its fundamental electronic charge, in solid-state devices. It is known that Skyrmions can be used as information carriers. They are a great candidate to make memory storage devices because they can be easily driven by currents. The most common type of device that has been proposed to use them is the Racetrack memory device.

However, the temperature range at which Skyrmions form in the B20 compounds are much to low for anything to be commercially accepted. Therefore it is necessary to find other

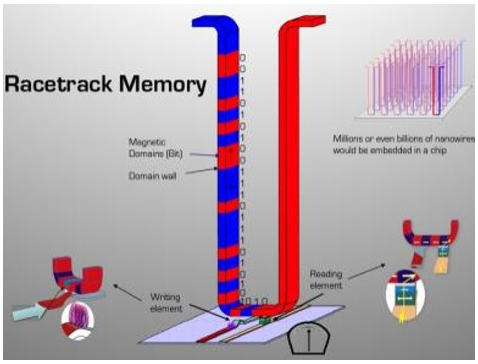

Figure 1.11 A common design for the Racetrack memory where the Skyrmion is the information carrier. [16]

materials that host Skyrmions at higher temperature. It could also be that moving away from the Skyrmion is another solution. This is why I discussed the Topological Insulator and the Hopfion. The former was found to host a THE and this could lead to materials that can be used in commercial applications. Although the Hopfion itself does not have an overall magnetic field and hence once would expect no Topological Hall signature in transport measurements this may not be true. This has been motivated because of another work [17] that shows even with this cancellation of the magnetic field on the global scale there can still be some Hall effect. Since the possibility of new memory devices that could launch technology into the future could be brought about because of the THE it is important to understand this phenomena at a microscopic level. It is only then that one can develop new technologies that society can benefit from.

To reiterate, quantum transport is deeply connected to TRS and Inversion symmetry. In Linear Hall effects it is a magnetic field that is produced by an external source, complicated band structures in the momentum space, or non-trivial spin textures in the real space that apply a Lorentz type force on electrons giving rise to asymmetric scattering. In non-linear cases it is the Inversion symmetry that must be broken to yield the asymmetry in scattering. The THE is the main focus of the works below. Not only the THE but what is exactly responsible for this kind of transport signature. Also, how does one measure this effect and how it is isolated in the date is discussed. This is an important part of the THE because it is

imperative to understand how exactly this effect occurs in materials and how experimentalists are sure that they are measuring this effect. There it will be formulated that the Skyrmion is not necessary for a THE response. It will be discussed how local symmetries being broken can give rise to it even though overall symmetry is preserved. Two of these main works will consist of the TI and the Hopfion.

Therefore the rest of these works will be organized as follows, chapter two will focus more on the Skyrmion and how it can arise in materials, chapter three explains the work on the interplay between momentum space berry phase and the real space magnetic field. It will also be focused in the strong regime. Chapter four discusses how I calculate the THE in the case of the TI and how it agrees with experiment. Also highlighting that the Skyrmion is not needed for THE. Chapter five briefly goes into the work of non-linear hall effects. The sixth and final chapter touches on the transport calculations for the case of the Hopfion. It is here where I calculate the differential cross section and discuss its' relation to the Hall effect. Also, some possible experiments that could detect the THE.

Chapter Two

Discussion of Skyrmions

This chapter will discuss how Skyrmions arise in certain materials. Ultimately it will be shown that Skyrmions can not be stable with just the Heisenberg and Dzyaloshinskii-Moriya interactions. Let us first discuss the history of the Skrymion and how it was experimentally discovered.

2.1 Skyrmion Formulation and Discovery

In 1962 Tony Skyrme first introduced the idea of a Skyrmion as a model for the nucleon. His main interest was to understand subatomic particles using convoluted twists in the quantum field. His ideas were actually quite accurate in making predictions of fundamental particle such as quarks or gluons. However, these ideas were superseded by the well known theory called quantum chromodynamics. Therefore, Skyrme's ideas fell into the shadows for some time. It was not until researchers studying chiral magnets realized that the magnetic fields they were working with could be modeled by the Skyrmion. The field lines for a Skyrmion wrap around one another like key rings hooking into other key rings. Thus, creating nanometer-scale size objcts that cannot be torn apart without breaking the rings. This is why it is a topological invariant since moving it around will not break the field lines. It is also why the Skyrmion can be used as the information carrier due to this invariance.

These field lines are shown below. Later we shall see what interactions are responsible to allow the Skyrmion to become stable.

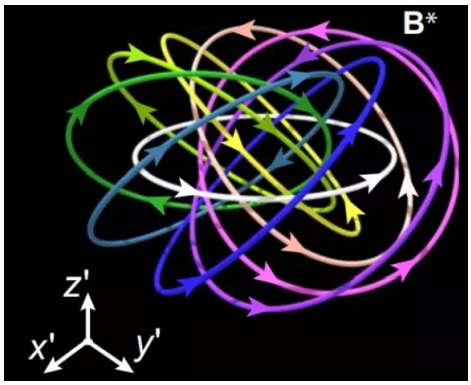

Figure 2.1 Artist representation of magnetic field lines of a Skyrmion. [18]

The first materials that the Skyrmion was observed in were what is known as B20 materials. They are a class of compounds that have cubic lattices, which can host nontrivial spin textures[19]. It is known that materials that fall into this family have broken inversion symmetry. The broken symmetry is seen in the spins of the electrons, which gives rise to spins competing to align with one another. This competition is what leads to the swirling vortex nature of the Skyrmion. There are to main interactions that cause this competition between spins. The first one being what is known as the Heisenberg interaction. It is well known in ferromagents/anti-ferromagnets where the spins want to be aligned/anti-aligned with each other. This can be seen in the form of the interaction.

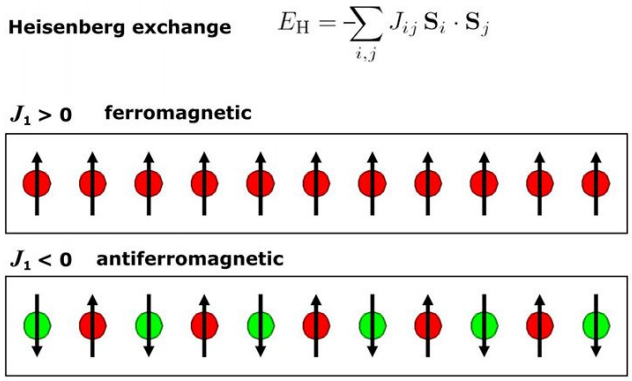

Figure 2.2 Heisenberg Interaction in Ferromagnet and Anti-Ferromagnet. [20]

However, E_H does not break the inversion symmetry is a lattice because of the dot product. This is where the Dzyaloshinskii-Moriya (DM) interaction is important. It causes spins to want to be perpendicular to each other. The DM interaction arises due to strong spin-orbit coupling and inversion symmetry breaking [46]. The inversion breaking can be seen in the form the DM takes.

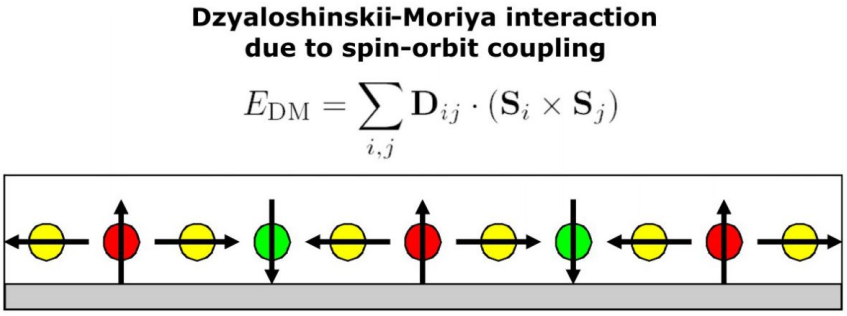

Figure 2.3 Dyzaloshinskii-Moriya (DM) Interaction. [20]

Due to the cross product nature of the DM interaction it is now easy to see how it breaks the inversion symmetry. If one simply flips the spins $S_i \rightarrow S_j$ and flip the cross product you will get $-E_{DM}$. One can see that the Heisenberg interaction is unchanged under this operation. Therefore these are the two main interactions playing the role of Skyrmion formation. So, the first question of this work is, are these two interactions enough to have a stable Skyrmion?

2.2 Stable Skyrmion

Let us first define what is meant by stable. As mentioned above a Skyrmion is a 2-D object that is a swirling vortex of spin with a finite radius. The Skyrmion can be parameterized by two angles, θ and ψ. The magnetization created by the Skyrmion can be written as,

$$\mathbf{M} = (\cos\psi \sin\theta, \sin\psi \sin\theta, \cos\theta) \tag{2.1}$$

where both angles are functions of the 2-D coordinate $\rho = (\rho, \phi)$. Since the radius is finite we expect the angles to drop off to zero as $\rho \to \infty$. The functional form of the angles will be found by writing down the Heisenberg and DM interactions in a continuous form then minimizing the energy to solve differential equations to get $\theta(\rho)$ and $\psi(\rho)$. The energy is written as,

$$E[\theta(\rho), \psi(\rho)] = \int \left[J(\nabla \mathbf{M})^2 + D\mathbf{M} \cdot (\nabla \times \mathbf{M}) \right] d\mathbf{r}. \tag{2.2}$$

The way I solved this problem was to switch to cylindrical coordinates. So any derivatives will changed to derivatives with respect to ρ and ϕ. Also, I wrote the unit vectors in (2.1) in terms of $\hat{\rho}$ and $\hat{\phi}$ giving me a vector with components M_ρ, M_ϕ, and M_z. Then, plugging this into (2.2) I find,

$$\begin{aligned} E[\theta(\rho), \psi(\rho)] = 2\pi J \int_0^R \left[\left(\frac{d\theta}{d\rho} \right)^2 + \frac{\sin^2(\theta)}{\rho^2} + \left(\frac{d\psi}{d\rho} \right)^2 \sin^2(\theta) \right] \rho d\rho \\ + 2\pi D \int_0^R \left[\cos(\psi) \frac{d\theta}{d\rho} + \frac{\cos(\psi)\sin(2\psi)}{2\rho} - \frac{1}{2}\sin(2\theta)\sin(\psi) \right] \rho d\rho \end{aligned} \tag{2.3}$$

where R is the radius of the Skyrmion, details of how to get from (2.2) to (2.3) will be shown in appendix A. To find the equations of motion for $\theta(\rho)$ I will give it a slight deviation, i.e. $\theta \to \theta + \delta\theta$.

$$\begin{aligned} E[\theta + \delta\theta, \psi] = 2\pi J \int_0^R \left[\left(\frac{d}{d\rho}(\theta + \delta\theta) \right)^2 + \frac{\sin^2(\theta + \delta\theta)}{\rho^2} + \left(\frac{d\psi}{d\rho} \right)^2 \sin^2(\theta + \delta\theta) \right] \rho d\rho \\ + 2\pi D \int_0^R \left[\cos(\psi) \frac{d}{d\rho}(\theta + \delta\theta) + \frac{\cos(\psi)\sin(2\psi)}{2\rho} - \frac{1}{2}\sin(2(\theta + \delta\theta))\sin(\psi) \right] \rho d\rho \end{aligned} \tag{2.4}$$

Here I can do an expansion in $\delta\theta$ where I will ignore the second order terms since I am considering $\delta\theta$ to be small. With this expansion I calculate,

$$\delta E = E[\theta+\delta\theta,\psi] - E[\theta,\psi] \approx 2\pi J \int_0^R \left[2\frac{d\theta}{d\rho}\frac{d\delta\theta}{d\rho} + \frac{\sin(2\theta)}{\rho^2}\delta\theta + \left(\frac{d\psi}{d\rho}\right)^2 \sin(2\theta)\delta\theta \right] \rho d\rho$$
$$+ 2\pi D \int_0^R \left[\frac{d\delta\theta}{d\rho}\cos(\psi) + \frac{\cos(\psi)\cos(2\theta)}{\rho}\delta\theta - \frac{d\psi}{d\rho}\sin(\psi)\cos(2\theta)\delta\theta \right] \rho d\rho \quad (2.5)$$

to arrive at (2.5) I was able to pull together all terms that were on the order of $\delta\theta^0$, then moving it to the left hand side. After performing an integration by parts on the terms that contain $\frac{d\delta\theta}{d\rho}$ and ignoring the bulk terms I find,

$$\frac{\delta E}{\delta\theta} = 2\pi J \int_0^R \left[-2\left(\frac{d^2\theta}{d\rho^2} + \frac{1}{\rho}\frac{d\theta}{d\rho}\right) + \frac{\sin(2\theta)}{\rho^2} + \left(\frac{d\psi}{d\rho}\right)^2 \sin(2\theta) \right] \rho d\rho$$
$$+ 2\pi D \int_0^R \left[-\frac{\sin^2(\theta)}{\rho} + \frac{d\psi}{d\rho}\sin(\psi)\sin^2(\theta) \right] \rho d\rho. \quad (2.6)$$

When I set this to zero I find a complicated second order coupled differential equation,

$$\frac{d^2\theta}{d\rho^2} = -\frac{1}{\rho}\frac{d\theta}{d\rho} + \frac{\sin(2\theta)}{2\rho^2} + \frac{1}{2}\left(\frac{d\psi}{d\rho}\right)^2 \sin(2\theta) - \frac{2\sin^2(\theta)}{\xi\rho} + \frac{2}{\xi}\frac{d\psi}{d\rho}\sin(\psi)\sin^2(\theta) \quad (2.7)$$

here I have defined $\xi = 2J/D$, which is the characteristic length scale due to the DM interaction. Since this is a coupled equation, in order to solve it I will need the differential equation for $\psi(\rho)$. This is done similarly by varying ψ slightly by some small infinitesimal change. The process is the same as for θ so the details will be left to appendix A. The differential equation I find is,

$$\frac{d^2\psi}{d\rho^2} = -\frac{1}{\rho}\frac{d\psi}{d\rho} - 2\frac{d\theta}{d\rho}\frac{d\psi}{d\rho}\cot(\theta) + \frac{2}{\xi}\frac{d\theta}{d\rho}\sin(\psi) \quad (2.8)$$

these equations were solved numerically in mathematica. To find the minimum energy

solution the energy was plotted against different initial conditions $\frac{d\theta}{d\rho}|_{\rho=0}$.

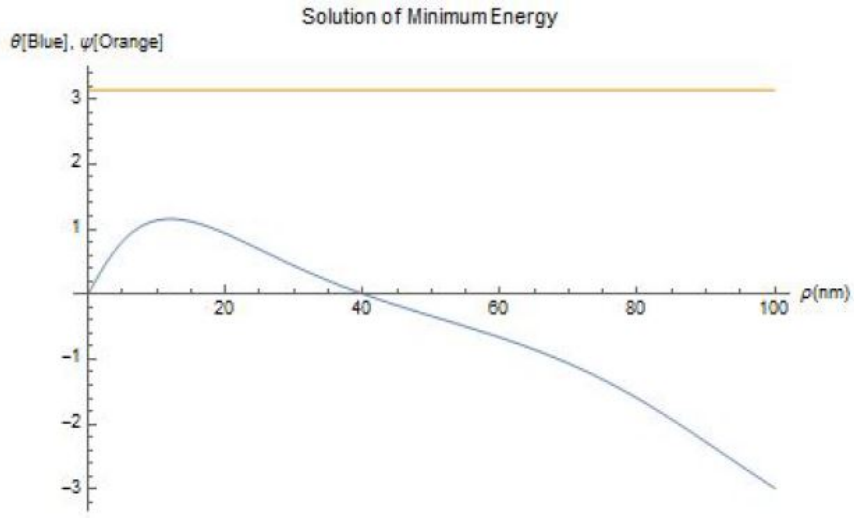

Figure 2.4 Solutions for $\theta(\rho)$ and $\psi(\rho)$ using the following parameters; $\theta(0) = 0, \psi(0) = \pi, \frac{d\theta}{d\rho}|_{\rho=0} = -.62, \frac{d\psi}{d\rho}|_{\rho=0} = 0, J = 16pj/m, D = 3mJ/m^2, \xi = 10.67nm$

I was confident that this was a minimum energy solution because when I plotted the energy against the initial condition $\alpha \equiv \theta'(\rho = 0)$, the value became apparent.

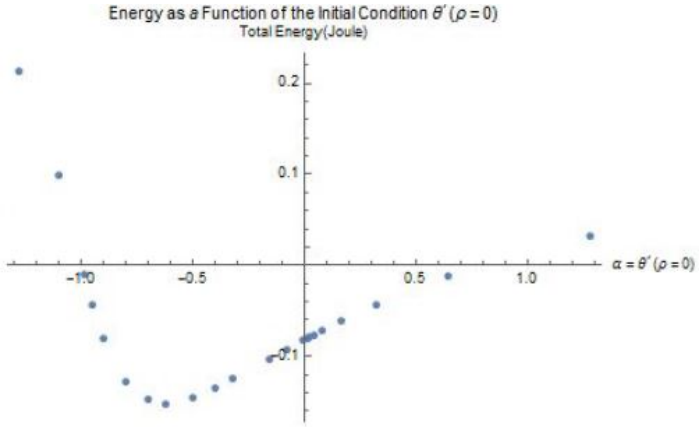

Figure 2.5 Plot of Total Energy vs. the Initial Condtion α to find Minimum Energy

However, as one can see from the discussion above about stability, it can be seend from Fig. (2.4) that $\theta(\rho)$ is not a stable solution. That is because $\theta(\rho \to \infty) \to -\infty$. Therefore, what I have shown is that there is no stable Skyrmion for just these two interactions. So, what is needed to have a stable Skyrmion? This will be discussed shortly. A quick point to

make about these solutions is the interesting magnetic structure I found when I plugged the solutions back into the magnetization **M**.

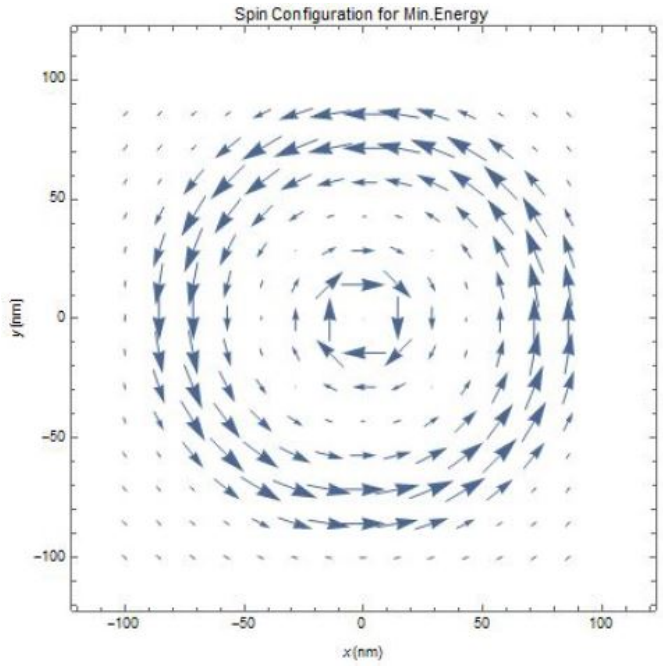

Figure 2.6 Magnetic Structure of Minimum Energy Solution

What I found here is what is known as a Target Skyrmion, which is just one Skyrmion embedded into another except their rotations are opposite as can be seen in the figure. Since this work was established to show that just the Heisenberg and DM interactions can not create stable solutions, it would be interesting to further study this magnetic structure, namely are there any interesting transport phenomena with it. This could be a future work for this project, however it is not in the scope of this work. To give an idea of what actually does yield a stable Skyrmion, I will write down the well known Ginzburg-Landau energy functional[47],

$$F[\mathbf{M}] = \int \left[r_0 \mathbf{M}^2 + J(\nabla \mathbf{M})^2 + D\mathbf{M} \cdot (\nabla \times \mathbf{M}) + U\mathbf{M}^4 - \mathbf{B} \cdot \mathbf{M} \right] d^2 r. \tag{2.9}$$

Here, there are three extra terms in contrast to (2.2), the first one is just an additional contribution the Heisenberg interaction. The Zeeman coupling or the coupling to external

magnetic field, $\mathbf{B}$, along with the quartic term help to keep the Skyrmion structure stable. The main reason this happens is because the quartic term can produce interactions that mimic regular crystal formation of ordinary solids out of the liquid state. For example, if there is a finite uniform component of the magnetization, $\mathbf{M}_f$, the quartic term in momentum space will produce a term that looks third order in the magnetization,

$$\sum_{\mathbf{q}_1,\mathbf{q}_2,\mathbf{q}_3} (\mathbf{M}_f \cdot \mathbf{m}_{q1})(\mathbf{m}_{q2} \cdot \mathbf{m}_{q3})\delta(\mathbf{q}_1 + \mathbf{q}_2 + \mathbf{q}_3) \tag{2.10}$$

where $\mathbf{m}_q$ is the Fourier transform of $\mathbf{M}(\mathbf{r})$. This is similar to the case of an ordinary crystal where one can gain energy from this term for a structure with three $\mathbf{Q}$ vectors adding up to zero[47]. These stable Skyrmions were first found in the B20 compounds, the first one notably being MnSi. The phase diagram revealed what was known as the A-phase. It was also confirmed in neutron scattering experiments that revealed the crystal structure.

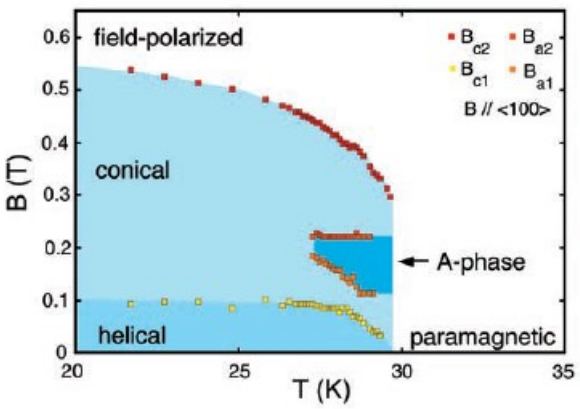

Figure 2.7 Phase Diagram for MnSi revealing the A-phase that hosts Stable Skyrmions[47]

It was also in MnSi where transport measurements were observed to host a strange Hall effect. In the next section I will discuss how the Skyrmion is directly related to this Hall effect.

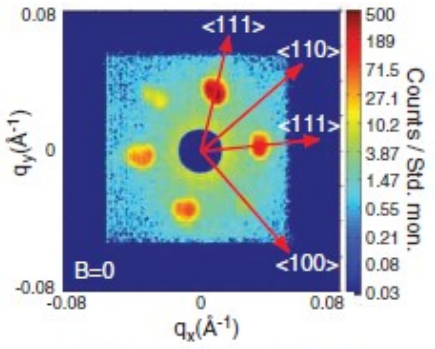

Figure 2.8 Neutron Scattering Intensities of MnSi in the A-phase[47]

2.3 Topological Hall Effect

The ordinary Hall effect occurs in metals when an external magnetic field is applied to it. This induces a Lorentz force that acts on electrons from the applied current. The Lorentz force deflects the electrons to one side of the material building up what is known as the Hall Voltage.

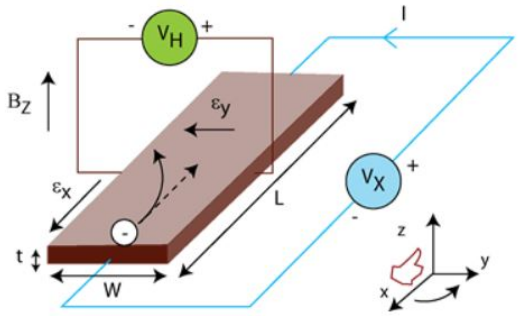

Figure 2.9 Ordinary Hall Effect [21]

Measurement of the transverse resistivity, ρ_{xy}, reveals that it is proportional to the applied magnetic field. After the discovery of the ordinary Hall effect another contribution to the resistivity was found. This time it was found to be proportional to the Magnetization. Therefore, the total transverse resistivity can be written as,

$$\rho_{xy} = R_0 B + R_s M \tag{2.11}$$

where R_0 is the ordinary Hall constant and R_s is the coefficient for what is known as the anomalous Hall effect. This Hall effect arises due to a Lorentz type force that acts on the electron except the magnetic field is from the wave function of the electron. In materials with complicated band structures the electron will obtain what is known as a Berry Phase. This phase will give rise to a "magnetic" field that will in principle act on the electron just as the external magnetic field does, thus giving rise to this type of Hall effect.

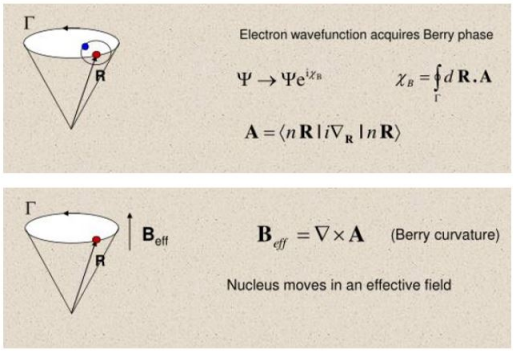

Figure 2.10 Electron Wave Function Acquiring a Berry Phase Leading to the Berry Curvature. [22]

Then, the resistivity was measured in the A-phase of MnSi giving way to a third contribution. Experiments found that this contribution was not proportional to either the applied field nor magnetization. Since this deviation was found it was understood that one had another contribution that added to ρ_{xy}.

$$\rho_{xy} = R_0 B + R_s M + \Delta\rho_{xy} \tag{2.12}$$

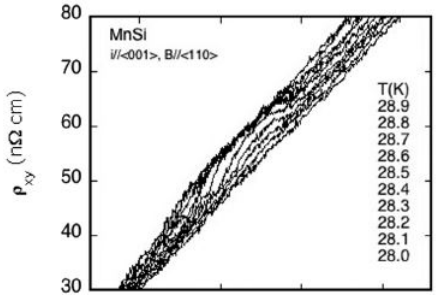

Figure 2.11 Total Resistivity in A-phase of MnSi[10]

This last contribution is caused by the magnetic field that is created by the Skyrmion. Just like the ordinary and anomalous contributions, the Skyrmion produces a magnetic field from the magnetization given by,

$$B_z = \mathbf{M} \cdot (\partial_x \mathbf{M} \times \partial_y \mathbf{M}) \tag{2.13}$$

this magnetic field will also yield a Lorentz type force that acts on the electron. This field is compeltely formed by the topology of the spins that make up the Skyrmion. Hence the name, Topological Hall Effect(THE). It is known that the Skyrmion is responsible for this additional contribution because one can isolate this term $\Delta\rho_{xy}$ and compare to the phase diagram of MnSi. The way to isolate it is to subtract off the ordinary and anomalous contributions. To do you need to determine the coefficients R_0 and R_s. This is done by examining the total resistivity away from the A-phase. There, only the ordinary and anomalous and Hall effects are non-zero. Then, by performing a linear fit using the equation,

$$\rho_{xy}/B = R_0 + R_s(M/B) \tag{2.14}$$

one can figure out the coefficients allowing you to subtract off these terms from the total. This is a common way experiments will isolate the THE. Later in this chapter I will discuss some other ways experimentalists have isolated this term, along with the advantages and disadvantages to these methods. Once isolated the THE is found to be,

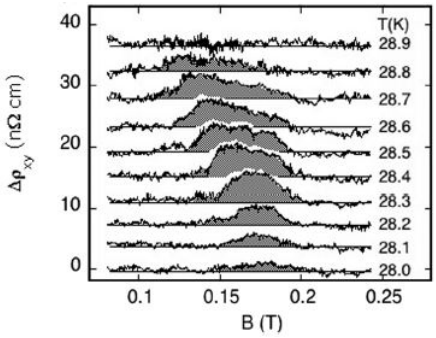

Figure 2.12 $\Delta\rho_{xy}$ in MnSi[10]

which is compared to the A-phase in the phase diagram.

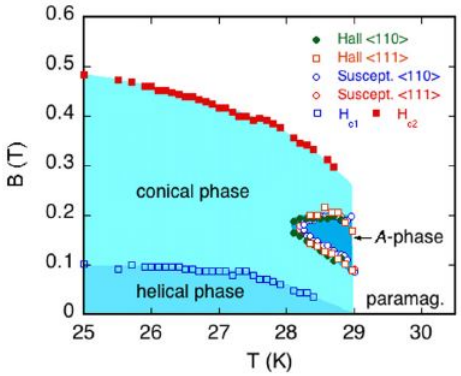

Figure 2.13 $\Delta\rho_{xy}$ compared to the A-phase in MnSi[10]

Thus, it really does seem that this contribution to the resistivity is created by the Skyrmion. Other B20 materials were reported to host this Hall effect as well, such as MnGe and FeGe. The ultimate goal being to find this effect at higher temperatures than the ones in MnSi. Higher temperatures are wanted because then the materials could be considered for magnetic nonvolatile high memory devices with ultra high density[23]. Therefore, I think it makes it important to understand the THE microscopically. In the next couple of chapters I will show exactly how that is done. Before that though, let me discuss some other interesting features of the THE. Namely, I will discuss other materials that host this effect along with some methods they used to isolate $\Delta\rho_{xy}$. Also, I will show some examples of materials that are known to not host Skyrmions bringing up the question, is the Skyrmion always responsible for this Hall effect?

2.4 Examples and Methods to measure the Topological Hall Effect

Although the linear fitting method to determine the coefficients for the ordinary and anomalous effects is a common method [10, 13, 23], it is not the only method. Another method was developed due to the fact that in some materials, this linear fit does not work.

It is known that the OHE and AHE can deviate from the linear relationship with magnetic field and magnetization. So, another way to isolate the THE is what I call the tilting method. According to neutron scattering, the plane of the Skyrmion where the three spins lie is strictly perpendicular to the applied field. This means that the energy gain from the spins interacting being on the same plane as the field is crucial for stabalizing Skyrmions. Thus, once one tilts the materials the Skyrmion is easily destabalized[56]. What is done to extract the THE is the following, the total resistivity is measured for when the material is completely perpendicular to the field. Then, the material is tilted at different angles until the THE is not seen in the measurements. Once the angle is found that eliminates the Skyrmion phase it can be subtracted from the lower angle measurements which should leave only the THE.

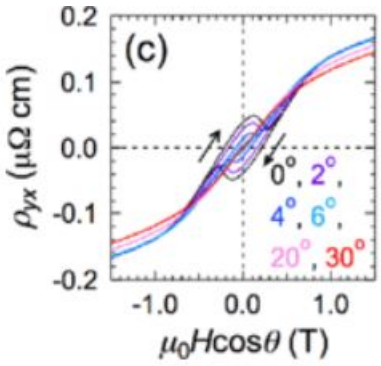

Figure 2.14 Total Resistivity Measured in FeGe at Different Angles with respect to the Applied Field[9]

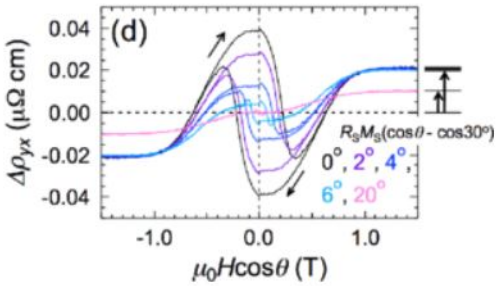

Figure 2.15 Extracted THE using the Tilt Method[9]

One more method to measure the THE was actually used in the Nature Materials paper

that I am part of. Here the THE was isolated by examining the hysteresis loop[45]. In the downward sweep (red curve) the TI will be in a ferromagnetic (FM) state without any chiral spin textures and thus the resistivity should only inculde the ordinary and anomalous terms. When the upward sweep is taken (blue curve) then it will undergo a magnetic transition around the critical field where chiral structures, in this case chiral domain walls form. Here, all three contributions are present. Then the THE can be extracted by simply subtracting the blue and red curves and what is leftover should be the THE.

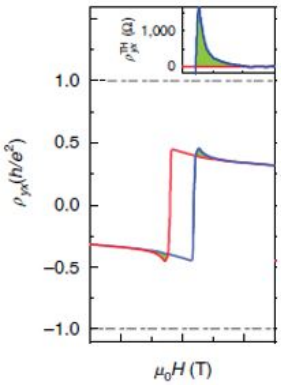

Figure 2.16 Subtracting Red and Blue Curves to Isolate ρ_{xy}^{THE}[14]

In conclusion, the first two methods have been popular ways to isolate the THE. However, the method of assuming the form of the ordinary and anomalous Hall effects poses the problems in materials that exhibit nonlinear behaviors in the applied field and magnetization. Also, in determining the coefficient for the anomalous term can be difficult because of the intrinsic and extrinsic terms. The tilting method is a good way to get around materials that break the linear relationships for the ordinary and anomalous terms. The problem with this method though is that in tilting the material will most likely change the magnetization and thus changing anomalous term. If the angle is not to steep it could be that the tilting does not change it all that much. The last method could be one that could be the most general but it could be a specific case for Topological Insulators. However, I have not read to many other experiments using this method. Essentially, knowing the band structure of

your material will most likely determine which method one should choose. Now that some discussion of experiments have been established it will be the main focus for the next few chapters to develop the theory to explain these measurements.

2.5 Conclusion

In this chapter the Skyrmion was extensively explored. Showing how it is stable to what materials it is found in. Also, the relationship it has to the Topological Hall Effect. In the following chapter I will dive further into this relationship by studying exactly how this type of Hall effect arises from the Skyrmion. I will also discuss further into the weak and strong coupling regimes.

Chapter Three

Electron Scattering Off Skyrmion in Strong Coupling Regime

This chapter will focus on the theory of the Topological Hall effect. My first work in this area was to understand the scattering of an electron off a Skyrmion. My goal was to give some analytical calculations that should agree with the numerical ones of our collaborators, Zhang and Liu [24]. I will go through my first attempt at this, followed by some discussion with the referees from the journal that we submitted the paper too, then I will show another attempt at my calculation, and finally talk about how this second attempt led me into understanding the weak and strong coupling regime of the THE that gave way to the final calculation of the problem.

3.1 Model Hamiltonian

This work was to focus on a Skyrmion in a Topological Insulator film with magnetic doping, dubbed Magnetic Topological Insulator(MTI). The reason to study this MTI is because it gives an ideal platform to study the interaction between the AHE and THE. As mentioned before the AHE intrinsic part arises due to momentum space berry phase while the THE is caused by the real space spin texture that gives rise to a magnetic field. Since

it is known that MTI's host a strong spin orbit coupling[24], along with the surface states can also mediate DM interactions[24]. Therefore, these materials should host both effects. More importantly we are interested if the spin orbit coupling (SOC) has any effect on the THE. The numerical work done showed that there was no effect from the SOC. This was displayed in the conductance calculated by our collaborators. They were able to decompose the conductance into the THE and AHE, please refer to [24].

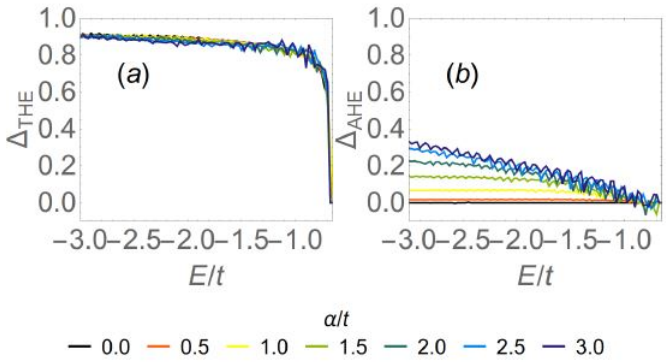

Figure 3.1 (a) and (b) show the decomposition of THE and AHE, respectively. [24]

Here α is the SOC and t is the hopping strength. As the SOC is varied it was found that the THE did not change. It was my goal to reproduce figure (3.1a) by analytical calculation. To do this I will start with the unperturbed Hamiltonian used to describe an MTI.

$$H_0 = (Bp^2 + M)\sigma_0 \otimes \tau_z + \lambda(p_x\sigma_x + p_y\sigma_y) \otimes \tau_x \tag{3.1}$$

Here B and M are constants λ is the SOC parameter, σ_i are the Pauli matrices and I have taken into consideration the orbitals which are represented by the $4x4$ matrices τ_z and τ_x with the product operator $\otimes$ defining the matrix product between a 2x2 and 4x4 matrix. These are $4x4$ extensions of the pauli matrices and are given by,

$$\tau_z = \begin{pmatrix} 1 & 0 & 0 & 0 \\ 0 & 1 & 0 & 0 \\ 0 & 0 & -1 & 0 \\ 0 & 0 & 0 & -1 \end{pmatrix}, \tau_x = \begin{pmatrix} 0 & 0 & 1 & 0 \\ 0 & 0 & 0 & 1 \\ 1 & 0 & 0 & 0 \\ 0 & 1 & 0 & 0 \end{pmatrix}. \tag{3.2}$$

To include the Skyrmion I use the fact that it will couple to the spin of the electron. This is modeled by the interaction term,

$$V(r) = -J_H \mathbf{m}(r) \cdot \boldsymbol{\sigma} \otimes \tau_0 \tag{3.3}$$

where $\mathbf{m}(r) = (\sin(\theta(r))\cos\phi, \sin(\theta(r))\sin\phi, \cos(\theta(r)))$ and ϕ is the usual 2-D coordinate and $\theta(r) = \pi\exp(-r/a)$ is the polar angle of the Skyrmion configuration with a being the radius of the Skyrmion and J_H is the constant that determines the strength of the coupling of the Skyrmion to the spin of the electron. What I did at first was just calculate the differential cross section using the perturbation $V(r)$. Then, I used the Boltzmann equation to calculate conductivity which should mimic Fig(3.1a). So, they should have the same behavior. Namely, they should both be independent of the SOC. I use scattering theory to calculate the cross section. In order to do this I added a ferromagnetic term to the unperturbed and perturbed Hamiltonian in order for $V(r) \to 0$ as $r \to \infty$. The unperturbed and perturbed Hamiltonians I used are,

$$H_0 = (Bp^2 + M)\sigma_0 \otimes \tau_z + \lambda(p_x\sigma_x + p_y\sigma_y) \otimes \tau_x - J_H\sigma_z \otimes \tau_0 \tag{3.4}$$

$$V(r) = -J_H(\mathbf{m}(r) \cdot \boldsymbol{\sigma} - \sigma_z) \otimes \tau_0 \tag{3.5}$$

Writing them out as $4x4$ matrices they are,

$$H_0 = \begin{pmatrix} Bp^2 + M - J_H & 0 & 0 & \lambda p_- \\ 0 & Bp^2 + M + J_H & \lambda p_+ & 0 \\ 0 & \lambda p_- & -Bp^2 - M - J_H & 0 \\ \lambda p_+ & 0 & 0 & -Bp^2 - M + J_H \end{pmatrix} \tag{3.6}$$

$$V(r) = -J_H \begin{pmatrix} m_z - 1 & m_- & 0 & 0 \\ m_+ & -(m_z - 1) & 0 & 0 \\ 0 & 0 & m_z - 1 & m_- \\ 0 & 0 & m_+ & -(m_z - 1) \end{pmatrix}. \tag{3.7}$$

here I define $p_\pm = p_x \pm ip_y$ and $m_\pm = m_x \pm im_y$. I will show in the next section that I need the eigenstates of the unperturbed Hamiltonian in order to calculate the differential cross section. In appendix B I calculate the eigenstates, they can be written as,

$$|1_{p+}\rangle = \begin{pmatrix} \cos\frac{\omega}{2} \\ 0 \\ 0 \\ e^{i\phi_p}\sin\frac{\omega}{2} \end{pmatrix}, |4_{p-}\rangle = \begin{pmatrix} \sin\frac{\omega}{2} \\ 0 \\ 0 \\ -e^{i\phi_p}\cos\frac{\omega}{2} \end{pmatrix}, |2_{p+}\rangle = \begin{pmatrix} 0 \\ \cos\frac{\psi}{2} \\ e^{-i\phi_p}\sin\frac{\psi}{2} \\ 0 \end{pmatrix}, |3_{p-}\rangle = \begin{pmatrix} 0 \\ \sin\frac{\psi}{2} \\ -e^{-i\phi_p}\cos\frac{\psi}{2} \\ 0 \end{pmatrix} \tag{3.8}$$

where $\cos\psi = \frac{Bp^2+M+J_H}{E_+(M+J_H)}$,$\cos\omega = \frac{Bp^2+M-J_H}{E_+(M-J_H)}$, $\tan\phi_p = \frac{p_y}{p_x}$ detrmine the polar angle and azimuth of the spinors. The energy levels for upper and lower block are, $E_\pm(M \pm J_H) = \pm\sqrt{(Bp^2 + M \pm J_H)^2 + (\alpha p)^2}$. I will write the eigenstates of the in-coming and out-going electron as $|\psi_{\mathbf{p}\beta\sigma}\rangle$, $|\psi_{\mathbf{p'}\alpha\sigma}\rangle$, where **p**, **p'** are the in-coming and out-going momentum,

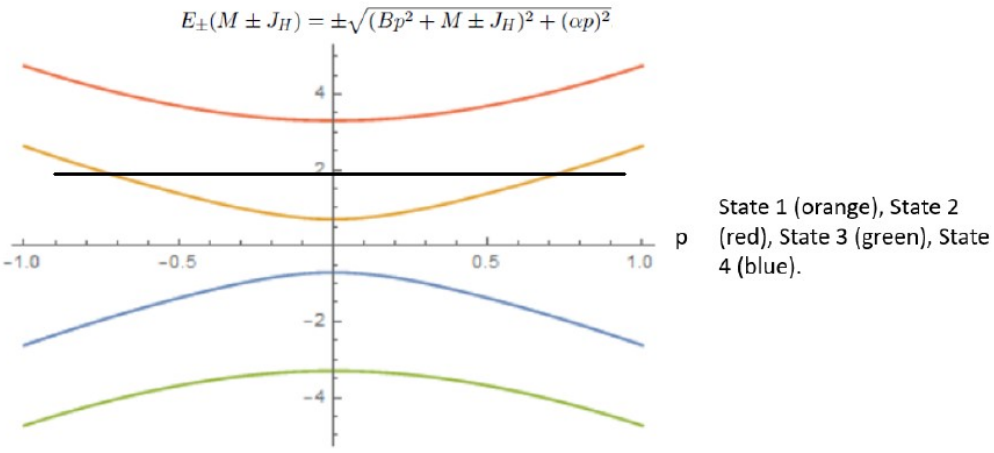

Figure 3.2 Dispersion Relation of H_0 B=1, $J_H = 1.3$, M=2, and $\alpha = 2$ and the black line indicates the energy chosen for the incoming electron

respectively, $\alpha, \beta = 1, 2, 3, 4$, and $\sigma = \pm$ corresponding to each energy. In the position representation the state reads, $\langle \mathbf{r}|\psi_{\mathbf{p}\alpha\sigma}\rangle = e^{i\mathbf{r}\cdot\mathbf{p}}\,|\alpha_{\mathbf{p}\sigma}\rangle$. I will take $\hbar = 1$. In fact the energy of the incoming electron used in the numerical work only crosses one band, so throughout the calculation I will take $\alpha = \beta$. I am also taking the initial electron to be along the x-axis, so $\phi_p = 0$.

In the next section I will go into detail about how I calculated the differential cross section using a perturbation method along with how the THE was extracted.

3.2 Perturbation and Differential Cross Section

Since I want to calculate the differential cross section that would ultimately produce a Hall effect I need to know exactly what to look for. Let's recall the discussion from chapter two about how the quartic term in the energy density produces a term that looks like this,

$$\sum_{\mathbf{q}_1,\mathbf{q}_2,\mathbf{q}_3} (\mathbf{M}_f \cdot \mathbf{m}_{q1})(\mathbf{m}_{q2} \cdot \mathbf{m}_{q3})\delta(\mathbf{q}_1 + \mathbf{q}_2 + \mathbf{q}_3). \tag{3.9}$$

Since I know it this term that is really responsible for the stabalization of Skyrmions, I know what to look for in the differential cross section calculation. Basically I will look for a

term that is third order in the magnetization. It is this term that describes the topological structure of the Skyrmion thus giving rise to the THE. So how do I calculate the cross section in order to find this third order term? The answer lies in the expansion of the scattering amplitude $F_{\alpha\beta}(\mathbf{p}, \mathbf{p}')$. As I will show below, the Born approximation for expanding F up to linear order in the potential $V(r)$ only yields a term proportional to m_z^2. Therefore, I need to expand up to second order in the potential. I find that the cross terms between first and second order give rise to this third order in magnetization. The scattering amplitude up to second order is,

$$F_{\alpha\beta}(\mathbf{p}, \mathbf{p'}) = \left\langle \psi_{\mathbf{p'}\alpha\sigma} \left| \hat{V} + \hat{V}\hat{G}_0\hat{V} \right| \psi_{\mathbf{p}\beta\sigma} \right\rangle \tag{3.10}$$

where $\hat{G}_0$ is the Green's function for the unperturbed Hamiltonian. The scattering amplitude is related to the differential cross section by,

$$\left(\frac{d\sigma(\varphi)}{d\varphi}\right)_{\alpha\beta} = |F_{\alpha\beta}(\mathbf{p}, \mathbf{p'})|^2 \tag{3.11}$$

here $\varphi = \phi_{p'} - \phi_p$ is the scattering angle. The first term in (3.10) is,

$$\left\langle \psi_{\mathbf{p'}\alpha\sigma} \left| \hat{V} \right| \psi_{\mathbf{p}\alpha\sigma} \right\rangle = -J_H \left\langle \alpha_{\mathbf{p'}\sigma} \left| \int d\mathbf{r} e^{-i(\mathbf{p'}-\mathbf{p})\cdot\mathbf{r}} (\mathbf{m}(\mathbf{r}) \cdot \boldsymbol{\sigma} - \sigma_z) \otimes \tau_0 \right| \alpha_{\mathbf{p}\sigma} \right\rangle. \tag{3.12}$$

The integrals I need to solve are the following,

$$\int (\cos(\pi e^{-r/a}) - 1) e^{-iqr\cos\phi} r dr d\phi \tag{3.13}$$

$$\int \sin(\pi e^{-r/a}) e^{\mp i\phi} e^{-iqr\cos\phi} r dr d\phi \tag{3.14}$$

these integrals come from the diagonal and off-diagonal terms in the scattering potential

matrix, respectively. I can integrate the first one in the following way,

$$\begin{aligned}\int(\cos(\pi e^{-r/a})-1)e^{-iqr\cos\phi}rdrd\phi &= 2\pi\int_0^a(\cos(\pi e^{-r/a})-1)J_0(qr)rdr\\ &\approx 2\pi\int_0^a(\cos(\pi e^{-r/a})-1)rdr\\ &= 2\pi a^2\int_0^1(\cos(\pi e^{-x})-1)xdx\\ &= 2\pi a^2 A\end{aligned} \tag{3.15}$$

similarly for the second one,

$$\begin{aligned}\int\sin(\pi e^{-r/a})e^{\mp i\phi}e^{-iqr\cos\phi}rdrd\phi &= 2\pi i\int_0^a\sin(\pi e^{-r/a})J_1(qr)rdr\\ &\approx 2\pi i\int_0^a\sin(\pi e^{-r/a})\frac{qr}{2}rdr\\ &= \pi i a^3 q\int_0^1\sin(\pi e^{-x})x^2dx\\ &= i\pi a^3 qD\end{aligned} \tag{3.16}$$

where I have used a small argument limit $qr << 1$ for the Bessel functions $J_0(x)$,$J_1(x)$, and $q = |\mathbf{p}' - \mathbf{p}|$. Therefore, we can write the Born approximation as,

$$\left\langle \alpha_{\mathbf{p'}\sigma}\left|\begin{pmatrix}2\pi a^2 A & i\pi a^3 qD\\ i\pi a^3 qD & -2\pi a^2 A\end{pmatrix}\otimes\tau_0\right|\alpha_{\mathbf{p}\sigma}\right\rangle \tag{3.17}$$

The second term in (3.10) is,

$$\left\langle\psi_{\mathbf{p'}\alpha\sigma}\left|\hat{V}\hat{G}\hat{V}\right|\psi_{\mathbf{p}\alpha\sigma}\right\rangle = \int d\mathbf{r}d\mathbf{r'}e^{-i\mathbf{p'}\cdot\mathbf{r'}}e^{-i\mathbf{p}\cdot\mathbf{r}}\left\langle\alpha_{\mathbf{p'}\sigma}\left|V(\mathbf{r'})G(\mathbf{r'}-\mathbf{r})V(\mathbf{r})\right|\beta_{\mathbf{p}\sigma}\right\rangle \tag{3.18}$$

If we let $\mathbf{R} = \mathbf{r'} - \mathbf{r}$ and change to a momentum representation we get,

$$\begin{aligned}
\left\langle \psi_{\mathbf{p'}\alpha\sigma} \left| \hat{V}\hat{G}\hat{V} \right| \psi_{\mathbf{p}\alpha\sigma} \right\rangle &= \int d\mathbf{r}d\mathbf{R}e^{-i\mathbf{p'}\cdot(\mathbf{R}+\mathbf{r})}e^{-i\mathbf{p}\cdot\mathbf{r}} \left\langle \alpha_{\mathbf{p'},\sigma} \left| V(\mathbf{r}+\mathbf{R})G(\mathbf{R})V(\mathbf{r}) \right| \alpha_{\mathbf{p}\sigma} \right\rangle \\
&= \int d\mathbf{r}d\mathbf{R}d\mathbf{p}_1 d\mathbf{p}_2 e^{-i\mathbf{p'}\cdot\mathbf{R}}e^{-i(\mathbf{p'}-\mathbf{p})\cdot\mathbf{r}}e^{i\mathbf{p}_1\cdot\mathbf{R}}e^{i\mathbf{p}_2\cdot(\mathbf{R}+\mathbf{r})} \left\langle \alpha_{\mathbf{p'},\sigma} \left| V(\mathbf{p}_2)G(\mathbf{p}_1)V(\mathbf{r}) \right| \alpha_{\mathbf{p}\sigma} \right\rangle \\
&= \int d\mathbf{r}d\mathbf{p}_1 d\mathbf{p}_3 \delta((\mathbf{p}_1+\mathbf{p}_2)-\mathbf{p'})e^{-i(\mathbf{p'}-\mathbf{p})\cdot\mathbf{r}+i\mathbf{p}_2\cdot\mathbf{r}} \left\langle \alpha_{\mathbf{p'},\sigma} \left| V(\mathbf{p}_3-\mathbf{p}_1)G(\mathbf{p}_1)V(\mathbf{r}) \right| \alpha_{\mathbf{p}\sigma} \right\rangle \\
&= \int d\mathbf{p}_1 \left\langle \alpha_{\mathbf{p'},\sigma} \left| V(\mathbf{p'}-\mathbf{p}_1)G(\mathbf{p}_1)V(\mathbf{p}_1-\mathbf{p}) \right| \alpha_{\mathbf{p}\sigma} \right\rangle
\end{aligned} \tag{3.19}$$

where $G(\mathbf{p}_1) = \sum_\delta |\delta\rangle \langle\delta| (E - E_\lambda(p_1) + i\epsilon)^{-1}$ and $\mathbf{p}_1$ is an intermediate momentum between the initial and final scattering event. To find the forms of $V(\mathbf{p}' - \mathbf{p}_1)$ and $V(\mathbf{p}_1 - \mathbf{p})$ all I need to do is replace $q = |\mathbf{p}' - \mathbf{p}|$ with the magnitudes, $|\mathbf{p}' - \mathbf{p}_1|$ and $|\mathbf{p}_1 - \mathbf{p}|$ in (3.17). These magnitudes are the following,

$$|\mathbf{p}' - \mathbf{p}_1| = 2p \sin \frac{\phi_{p'} - \phi_{p_1}}{2} \tag{3.20}$$

$$|\mathbf{p}_1 - \mathbf{p}| = 2p \sin \frac{\phi_{p_1}}{2} \tag{3.21}$$

where $\phi'_p - \phi_{p_1}$ and ϕ_{p_1} are the angles between $\mathbf{p}'$, $\mathbf{p}_1$ and $\mathbf{p}$, $\mathbf{p}_1$, respectively. Details will be given in appendix B but when integrating over ϕ_{p_1} and changing the momentum to energy integral I find the second Born approximation to be,

$$
\begin{aligned}
&-i\pi J_H^2 \Big[D(E_+(M-J_H)) \left\langle \alpha_{p'_E\sigma} \left| \cos^2\frac{\omega_E}{2} a\otimes u + \sin^2\frac{\omega_E}{2} b\otimes w + \frac{1}{2}\sin\omega_E (c\otimes x + d\otimes y) \right| \alpha_{p_E\sigma} \right\rangle \\
&+ D(E_+(M+J_H)) \left\langle \alpha_{p'_E\sigma} \left| \cos^2\frac{\omega_E}{2} b\otimes u + \sin^2\frac{\omega_E}{2} a\otimes w + \frac{1}{2}\sin\omega_E (c\otimes y + d\otimes x) \right| \alpha_{p_E\sigma} \right\rangle \\
&+ D(E_-(M-J_H)) \left\langle \alpha_{p'_E\sigma} \left| \cos^2\frac{\omega_E}{2} a\otimes u + \sin^2\frac{\omega_E}{2} b\otimes w + \frac{1}{2}\sin\omega_E (c\otimes y - d\otimes x) \right| \alpha_{p_E\sigma} \right\rangle \\
&+ D(E_-(M+J_H)) \left\langle \alpha_{p'_E\sigma} \left| \cos^2\frac{\omega_E}{2} b\otimes u + \sin^2\frac{\omega_E}{2} a\otimes w + \frac{1}{2}\sin\omega_E (c\otimes x + d\otimes y) \right| \alpha_{p_E\sigma} \right\rangle
\end{aligned}
\tag{3.22}
$$

I have defined the $2x2$ matrices a,b,c, and d as

$$
a = \begin{pmatrix} 8\pi^3 a^4 A^2 & 16 i\pi^2 a^5 p_E A D \\ -16 i\pi^2 a^5 p_E A D \cos\frac{\phi_{p'}}{2} & 0 \end{pmatrix} \tag{3.23}
$$

$$
b = \begin{pmatrix} 0 & -16 i\pi^2 a^5 p_E A D \\ 16 i\pi^2 a^5 p_E A D \cos\frac{\phi_{p'}}{2} & 8\pi^3 a^4 A^2 \end{pmatrix} \tag{3.24}
$$

$$
c = \begin{pmatrix} -\frac{16}{3} i\pi^2 a^5 p_E A D & 0 \\ 0 & \frac{16}{3} i\pi^2 a^5 p_E A D \end{pmatrix} \tag{3.25}
$$

$$
d = \begin{pmatrix} -\frac{16}{3} i\pi^2 a^5 p_E A D[\cos\frac{\phi_{p'}}{2} + 2i\sin\frac{\phi_{p'}}{2}] & 0 \\ 0 & \frac{16}{3} i\pi^2 a^5 p_E A D[\cos\frac{\phi_{p'}}{2} + 2i\sin\frac{\phi_{p'}}{2}] \end{pmatrix} \tag{3.26}
$$

and the $4x4$ matrices u, w, x,and y as

$$u = \begin{pmatrix} 1 & 0 & 0 & 0 \\ 0 & 1 & 0 & 0 \\ 0 & 0 & 0 & 0 \\ 0 & 0 & 0 & 0 \end{pmatrix} \tag{3.27}$$

$$w = \begin{pmatrix} 0 & 0 & 0 & 0 \\ 0 & 0 & 0 & 0 \\ 0 & 0 & 1 & 0 \\ 0 & 0 & 0 & 1 \end{pmatrix} \tag{3.28}$$

$$x = \begin{pmatrix} 0 & 0 & 1 & 0 \\ 0 & 0 & 0 & 1 \\ 0 & 0 & 0 & 0 \\ 0 & 0 & 0 & 0 \end{pmatrix} \tag{3.29}$$

$$y = \begin{pmatrix} 0 & 0 & 0 & 0 \\ 0 & 0 & 0 & 0 \\ 1 & 0 & 0 & 0 \\ 0 & 1 & 0 & 0 \end{pmatrix} \tag{3.30}$$

and p_E is the momentum as a function of energy obtained by from the dispersion relation. When changing the momentum integral to an energy one I wrote $(E - E(p_1) + i\epsilon)^{-1} = P\frac{1}{E-E(p)} - i\pi\delta(E - E(p_1))$ where $P\frac{1}{x}$ is the principal part but only the imaginary part has been considered and $D(E_\pm(M \pm J_H))$ is the density of states. Now that I have calculate the first and second Born approximations I can calculate the differential cross section for the THE.

3.3 Calculating Differential Cross Section

I am looking to calculate the asymmetric contribution to the differential cross section. This is found for terms with J_H^3. I am again taking lowest order in momentum and since I am only interested in the scattering events with initial and final states being $|1_{p+}\rangle$ and $|1_{p'+}\rangle$. Squaring the scattering amplitude and considering only third order term that is asymmetric in the scattering angle I find it to be,

$$\left(\frac{d\sigma}{d\varphi}\right)_{11}^{A} = Z(E_+(M-J_H))\left[(1-\cos\omega_E)\cos^4\frac{\omega_E}{2} + (1+\cos\omega_E)\sin^4\frac{\omega_E}{2}\right]\sin\varphi \qquad (3.31)$$

where $Z(E_+(M-J_H)) = 4\pi^2 a^4 A^2 D(E_+(M-J_H))J_H^3$.

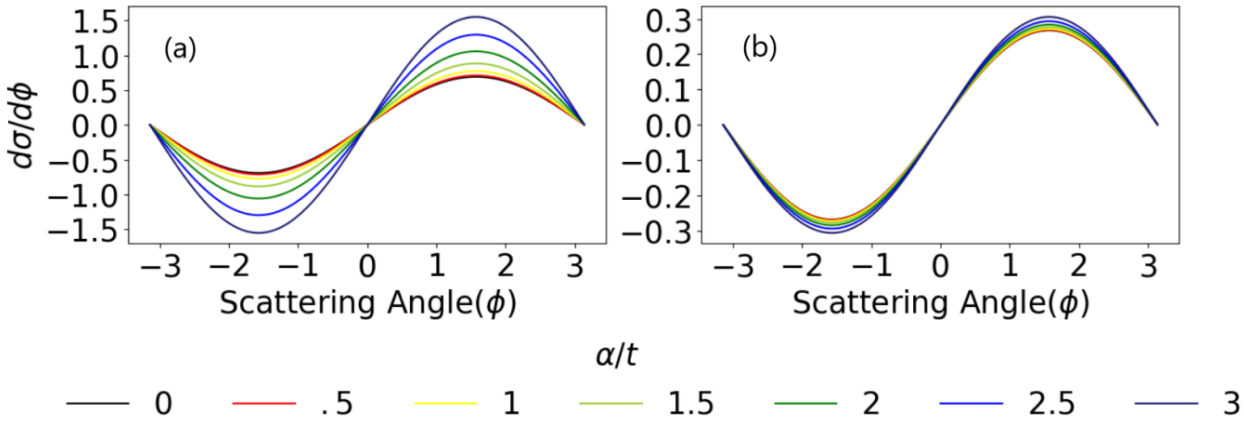

Figure 3.3 Differential Cross Section responsible for THE here α is the SOC parameter (a) small J_H limit (b) large J_H limit. [24]

In (a) I have used a value for J_H that is on the order of magnitude as the values used for the SOC parameter. The plot in (b) is where J_H is an order magnitude larger than the SOC values. It is in (b) where I saw the SOC dependence disappear. However, after discussing with collaborators there were some blatant discrepancies. First and foremost the numerical calculations did not need to increase the value of J_H to get rid of the SOC dependence. In the numerical work a value of J_H was used that was on the same order of magnitude as the SOC and still they saw no dependence. Another problem is that when increasing the

J_H value the perturbation becomes less credible. Also, this original work was submitted to PRB and these issues came up after the referees brought up some questions that made use rethink the calculation. A specific question for my calculation was the definition of the cross section. I simply used $\frac{d\sigma}{d\varphi} = |F|^2$ where I did not include the coefficient that includes correct dimensions. In the next section where I attempt to fix the calculation I will include this coefficient and I will derive it in appendix B. Some other things to note about the second attempt at the problem is that I write the states differently, I go into more detail of the second Born approximation part to show how this third order term arises, and I will calculate the conductivity σ_{xy} using the asymmetric part of the differential cross section.

3.4 States and Unperturbed Hamiltonian

To reiterate I am using a 4 band Hamiltonian with a ferromagnetic background. This model correctly describes the bulk MTI. This model Hamiltonian and states are,

$$H_0 = (Bp^2 + M)\sigma_0\tau_z + \alpha(p_x\sigma_x + p_y\sigma_y)\tau_x - J_H\sigma_z\tau_0 \tag{3.32}$$

$$|1_{p+}\rangle = N\begin{pmatrix} e^{-i\phi_p}W \\ 0 \\ 0 \\ 1 \end{pmatrix}, |4_{p-}\rangle = \bar{N}\begin{pmatrix} e^{-i\phi_p}W^{-1} \\ 0 \\ 0 \\ -1 \end{pmatrix}, |2_{p+}\rangle = M\begin{pmatrix} 0 \\ 1 \\ e^{-i\phi_p}Z \\ 0 \end{pmatrix}, |3_{p-}\rangle = \bar{M}\begin{pmatrix} 0 \\ -1 \\ e^{-i\phi_p}Z^{-1} \\ 0 \end{pmatrix} \tag{3.33}$$

where

$$W = \sqrt{\frac{E_+(M - J_H) + Bp^2 + M - J_H}{E_+(M - J_H) - Bp^2 - M + J_H}} \tag{3.34}$$

$$Z = \sqrt{\frac{E_+(M+J_H) - Bp^2 - M - J_H}{E_+(M+J_H) + Bp^2 + M + J_H}} \tag{3.35}$$

$$N = \sqrt{\frac{E_+(M-J_H) - Bp^2 - M + J_H}{2E_+(M-J_H)}} \tag{3.36}$$

$$\bar{N} = \sqrt{\frac{E_+(M-J_H) + Bp^2 + M - J_H}{2E_+(M-J_H)}} \tag{3.37}$$

$$M = \sqrt{\frac{E_+(M+J_H) + Bp^2 + M + J_H}{2E_+(M+J_H)}} \tag{3.38}$$

$$\bar{M} = \sqrt{\frac{E_+(M+J_H) - Bp^2 - M - J_H}{2E_+(M+J_H)}} \tag{3.39}$$

are the normalization constants and I have defined the other quantities above. I will now show how I was able to calculate the cross section with the updates to the states and formula of the cross section.

3.5 Differential Cross Section for Newly Obtained States

With the appropriate coefficient the differential cross section is,

$$\left(\frac{d\sigma(\varphi)}{d\varphi}\right)_{\alpha\beta} = \frac{D(E)^2}{8\pi p} \left|F_{\alpha\beta}(\mathbf{p}, \mathbf{p'})\right|^2 \tag{3.40}$$

again, I will discuss how I derived this is appendix B. The denisty of states in (3.40) is the energy of the incoming electron. Since I have given the set-up of the first and second Born approximations I will just focus on calculating those terms for the new states.

$$-J_H \int d\mathbf{r} e^{-i(\mathbf{p'}-\mathbf{p})\cdot\mathbf{r}} \left\langle 1_{\mathbf{p'}+} \left|(\mathbf{m}\cdot\boldsymbol{\sigma} - \sigma_z) \otimes \tau_0\right| 1_{\mathbf{p}+}\right\rangle \tag{3.41}$$

the expectation value is,

$$\langle 1_{\mathbf{p}'+}|(\mathbf{m}\cdot\boldsymbol{\sigma}-\sigma_z)\otimes\tau_0|1_{\mathbf{p}+}\rangle = N^2\begin{pmatrix} e^{i\phi_{p'}}W & 0 & 0 & 1\end{pmatrix}\begin{pmatrix} m_z-1 & m_- & 0 & 0\\ m_+ & -m_z+1 & 0 & 0\\ 0 & 0 & m_z-1 & m_-\\ 0 & 0 & m_+ & -m_z+1\end{pmatrix}\begin{pmatrix} W\\ 0\\ 0\\ 1\end{pmatrix} \tag{3.42}$$

$$V_{11}(\mathbf{p}'-\mathbf{p}) = -J_H\int d\mathbf{r}e^{-i(\mathbf{p}'-\mathbf{p})\cdot\mathbf{r}}N^2(m_z(r)-1)(e^{i\phi_{p'}}W^2-1) \tag{3.43}$$

For the second born approximation term, there are 4 terms that correspond to the transitions, $1\to1\to1$, $1\to2\to1$, $1\to3\to1$, $1\to4\to1$. Since I know the form of V_{11} and the states $|1\rangle$ and $|4\rangle$ are similar, I will examine the $1\to2\to1$ term. This is,

$$\int d\mathbf{p}_1\frac{V_{12}(\mathbf{p}'-\mathbf{p}_1)V_{21}(\mathbf{p}_1-\mathbf{p}')}{E-E_2(p_1)+i\epsilon} \tag{3.44}$$

I will first examine the term V_{12}.

$$V_{12}(\mathbf{p}'-\mathbf{p}_1) = -J_H\int d\mathbf{r}e^{-i(\mathbf{p}'-\mathbf{p}_1)\cdot\mathbf{r}}\left\langle 1_{\mathbf{p}'+}|(\mathbf{m}\cdot\boldsymbol{\sigma}-\sigma_z)\otimes\tau_0|2_{\mathbf{p}_1+}\right\rangle \tag{3.45}$$

$$\left\langle 1_{\mathbf{p}'+}|V(r)|2_{\mathbf{p}_1+}\right\rangle = NM\begin{pmatrix} e^{i\phi_{p'}}W & 0 & 0 & 1\end{pmatrix}\begin{pmatrix} m_z-1 & m_- & 0 & 0\\ m_+ & -m_z+1 & 0 & 0\\ 0 & 0 & m_z-1 & m_-\\ 0 & 0 & m_+ & -m_z+1\end{pmatrix}\begin{pmatrix} 0\\ 1\\ e^{-i\phi_{p_1}}Z\\ 0\end{pmatrix} \tag{3.46}$$

$$V_{12}(\mathbf{p}'-\mathbf{p}_1) = -J_H\int d\mathbf{r}e^{-i(\mathbf{p}'-\mathbf{p}_1)\cdot\mathbf{r}}NM(e^{i\phi_{p'}}Wm_- - m_+Ze^{-i\phi_{p_1}}) \tag{3.47}$$

For V_{21} I find,

$$\left\langle 2_{\mathbf{p}_1+}\left|V(r)\right|1_{\mathbf{p}+}\right\rangle = NM\begin{pmatrix}0 & 1 & e^{i\phi_{p_1}}Z & 0\end{pmatrix}\begin{pmatrix} m_z-1 & m_- & 0 & 0 \\ m_+ & -m_z+1 & 0 & 0 \\ 0 & 0 & m_z-1 & m_- \\ 0 & 0 & m_+ & -m_z+1\end{pmatrix}\begin{pmatrix}W\\0\\0\\1\end{pmatrix} \tag{3.48}$$

this yields,

$$V_{21}(\mathbf{p}_1-\mathbf{p}) = -J_H\int d\mathbf{r}' e^{-i(\mathbf{p}_1-\mathbf{p})\cdot\mathbf{r}'}NM(Wm_+ - m_-Ze^{i\phi_{p_1}}). \tag{3.49}$$

Finally, I want to change the momentum integral to energy integral.

$$E_2(p_1) = \sqrt{(Bp_1^2+M-J_H)^2+(\alpha p_1)^2} \tag{3.50}$$

with simple algebra one finds,

$$p_1 = \sqrt{\sqrt{\frac{E^2-(M-J_H)^2}{B^2}+(1/4)\Gamma^2}-(1/2)\Gamma} \tag{3.51}$$

where, $\Gamma = \frac{2B(M-J_H)+\alpha^2}{B^2}$. Changing $p_1dp_1 = D(E)dE$ where,

$$D(E) = \frac{E}{2B^2}\frac{1}{\sqrt{\frac{E^2-(M-J_H)^2}{B^2}+(1/4)\Gamma^2}}. \tag{3.52}$$

Now, the advantage to my calculation to the prior is two-fold. First, I will not be making the approximations I did in the last attempt. Here, I will keep everything as general as I can and perform the integrals numerically for the differential cross section and conductivity. Second, I will directly show what terms produce the THE. I will show that this comes from inter and intra-scattering events mixing. So, let me examine the scattering amplitude for

the same inital and final states just as before,

$$F_{11}(p,p') = V_{11}(p,p') + \int d\mathbf{p}_1 \left\langle 1_{\mathbf{p'}\sigma} \right| V(\mathbf{p'} - \mathbf{p}_1) G(\mathbf{p}_1) V(\mathbf{p}_1 - \mathbf{p}) \left| 1_{\mathbf{p}\sigma} \right\rangle \tag{3.53}$$

where $V_{11}(p,p')$ is given by (3.43). Plugging in the Green's function the amplitude can be written as,

$$F_{11}(p,p') = V_{11}(p,p') + \int d\mathbf{p}_1 \sum_{\delta} \left\langle 1_{\mathbf{p'}\sigma} \left| V(\mathbf{p'} - \mathbf{p}_1) \frac{|\delta\rangle \langle\delta|}{E_F - E_\delta(p_1) + i\varepsilon} V(\mathbf{p}_1 - \mathbf{p}) \right| 1_{\mathbf{p}\sigma} \right\rangle \tag{3.54}$$

Squaring F_{11} and taking just the cross terms gives,

$$(V_{11}(p,p'))^* \left(\int d\mathbf{p}_1 \sum_{\delta} \left\langle 1_{\mathbf{p'}\sigma} \left| V(\mathbf{p'} - \mathbf{p}_1) \frac{|\delta\rangle \langle\delta|}{E_F - E_\delta(p_1) + i\varepsilon} V(\mathbf{p}_1 - \mathbf{p}) \right| 1_{\mathbf{p}\sigma} \right\rangle \right) + h.c. \tag{3.55}$$

Now, from here we can separate it into to intra and inter band components. Say, for the intra band part, that is when $\delta = 1$.

$$(V_{11}(p,p'))^* \left(\int d\mathbf{p}_1 \left\langle 1_{\mathbf{p'}\sigma} \left| V(\mathbf{p'} - \mathbf{p}_1) \frac{|1\rangle \langle 1|}{E_F - E_1(p_1) + i\varepsilon} V(\mathbf{p}_1 - \mathbf{p}) \right| 1_{\mathbf{p}\sigma} \right\rangle \right) + h.c. \tag{3.56}$$

Then the three inter band parts,

$$(V_{11}(p,p'))^* \left(\int d\mathbf{p}_1 \left\langle 1_{\mathbf{p'}\sigma} \left| V(\mathbf{p'} - \mathbf{p}_1) \frac{|2\rangle \langle 2|}{E_F - E_2(p_1) + i\varepsilon} V(\mathbf{p}_1 - \mathbf{p}) \right| 1_{\mathbf{p}\sigma} \right\rangle \right) + h.c. \tag{3.57}$$

$$(V_{11}(p,p'))^* \left(\int d\mathbf{p}_1 \left\langle 1_{\mathbf{p'}\sigma} \left| V(\mathbf{p'} - \mathbf{p}_1) \frac{|3\rangle \langle 3|}{E_F - E_3(p_1) + i\varepsilon} V(\mathbf{p}_1 - \mathbf{p}) \right| 1_{\mathbf{p}\sigma} \right\rangle \right) + h.c. \tag{3.58}$$

$$(V_{11}(p,p'))^* \left(\int d\mathbf{p}_1 \left\langle 1_{\mathbf{p'}\sigma} \left| V(\mathbf{p'}-\mathbf{p}_1) \frac{|4\rangle\langle 4|}{E_F - E_4(p_1) + i\varepsilon} V(\mathbf{p}_1 - \mathbf{p}) \right| 1_{\mathbf{p}\sigma} \right\rangle \right) + h.c. \quad (3.59)$$

physically, these represent scattering from the initial state, 1 to the final state 1, with intermediate states, 1, 2, 3, or 4.

For this work, I need to calculate the THE. To find the THE the chirality aware term must be extracted from the total cross section. The chirality aware term is of the form $m(r) \cdot (m(r') \times m(r''))$. Where I find this term is in the interband parts involving the states 2 and 3. Examining equations (3.43), (3.47), and (3.49), I find that the chirality aware term comes from the cross terms of m_+ and m_-. Since $m_\pm = m_x \pm i m_y$ when multiplying (3.43), (3.47), and (3.49) together I find a term such as $m_z(r)(m_x(r')m_y(r'') - m_y(r')m_x(r''))$. To show this in detail, I will start with the interband terms.

$$Re\left[V_{11}(p,p')^* \int dp_1 V_{12}(p'-p_1) G(p_1) V_{21}(p_1-p)\right] + Re\left[V_{11}(p,p')^* \int dp_1 V_{13}(p'-p_1) G(p_1) V_{31}(p_1-p)\right] \quad (3.60)$$

Plugging in equations (3.43), (3.47), and (3.49) to the first term of 34 gives,

$$\begin{aligned} &Re[(...)N^4 M^2(p_1)(m_z(r'')-1)(e^{-i\phi_{p'}}W^2 - 1)(e^{i\phi_{p'}}W(p_1)m_-(r) - m_+(r)Z(r)e^{-i\phi_{p_1}}) \\ &(W(p_1)m_+(r') - m_-(r')Z(p_1)e^{i\phi_{p_1}})] \end{aligned} \quad (3.61)$$

Where (...) are just the integrals, Green's function, exponentials, and constant J_H.

$$(...) = -J_H^3 \int dr dr' dr'' dp_1 \frac{1}{E_F - E_2(p_1) + i\epsilon} e^{i(\mathbf{p'}-\mathbf{p})\cdot\mathbf{r}''} e^{-i(\mathbf{p'}-\mathbf{p}_1)\cdot\mathbf{r}} e^{-i(\mathbf{p}_1-\mathbf{p})\cdot\mathbf{r}'} \quad (3.62)$$

Looking at the second term I find it to be,

$$Re[(...)N^4\bar{M}^2(p_1)(m_z(r'')-1)(e^{-i\phi_{p'}}W^2-1)(-e^{i\phi_{p'}}W(p_1)m_-(r)+m_+(r)Z(r)^{-1}e^{-i\phi_{p_1}})$$
$$(-W(p_1)m_+(r')+m_-(r')Z(p_1)^{-1}e^{i\phi_{p_1}})] \tag{3.63}$$

The term (...) is the same as in (3.62) except the Green's function has the denominator $E_F - E_3(p_1) + i\epsilon$. Since the THE involves the chirality aware term, I only want to keep terms that have the form $m_z(r'')(m_x(r)m_y(r') - m_y(r)m_x(r'))$. This comes from terms like $m_z(r'')m_-(r)m_+(r')$ more specifically it is the imaginary part of $m_-(r)m_+(r') = (m_x(r) - im_y(r))(m_x(r') + im_y(r'))$. Keeping these terms only, the first and second term of (3.60) are,

$$Re[(...)N^4(e^{-i\phi_{p'}}W^2-1)\left(\frac{(M^2(p_1)(e^{i\phi_{p'}}W^2-Z^2(p_1))}{E_F-E_2(p_1)+i\epsilon}+\frac{\bar{M}^2(p_1)(e^{i\phi_{p'}}W^2-Z^{-2}(p_1))}{E_F-E_3(p_1)+i\epsilon}\right)$$
$$m_z(r'')[\mathbf{m}(r)\times\mathbf{m}(r')]_z] \tag{3.64}$$

In the parantheses (...) is,

$$(...) = -iJ_H^3\int drdr'dr''dp_1e^{i(\mathbf{r''}-\mathbf{r})\cdot\mathbf{p'}}e^{i(\mathbf{r}-\mathbf{r'})\cdot\mathbf{p}_1}e^{i(\mathbf{r'}-\mathbf{r''})\cdot\mathbf{p}} \tag{3.65}$$

Now that I have isolated the chirality aware term, I need to isolate the terms that will produce asymmetry in the cross section, i.e. $\frac{d\sigma}{d\varphi}(\varphi) = -\frac{d\sigma}{d\varphi}(-\varphi)$. I want to find the asymmetry so that there can be a non-zero Hall current. To do this I can examine the terms, $e^{i(\mathbf{r''}-\mathbf{r})\cdot\mathbf{p'}}(e^{-i\varphi}W^2-1)(e^{i\varphi}W^2-Z^2)$ and $e^{i(\mathbf{r''}-\mathbf{r})\cdot\mathbf{p'}}(e^{-i\varphi}W^2-1)(e^{i\varphi}W^2-Z^{-2})$. Now, the exponential can be written as,

$$e^{i(\mathbf{r''}-\mathbf{r})\cdot\mathbf{p'}} = e^{i(x''-x)p'_x}e^{i(y''-y)p'_y} = (\cos(\Delta Xp\cos\varphi)+i\sin(\Delta Xp\cos\varphi))(\cos(\Delta Yp\sin\varphi)+i\sin(\Delta Yp\sin\varphi)) \tag{3.66}$$

Where $\Delta X = x'' - x$ and $\Delta Y = y'' - y$. I can write this as a sum of an even and odd function of the scattering angle, $e^{i(\mathbf{r}''-\mathbf{r})\cdot\mathbf{p}'} = f(\varphi) + g(\varphi)$. Where f is an even function and g is odd with respect to φ. I can do the same for the other terms. Examining, $(e^{-i\varphi}W^2 - 1)(e^{i\varphi}W^2 - Z^2)$,

$$(e^{-i\varphi}W^2 - 1)(e^{i\varphi}W^2 - Z^2) = W^4 + Z^2 - e^{-i\varphi}W^2Z^2 - e^{-i\varphi}W^2 + Z^2 \tag{3.67}$$

Again, I can write this as a sum of an even and odd function. $(e^{-i\varphi}W^2-1)(e^{i\varphi}W^2-Z^2) = \bar{f}(\varphi) + \bar{g}(\varphi)$. Now, the cross section will have terms like $(f(\varphi) + g(\varphi))(\bar{f}(\varphi) + \bar{g}(\varphi))$ and the asymmetric terms will come from the cross terms. So, the cross section for the THE looks like,

$$\left(\frac{d\sigma(\varphi)}{d\phi}\right)_{THE} = Re[(...)N^4\left(\frac{(M^2(p_1)\left(f(\varphi)\bar{g}(\varphi) + g(\varphi)\bar{f}(\varphi)\right)}{E_F - E_2(p_1) + i\epsilon} + \frac{\bar{M}^2(p_1)\left(f(\varphi)\bar{g}'(\varphi) + g(\varphi)\bar{f}'(\varphi)\right)}{E_F - E_3(p_1) + i\epsilon}\right) m_z(r'')[\mathbf{m}(r) \times \mathbf{m}(r')]_z] \tag{3.68}$$

where

$$(...) = -iJ_H^3 \int dr dr' dr'' dp_1 e^{i(\mathbf{r}-\mathbf{r}')\cdot\mathbf{p}_1} e^{i(\mathbf{r}'-\mathbf{r}'')\cdot\mathbf{p}} \tag{3.69}$$

$$f(\varphi) = \cos(\Delta X p\cos\varphi)\cos(\Delta Y p\sin\varphi) + i\sin(\Delta X p\cos\varphi)\cos(\Delta Y\sin\varphi) \tag{3.70}$$

$$g(\varphi) = i\cos(\Delta X p\cos\varphi)\sin(\Delta Y p\sin\varphi) - \sin(\Delta X p\cos\varphi)\sin(\Delta Y\sin\varphi) \tag{3.71}$$

$$\bar{f}(\varphi) = W^4 + Z^2 - W^2Z^2\cos\varphi - W^2\cos\varphi \tag{3.72}$$

$$\bar{g}(\varphi) = iW^2Z^2\sin\varphi - iW^2\sin\varphi \tag{3.73}$$

$$\bar{f}'(\varphi) = W^4 + Z^{-2} - W^2Z^{-2}\cos\varphi - W^2\cos\varphi \tag{3.74}$$

$$\bar{g}'(\varphi) = iW^2Z^{-2}\sin\varphi - iW^2\sin\varphi \tag{3.75}$$

Clearly, $\left(\frac{d\sigma(\varphi)}{d\varphi}\right)_{THE}$ goes to $-\left(\frac{d\sigma(\varphi)}{d\varphi}\right)_{THE}$ when $\varphi \to -\varphi$. To confirm my calculation I will antisymmetrize equation 38 numerically by calculating,

$$\frac{\frac{d\sigma(\varphi)}{d\varphi} - \frac{d\sigma(-\varphi)}{d\varphi}}{2} \tag{3.76}$$

where $\frac{d\sigma(\varphi)}{d\varphi}$ is the cross section from (3.64).

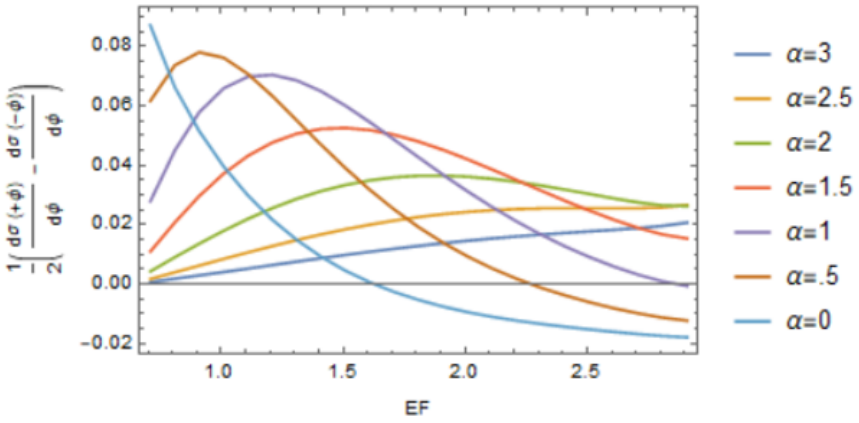

Figure 3.4 Calculating (42) by using (38) B=1, M=2, J_H=1.3, ϕ=π/4

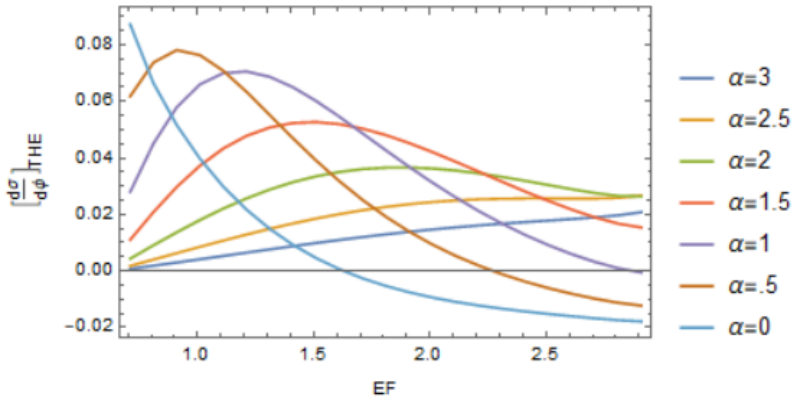

Figure 3.5 Fermi Dependence of (42) B=1, M=2, J_H=1.3, ϕ=π/4

Again, I see that the cross section is varying with SOC. However, I will discuss the conductivity calculation to see if in the process perhaps the SOC dependence drops out.

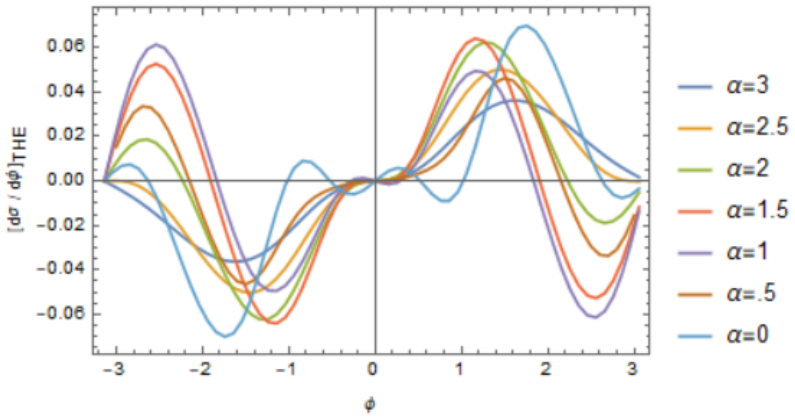

Figure 3.6 Angular Dependence of (42) with varying α, B=1, M=2, J_H=1.3, E_F/t = 2

3.6 Conductivity Calculation

Since, ultimately the main result from the numerical work was the transverse conductance, G_{xy} it is necessary for me to calculate the conductivity, σ_{xy}. Since the differential cross section calculations have shown SOC dependence my initial thought was that could the conductivity calculation make it so that it some how drops out? To answer this question let me start with a Boltzmann approach,

$$e\mathbf{E}\frac{\partial f(\mathbf{p})}{\partial \mathbf{p}} = \int d\phi_{p'} \left(R_{\mathbf{pp'}} f(\mathbf{p'}) - R_{\mathbf{p'p}} f(\mathbf{p})\right) \tag{3.77}$$

where e is the electron charge, $\mathbf{E}$ is a uniform electric field, which I will take to be in the x-direction, $f(\mathbf{p})$ is the electron distribution function, and the scattering rate $R_{\mathbf{p'p}}$ is given by,

$$R_{\mathbf{p'p}} = R_{imp}(\theta) + n_{sk} v \left(\frac{d\sigma(\theta)}{d\theta}\right)_{THE} \tag{3.78}$$

$R_{imp}(\theta)$ is scattering off of nonmagnetic impurities, n_{sk} is a skyrmion denisty, v is the velocity, and I have generalized the scattering angle to $\theta = \phi_{p'} - \phi_p$ where $\phi_{p'}$ and ϕ_p correspond to the final and initial momentum, respectively. The left hand side of (3.77) will only have $\cos\phi_p$ contribution, therefore I want to expand the distribution function up to,

$$f(\mathbf{p}) = f_0 + f_+ \cos\phi_p + f_- \sin\phi_p \tag{3.79}$$

So, the left hand side will be to first order in electric field, E is, $eE\frac{\partial\epsilon}{\partial p}\frac{\partial f_0}{\partial\epsilon}\cos\phi_p$. Examining the first term on the right hand side,

$$\int d\phi_{p'} R_{\mathbf{pp'}} f(\mathbf{p'}) = \int d\phi_{p'} \left(R(-\theta)_{imp} - n_{sk} v \left(\frac{d\sigma(\theta)}{d\theta} \right)_{THE} \right) (f_0 + f_+ \cos\phi_{p'} + f_- \sin\phi_{p'}) \tag{3.80}$$

Here, I am using the fact that the cross section is asymmetric with respect to the scattering angle. Looking at terms that will be linear in electric field, I find,

$$\Omega \sin\phi f_+ - \Omega \cos\phi f_- \tag{3.81}$$

$$\Omega = n_{sk} v \int \left(\frac{d\sigma(\theta)}{d\theta} \right)_{THE} \sin\theta d\theta \tag{3.82}$$

For the second term, the only terms surviving after integration are,

$$\frac{f_+}{\tau}\cos\phi_p + \frac{f_-}{\tau}\sin\phi_p \tag{3.83}$$

where $\frac{1}{\tau} = \int R_{imp}(\theta) d\theta$Therefore the Boltzmann equation reads,

$$eE\frac{\partial\epsilon}{\partial p}\frac{\partial f_0}{\partial\epsilon}\cos\phi_p = \cos\phi_p \left(-\Omega f_- - \frac{f_+}{\tau} \right) + \sin\phi_p \left(\Omega f_+ - \frac{f_-}{\tau} \right) \tag{3.84}$$

Solving this for f_- and f_+,

$$f_+ = -eE\tau\frac{\partial\epsilon}{\partial p}\frac{\partial f_0}{\partial\epsilon}\frac{1}{1+(\Omega\tau)^2} \tag{3.85}$$

$$f_- = -eE\tau \frac{\partial \epsilon}{\partial p} \frac{\partial f_0}{\partial \epsilon} \frac{\Omega\tau}{1+(\Omega\tau)^2} \tag{3.86}$$

To find the conductivity, I will look at the current

$$\mathbf{j} = e \int \mathbf{v} f(\mathbf{p}) d^2p \tag{3.87}$$

Here is where I can find σ_{xy} by looking at the y-component of $\mathbf{v}$ and since the E field is in the x-direction, the transverse conductivity is,

$$\sigma_{xy} = e^2\tau \frac{\Omega\tau}{1+(\Omega\tau)^2} \int v^2 \frac{\partial f_0}{\partial \epsilon} p dp \tag{3.88}$$

If I change to an energy integral, the integrand should peak around the fermi-energy, therefore I can approximate,

$$\sigma_{xy} \sim e^2\tau \frac{\Omega\tau}{1+(\Omega\tau)^2} v(EF)^2 D(EF) \tag{3.89}$$

where $D(EF)$ is the density of states at the fermi-energy.

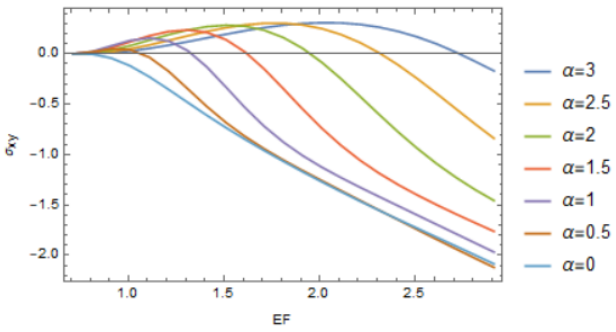

Figure 3.7 Fermi energy Dependence of σ_{xy}, B=1, M=2, J_H=1.3

Unfortunately, I find that the SOC dependence is still strong with σ_{xy}. So, how can I explain this dependence? Well, what is really happening is that neither the numerical work nor the analytical work is necessarily wrong it is in fact my analytical calculation is examining a particular case that is opposite of the numerical work.

3.7 Adiabatic and Non-Adiabatic Regime

It was found that after some careful consideration into the physics of the scattering problem where the issue lies between analytical and numerical. In my calculation I attempted to use a perturbation technique. This of course only works when the the potential is the smallest energy scale. Along with that, one can determine certain regimes for an electron scattering off a Skyrmion based on a single parameter. This is known as the adiabatic parameter defined as,

$$\lambda_{ad} \equiv \frac{J_H \tau}{\hbar} = \frac{2 J_H R}{\hbar v_F}. \tag{3.90}$$

and depending on the value will describe the scattering. Here, τ is the time for the electron to traverse the Skyrmion and v_F is the Fermi velocity. What I mean by this is that if $\lambda_{ad} \gg 1$ then the interaction between the electron's spin and the magnetization of the Skyrmion is dominant compared to say the spin orbit coupling term in (3.4). The potential will not be the smallest energy scale and thus can not be used as a perturbation. This is known as the adiabatic regime because the electron wants to align with the magnetization. For the opposite case, $\lambda_{ad} \ll 1$, this is known as the non-adiabatic regime. Here the electron does not feel the magnetization as much, which allows the perturbation to be used. It does turn out that when plugging in the values that were used in the numerical work, $\lambda_{ad} \gg 1$, so that the perturbation can not be used. This really amounts to the fact that spin flip processes are suppressed during scattering. Since the numerical work in fact used these assumptions the way to translate it to an analytical calculation is quite simple. In the adiabatic region one can implement a semi-classical Drude approach. Taking the original Hamiltonian,

$$H = (Bp^2 + M)\tau_z + \lambda(\sigma_x p_x + \sigma_y p_y)\tau_x - J_H \mathbf{m}(\mathbf{r}) \cdot \boldsymbol{\sigma} \tau_0 \tag{3.91}$$

since the original scattering potential can not be used a perturbation one can rotate

this Hamiltonian such that it is completely removed. This can be achieved by using a 2x2 matrix, $U(\mathbf{r})$, such that, $U^{\dagger}(\mathbf{m}(\mathbf{r})\cdot\sigma)U = \sigma_z$. Applying this to H I find,

$$H' = (B(p - iA)^2\tau_z + \lambda((p - iA)\cdot\bar{\boldsymbol{\sigma}}\tau_x - J_H\sigma_z \tag{3.92}$$

where, $A_\mu = -iU^{\dagger}\partial_\mu U$ and $\bar{\boldsymbol{\sigma}} = U^{\dagger}\boldsymbol{\sigma}U$. Now, what is important of this rotation is what arises is the gauge potential A. This is a 2x2 matrix that encodes the adiabatic(diagonal) and non-adiabatic(off-diagonal) terms. Since the electron only cross one band Fig. 3.2, along with being in the adiabatic region I only care about the first diagonal element in A. This can be thought of as a vector potential as is found in electromagnetism, which will give rise to a magnetic field, $B_z^{\uparrow} = \partial_x A_y^{\uparrow} - \partial_y A_x^{\uparrow}$ here I am just calling the diagonal element of A as $A^{\uparrow}$. This magnetic field will induce a Lorentz force on the scattered electron. I can use a simple Drude model to directly calculate the transverse conductivity,

$$\frac{d\langle\mathbf{p}\rangle}{dt} = -e\left(\mathbf{E} + \frac{\langle\mathbf{p}\rangle}{mc}\times\left\langle\mathbf{B}^{\uparrow}\right\rangle\right) - \frac{\langle\mathbf{p}\rangle}{\tau} \tag{3.93}$$

where I have taken the averages of momentum and the magnetic field, taking a steady state $\frac{d\langle\mathbf{p}\rangle}{dt} = 0$ I find,

$$0 = -eE_x - \frac{e\left\langle B_z^{\uparrow}\right\rangle}{mc}\langle p_y\rangle - \frac{\langle p_x\rangle}{\tau} \tag{3.94}$$

and

$$0 = -eE_y + \frac{e\left\langle B_z^{\uparrow}\right\rangle}{mc}\langle p_x\rangle - \frac{\langle p_y\rangle}{\tau}. \tag{3.95}$$

If I multiply this by $\sigma_0 = -\frac{ne\tau}{m}$ and using $\mathbf{j} = -ne\langle\mathbf{v}\rangle$ these equations become,

$$0 = \sigma_0 E_x - \frac{e\tau\left\langle B_z^{\uparrow}\right\rangle}{mc}j_y - j_x \tag{3.96}$$

$$0 = \sigma_0 E_y + \frac{e\tau\left\langle B_z^{\uparrow}\right\rangle}{mc}j_x - j_x \tag{3.97}$$

setting $j_y = 0$ since the applied current is only in the x-direction I can solve for j_x,

$$j_x = \frac{\sigma_0}{1 - \frac{e\tau\left\langle B_z^{\uparrow}\right\rangle}{mc}}(E_x + E_y) \tag{3.98}$$

approximating the denominator up to first order in $\frac{e\tau\left\langle B_z^{\uparrow}\right\rangle}{mc}$ the conductivity is,

$$\sigma_{xy} = \sigma_0 \frac{e\tau\left\langle B_z^{\uparrow}\right\rangle}{mc} \tag{3.99}$$

where it is in this final equation that I have found no SOC dependence. Where this result is also a well known strong coupling result[25]. To reiterate, it is found that in the strong coupling regime that there is no spin orbit coupling dependence on the conductivity due to the fact that the spin flip processes are suppressed during the scattering event. In the next chapter I will continue my work with Magnetic Topological Insulators. This time however, there will be no Skyrmion in the material but some how I still find a Topological Hall Effect. My work backed up experimental findings and is the reason I will discuss why the Topological Hall Effect does not imply Skyrmions.

3.8 Conclusion

So, to conclude this chapter it was found that the cross terms between the first and second Born approximations give rise to the spin chirality term that was mentioned in the two previous chapters. I also found that the distinction between the strong and weak coupling are important in the Topological Hall Effect. Now, I will start to show works that depart from the normal arguments of this type of Hall effect. Namely, are Skyrmions the only cause of the Topological Hall Effect? As will be seen through the rest of the remaining chapters, it will not be the case that they are.

Chapter Four

Spin Susceptibility Calculation

This chapter continues the trend of the last one in discussing the Topological Hall Effect. However, I begin to move away from the topic of Skyrmions. These latter half chapters serve as demonstrations of the THE without the Skyrmion. These works are my way to change the communities mind when it comes to the discussion of the THE. The work in this chapter will again discuss the Magnetic Topological Insulators. The Hall effect was measured and it was found to host the THE. My part was to calculate what is known as the spin susceptibility(SS). This describes the likely-hood of an electron's spin aligning with the magnetization produced by the material. I use a model similar to the 4x4 model from the last chapter. I show how the surface states and the bulk of the material both contribute to the THE. Also, I will discuss how the SS relates to the THE thorugh the DM interaction. First, let me discuss the set-up of the experiment, the measurements taken, and how the THE was measured.

4.1 Experimental Work

The material used for transport measurements was a topological insulator(TI) sandwich structure with an undoped TI layer (5 quintuple $(Bi, Sb)_2Te_3$ layers) inserted between two magnetic TI layers (two 3 quintuple Cr-doped $(Bi, Sb)_2Te_3$ layers). Such a 3-5-3 sandwich heterostructure has two distinct advantages. First, the non-magnetic TI layer serves as a

spacer that separates the magnetic exchange interaction(interaction between electron's spin and magnetization) between the two magnetic TI layers[14]. As a result, the influence of the DM interaction can be maximized because the magnetic moments in each MTI layer interact only with their own surface states. Second, both the top and bottom surface states are separately gapped by the magnetization, which makes the Quantum Anomalous Hall(QAH) effect possible[14]. To note the experiment was able to demonstrate a transition from the QAH, which reveals integer value of the conductivity/resistivity, σ_{yx}/ρ_{yx} to the THE. Since my work for this project was to understand the THE I will not go into details of the QAH. The reader is encouraged to read the experimental work in the paper[14]. The electrical transport measurements on the 3-5-3 heterostructure with standard dHall bar geometry. When the bottom gate, $V_g = 0V$ the ferromagnetic(FM) order at low temperatures gaps out the top and bottom surface states, and the chemical potential is located inside the magnetic exchange gaps of both surfaces. This is confirmed by the observation of a quantized Hall resistance (ρ_{yx}) and a vanishing longitudinal resistance (ρ_{xx}) at $T = 30$mK. Increasing the temperature , the sample deviates from the QAH state and shows transport properties of a conventional FM material, namely, hysteretic ρ_{yx} loops and butterfly-shaped ρ_{xx}.

4.1.1 Measuring THE in 3-5-3 MTI Heterostructure

Figure (4.2) shows the magnetic field $\mu_0 H$ dependence of the Hall resistance ρ_{yx} and the longitudinal resistance ρ_{xx} of the 3-5-3 heterostructure at different gate voltages$(V_g - V_g^0)$. When $V_g = V_g^0 = 20V$, the sample displays a perfect QAH state: at zero magnetic field, $\rho_{yx}(0) = \pm h/e^2$ and $\rho_{xx}(0) < 1\Omega$. When the magnetic field $\mu_0 H > \mu_0 H_c(\mu_0 H_c$ is the coercive field), the Hall curves completely overlap during the upward and downward magnetic field sweeps (Fig. 4.2d). When $V_g - V_g^0 = -100V$, hole carriers are injected into the sample and dissipative bulk channels are introduced. In this regime, $\rho_{yx}(0)$ deviates from h/e^2 but still remains as high as $\sim 0.76h/e^2$ and $\rho_{yx}(0)/\rho_{xx}1.2$, which indicates the persistence of the chiral

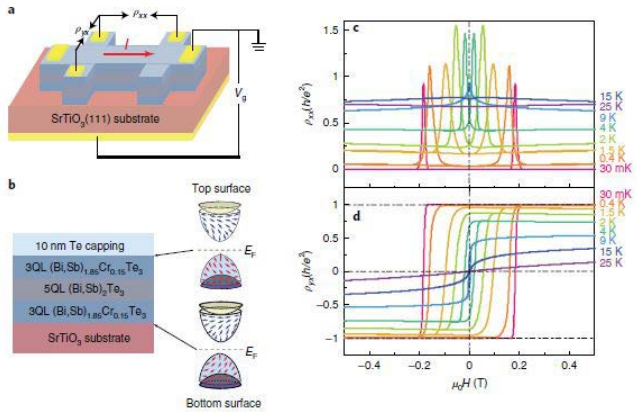

Figure 4.1 QAH effect in TI sandwich heterostructures. a, Schematic of the field-effect transistor device with a bottom gate (V_g) used in transport measurements. The electrical contacts on the Hall bar and the back-gate contact shown in yellow are made by pressed indium dots. The 0.5 mm $SrTiO_3(111)$ substrate is used as the dielectric layer for the bottom gate. b, Schematic of the magnetic TI sandwich heterostructure. The total thickness of the sample is 11 QLs. When T $< T_C$, an exchange gap opens at the Dirac points of the top and bottom surfaces. Blue (red) arrows represent the spin orientations of the top (bottom) section of gapped Dirac SSs. c,d, Magnetic field 0H dependence of the longitudinal resistance ρ_{xx} (c) and the Hall resistance ρ_{yx} (d) at $V_g = 0$ V. At T = 30 mK and $V_g = 0$ V, the quantized ρ_{yx} and the vanishing ρ_{xx} suggest this sandwich sample is in the QAH state.[14]

edge transport of the QAH state[14]. The existence of the chiral edge transport is further supported by the decrease in $\rho_{xx}(0)$ with decreasing temperature (Fig. 4.3e). Notably, over a range of a fraction of a Tesla above $\mu_0 H_c$, the hump feature appears in the ρ_{yx} curves(green shadow area); specifically, the Hall curve under a downward $\mu_0 H > \mu_0 H_c$ (Fig. 4.2c). The hump feature observed is interpreted as a signautre of the THE. It is considered as strong evidence for the existence of chiral spin texture in real space[14].

So how was the THE measured in the experiment? Well, re-call some of the ways I discussed how the THE was isolated from the total resistivity. One way was by simply subtracting off the normal and anomalous contributions. This was done by observing the total resistivity away from where the THE occurred to be able to write a linear relationship and identify the coefficients of the normal and anomalous Hall effects. The other way was by tilting the material such that the vector normal to the plane and the magnetic field in

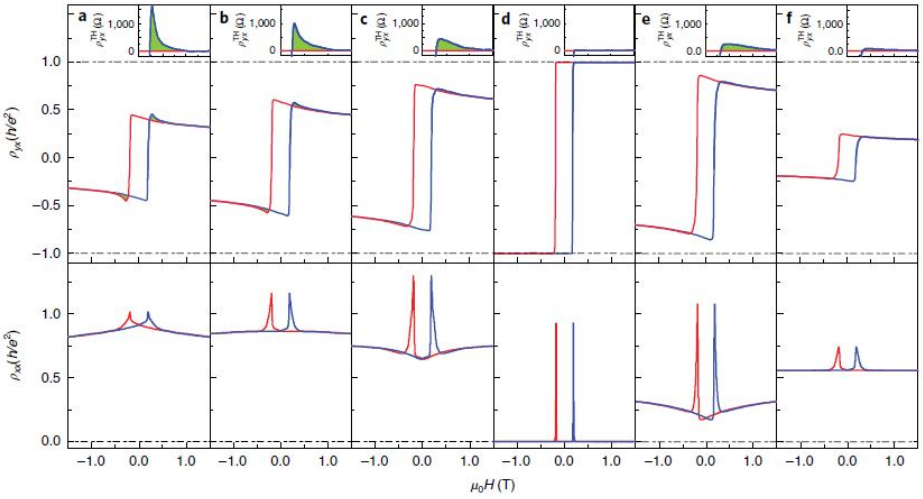

Figure 4.2 Gate-induced TH effect in TI sandwich heterostructures. a–f, Magnetic-field $\mu_0 H$ dependence of the Hall resistance ρ_{yx} (top) and the longitudinal resistance ρ_{xx} (bottom) at different gates (V_g – V_g^0) of –220 V (a), –140 V (b), –100 V (c), 0 V (d), +70 V (e) and +180 V (f) at T = 30 mK. The sample shows a perfect QAH state when $V_g = V_0$= +20 V. When V_g is tuned away from V_0, ρ_{yx} deviates from the quantized value (that is, h/e^2) and shows a hump (feature shaded in green), which is known as the TH effect. Insets a–f: the TH resistance ρ_{yx}^{TH}, which is subtracted using the offset resistance of ρ_{yx} as the external $\mu_0 H$ is swept upward and downward. Blue (red) curve represents the process for increasing (decreasing) $\mu_0 H$.[14]

the z-direction had some non-zero angle between them. The way the THE was isolated in this experiment does differentiate from the previous methods.

For a ferromagnetic material, the total ρ_{yx} is a result of three contributions as I have mentioned in prior chapters,

$$\rho_{yx} = \rho_{yx}^{NH} + \rho_{yx}^{AH} + \rho_{yx}^{THE}. \tag{4.1}$$

The following is how in this work the THE was isolated. It is the offset resistance under upward and downward $\mu_0 H$ sweeps (green shadow area in Fig. 4.2) as the THE for the following reasons. Consider the positive regime of $\mu_0 H$. During the downward sweep of $\mu_0 H$ (red curves in Fig. 4.2), the system should be in a ferromagnetic state without any chiral spin textures and thus ρ_{yx} should only include the normal and anomalous contributions. For the upward sweep of $\mu_0 H$ (blue curves in Fig. 4.2), the system undergoes a magnetic transition

around $\mu_0 H_c$ and chiral spin textures, particularly chiral magnetic domain walls (Fig. 4.4 a,b), can be formed. In this situation, all three Hall contributions are present and we do expect that the $\rho_{yx}^{NH} + \rho_{yx}^{AH}$ keeps the same value during the downward sweep of $\mu_0 H$. Thus, the THE can be extracted by taking the difference between the red and blue curves[14]. The reason the standard expressions of the normal and anomalous contributions($\rho_{yx}^{NH} = \mu_0 R_N H$ and $\rho_{yx}^{AH} = R_A M$) were not used is because of the following; these are only applicable in metalic systems and thus not valid for our samples close to the QAH insulating regime. When $V_g - V_g^0 = -220$, the maximum of ρ_{yx}^{TH} is $\sim 1.65 k\Omega$, which is much larger than the the THE resistances observed in all previous studies on metallic systems[14].

Once the THE part of ρ_{yx} was separated, is where my work comes in. As my role in this work was to explain the experimental results of (Fig. 4.3b). Specifically, my goal was to understand the features of the plot for the THE and determine for different regions of $(V_g - V_g^0)$ which contributions dominated, whether it would be from the surface state or the bulk of the MTI.

4.2 Calculating Spin Susceptibility

This section will show my calculation that was able to reproduce the experimental figure(Fig 4.3b). To start I want to fully describe all energy states in a MTI, which means I will include both the surface states and quantum well(QW) states. The Hamiltonian that describes the surface states is written as,

$$H_{surf} = \begin{pmatrix} v_F(\mathbf{k} \times \boldsymbol{\sigma}) \cdot \hat{\mathbf{z}} + \mathbf{M}^t \cdot \boldsymbol{\sigma} + U & m_k \\ m_k & -v_F(\mathbf{k} \times \boldsymbol{\sigma}) \cdot \hat{\mathbf{z}} + \mathbf{M}^b \cdot \boldsymbol{\sigma} - U \end{pmatrix} \tag{4.2}$$

where v_F is the velocity of surface state, $\mathbf{M}^t$ and $\mathbf{M}^b$ are the magnetization of top and bottom surface, m_k is the hybridization between the top and bottom surface while U is the asymmetric potential. For the QW state, the starting point is the 3D Topological Insulator

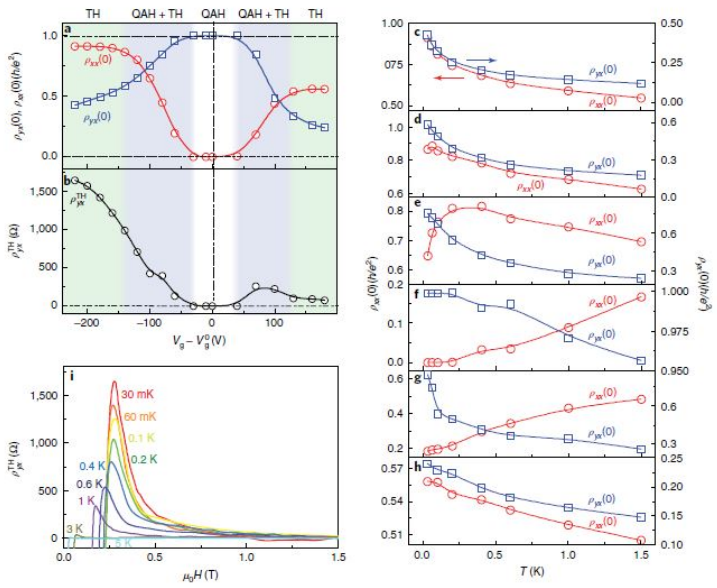

Figure 4.3 Concurrence of the QAH and THE in MTI sandwich heterostructures. a, Gate dependence of the Hall resistance $\rho_{yx}(0)$(empty blue squares) and the longitudinal resistance $\rho_{xx}(0)$ (empty red circles(at zero magetnic field and T=30mK. b, Gate dependence of the THE resistance ρ_{yx}^{THE} at T=30mK.The regions of concurrence of the QAH and THE are shaded light blue. c-h, Temperature dependence of the Hall resistance $\rho_{yx}(0)$ (empty blue squares) and the longitudinal resistance $\rho_{xx}(0)$(empty red circles) for different gates $(V_g - V_g^0)$ of -220V(c),-140V(d),-100V(e),0V(f),+70V(g) and +180V(h). i,μ_0H dependence of ρ_{yx}^{THE} for different T at $V_g = V_g^{THE,max}$. ρ_{yx}^{THE} decreases with increasing temperature. ρ_{yx}^{THE} is 1.65KΩ at T=30mK and disappears at T=5K. The uncertainty of the data shown in a-h is reflected by the size of the symbols. The primary source of the uncertainty is the hysteretic charging effect of the $SrTiO_3$ substrate. [14]

model.

$$H_{3D} = \epsilon_k + N_k\Gamma_5 + Bk_z\Gamma_4 + A(k_y\Gamma_1 - k_x\Gamma_2) \tag{4.3}$$

where, $\epsilon_k = C_0 + C_1k_z^2 + C_2(k_x^2 + k_y^2)$, $N_k = N_0 + N_1k_z^2 + N_2(k_x^2 + k_y^2)$ and $\Gamma_1 = \sigma_x\tau_x, \Gamma_2 = \sigma_y\tau_x, \Gamma_4 = \tau_y, \Gamma_5 = \tau_z$. In this model I assume an infinite potential along the z direction[24]. This confinement effect along the z direction can be approximated by choosing, $\langle k_z^2\rangle = (n\pi/L)^2$ and $\langle k_z\rangle = 0$ with $n = 1, 2, ...$ Thefore, $\epsilon_k = C_0 + C_1(n\pi/L)^2 + C_2(k_x^2 + k_y^2)$,

$N_k = N_0 + N_1(n\pi/L)^2 + N_2(k_x^2 + k_y^2)$ and the Hamiltonian is,

$$H_{QW_0} = \epsilon_k + \begin{pmatrix} N_k & A(k_y\sigma_x - k_x\sigma_y) \\ A(k_y\sigma_x - k_x\sigma_y) & -N_k \end{pmatrix}. \tag{4.4}$$

Along with the unperturbed Hamiltonian, the QW state will also have an asymmetric potential, $H_{QW,\tilde{U}} = \tilde{U}\tau_x$, along with an exchange coupling to magnetization, $H_{QW,M} = \mathbf{M}\cdot\boldsymbol{\sigma}$. So, the full QW Hamiltonian is,

$$H_{QW} = H_{QW,0} + H_{QW,\tilde{U}} + H_{QW,M} \tag{4.5}$$

The Hamiltonians for Surface and QW can be shown to be equivalent. This is done by performing a rotation of H_{surf} with the use of the unitary matrix, T. I do this because I will be taking the sum of the surface and QW Hamiltonians, which I will want to be in the same basis. The unitary matrix is given by,

$$T = \frac{1}{\sqrt{2}}(\sigma_z + \sigma_x) \tag{4.6}$$

applying this to H_{surf} gives,

$$
\begin{aligned}
T^{\dagger}H_{surf}T &= \frac{1}{2}\begin{pmatrix} 1 & 1 \\ 1 & -1 \end{pmatrix}\begin{pmatrix} v_F(\mathbf{k}\times\boldsymbol{\sigma})\cdot\hat{\mathbf{z}} + \mathbf{M}^t\cdot\boldsymbol{\sigma} + U & m_k \\ m_k & -v_F(\mathbf{k}\times\boldsymbol{\sigma})\cdot\hat{\mathbf{z}} + \mathbf{M}^b\cdot\boldsymbol{\sigma} - U \end{pmatrix}\begin{pmatrix} 1 & 1 \\ 1 & -1 \end{pmatrix} \\
&= \frac{1}{2}\begin{pmatrix} 1 & 1 \\ 1 & -1 \end{pmatrix}\begin{pmatrix} v_F(\mathbf{k}\times\boldsymbol{\sigma})\cdot\hat{\mathbf{z}} + \mathbf{M}^t\cdot\boldsymbol{\sigma} + U + m_k & v_F(\mathbf{k}\times\boldsymbol{\sigma})\cdot\hat{\mathbf{z}} + \mathbf{M}^t\cdot\boldsymbol{\sigma} + U - m_k \\ -v_F(\mathbf{k}\times\boldsymbol{\sigma})\cdot\hat{\mathbf{z}} + \mathbf{M}^b\cdot\boldsymbol{\sigma} - U + m_k & m_k + v_F(\mathbf{k}\times\boldsymbol{\sigma})\cdot\hat{\mathbf{z}} - \mathbf{M}^b\cdot\boldsymbol{\sigma} + U \end{pmatrix} \\
&= \frac{1}{2}\begin{pmatrix} 2m_k + (\mathbf{M}^t + \mathbf{M}^b)\cdot\boldsymbol{\sigma} & 2v_F(\mathbf{k}\times\boldsymbol{\sigma})\cdot\hat{\mathbf{z}} + (\mathbf{M}^t - \mathbf{M}^b)\cdot\boldsymbol{\sigma} + 2U \\ 2v_F(\mathbf{k}\times\boldsymbol{\sigma})\cdot\hat{\mathbf{z}} + (\mathbf{M}^t - \mathbf{M}^b)\cdot\boldsymbol{\sigma} + 2U & -2m_k + (\mathbf{M}^t + \mathbf{M}^b)\cdot\boldsymbol{\sigma} \end{pmatrix} \\
&= m_k\sigma_0\tau_z + v_F(k_y\sigma_x - k_x\sigma_y)\tau_x + U\sigma_0\tau_x + \mathbf{M}^+\cdot\boldsymbol{\sigma}\tau_0 + \mathbf{M}^-\cdot\boldsymbol{\sigma}\tau_x
\end{aligned}
\tag{4.7}
$$

where, $\mathbf{M}^+ = \frac{1}{2}(\mathbf{M}^t + \mathbf{M}^b)$ and $\mathbf{M}^- = \frac{1}{2}(\mathbf{M}^t - \mathbf{M}^b)$. Now that both these Hamiltonians are in the same basis I can derive the spin susceptibility by a field theory approach. The outline of this calculation is the following; (1) write down the actions for the unperturbed and perturbed parts of the Hamiltonian,(2) use the partition function to write a new effective action, and (3) identify the spin susceptibility tensor from the effective action. Since the Hamiltonians are in the same basis, at least the unperturbed parts are. I will show the calculation for H_{surf} then I will be able to write down the spin susceptibility tensor for H_{QW}.

4.2.1 Actions

Let us take a look at the Hamiltonian for the surface states in the rotated frame.

$$
H_{surf} = m_k\sigma_0\tau_z + v_F(k_y\sigma_x - k_x\sigma_y)\tau_x + U\sigma_0\tau_x + \mathbf{M}^+\cdot\boldsymbol{\sigma}\tau_0 + \mathbf{M}^-\cdot\boldsymbol{\sigma}\tau_x \tag{4.8}
$$

It is easy to identify the unperturbed part as,

$$H^0_{surf} = m_k\sigma_0\tau_z + v_F(k_y\sigma_x - k_x\sigma_y)\tau_x + U\sigma_0\tau_x \tag{4.9}$$

and the perturbation is,

$$H^I_{surf} = \mathbf{M}^+ \cdot \boldsymbol{\sigma}\tau_0 + \mathbf{M}^- \cdot \boldsymbol{\sigma}\tau_x \tag{4.10}$$

so the actions for each are,

$$S_0 = \beta \int d\mathbf{k}d\omega\bar{\psi}(-\mathbf{k},-\omega) \begin{pmatrix} -i\omega + m_k & v_F(\mathbf{k}\times\boldsymbol{\sigma})\cdot\hat{\mathbf{z}} + U \\ v_F(\mathbf{k}\times\boldsymbol{\sigma})\cdot\hat{\mathbf{z}} + U & -i\omega - m_k \end{pmatrix} \psi(\mathbf{k},\omega) \tag{4.11}$$

$$S_1 = \beta \int d\mathbf{k}d\omega\bar{\psi}(-\mathbf{k}),-\omega)(\mathbf{M}^+ \cdot \boldsymbol{\sigma}\tau_0 + \mathbf{M}^- \cdot \boldsymbol{\sigma}\tau_x)\psi(\mathbf{k},\omega) \tag{4.12}$$

4.2.2 Partition Function

With these actions the partition function is,

$$\mathcal{Z} = \int \mathcal{D}\bar{\psi}\mathcal{D}\psi e^{-(S_0+S_1)} \tag{4.13}$$

I can expand the perturbed Hamiltonian part,

$$\begin{aligned} \mathcal{Z} &= \int \mathcal{D}\bar{\psi}\mathcal{D}\psi e^{-S_0}e^{-S_1} \\ &\int \mathcal{D}\bar{\psi}\mathcal{D}\psi e^{-S_0}(1 - S_1 + \frac{1}{2}S_1^2) \\ &\mathcal{Z}_0(1 - \langle S_1\rangle + \frac{1}{2}\langle S_1^2\rangle) \\ &= e^{-\beta S_{eff}} \end{aligned} \tag{4.14}$$

therefore, the effective action is,

$$S_{eff} = -\frac{1}{\beta} ln \left[\langle -S_1 \rangle + \frac{1}{2} \langle S_1^2 \rangle - \frac{1}{2} \langle S_1 \rangle^2 \right]. \tag{4.15}$$

Since S_1 will be linear in momentum, the average will vanish. This leads only S_1^2 to be non-zero,

$$\frac{1}{2} S_1^2 = \frac{1}{2} \beta^2 \int d\omega_1 d\omega_2 d\mathbf{q}_1 d\mathbf{q}_2 d\mathbf{k}_1 d\mathbf{k}_2 \bar{\psi}(-\mathbf{k}_1 - \mathbf{q}_1, -\omega_1)(\mathbf{M}^+(\mathbf{q}_1) \cdot \boldsymbol{\sigma}\tau_0 + \mathbf{M}^-(\mathbf{q}_1) \cdot \boldsymbol{\sigma}\tau_x)$$
$$\psi(-\mathbf{k}_1, -\omega_1)\bar{\psi}(-\mathbf{k}_2 - \mathbf{q}_2, -\omega_2)(\mathbf{M}^+(\mathbf{q}_2) \cdot \boldsymbol{\sigma}\tau_0 + \mathbf{M}^-(\mathbf{q}_2) \cdot \boldsymbol{\sigma}\tau_x)\psi(-\mathbf{k}_2, -\omega_2) \tag{4.16}$$

I define the following, $\omega_1 = \omega_2$, $k_2 + q_2 = k_1$, and $k_2 = k_1 + q_1$ the latter two show, $q_2 = k_1 - k_2 = -q_1$. Now, with these definitions I use a Wick rotation when taking the average of S_1^2. In performing the wick rotation, I group up $\bar{\psi}$'s and ψ's, this combined with the definitons of the momenta, I find,

$$\frac{1}{2} \langle S_1^2 \rangle = \frac{1}{2} \beta^2 \int d\mathbf{q} d\mathrm{k} d\omega Tr \left[G_0(\mathbf{k} + \mathbf{q}, \omega)(\mathbf{M}^+(\mathbf{q}) \cdot \boldsymbol{\sigma}\tau_0 + \mathbf{M}^-(\mathbf{q}) \cdot \boldsymbol{\sigma}\tau_x) \right.$$
$$\left. G_0(\mathbf{k}, \omega)(\mathbf{M}^+(-\mathbf{q}) \cdot \boldsymbol{\sigma}\tau_0 + \mathbf{M}^-(-\mathbf{q}) \cdot \boldsymbol{\sigma}\tau_x) \right] \tag{4.17}$$

where I have used $G_0 \equiv \langle \bar{\psi}\psi \rangle$ and $G_0 = \left[\beta H^0_{surf} \right]^{-1}$. This yields an effective action of,

$$S_{eff} = \int d\mathbf{q} \frac{T}{2V} \sum_{\mathbf{k}, i\omega_n} Tr[G_0(\mathbf{q}+\mathbf{k}, i\omega_m + i\omega_n)(\mathbf{M}^+(\mathbf{q}) \cdot \boldsymbol{\sigma}\tau_0 + \mathbf{M}^-(\mathbf{q}) \cdot \boldsymbol{\sigma}\tau_x) G_0(\mathbf{k}, i\omega_n)(\mathbf{M}^+(\mathbf{q}) \cdot \boldsymbol{\sigma}\tau_0 + \mathbf{M}^-(\mathbf{q}) \cdot \boldsymbol{\sigma}\tau_x)$$
(4.18)

where I have switched the k and ω integrals to sums and defined the mastubara frequencies $\omega_n = 2n\pi T$ for bosons and $(2n+1)\pi T$ for fermions. With this effective action I can write down an effective Hamiltonian, which will reveal the spin susceptibility tensor.

4.3 Susceptibility Tensor

With this new action the effective surface state Hamiltonian is,

$$H_{surf}^{eff} = \chi_{\alpha\beta}^{M^+M^+} M_\alpha^+ M_\beta^+ + \chi_{\alpha\beta}^{M^+M^-} M_\alpha^+ M_\beta^- + \chi_{\alpha\beta}^{M^-M^+} M_\alpha^- M_\beta^+ + \chi_{\alpha\beta}^{M^-M^-} M_\alpha^- M_\beta^- \tag{4.19}$$

as I said, the Quantum Well Hamiltonian follows the same procedure except its S_1 has just $\mathbf{M} \cdot \boldsymbol{\sigma}$ as the perturbation. This gives,

$$H_{QW}^{eff} = \chi_{\alpha\beta} M_\alpha M_\beta \tag{4.20}$$

for the current work I only need to calculate, $\chi_{\alpha\beta}^{M^+M^+}$ which has the 4x4 matrix τ_0, thus we are only considering this intraband orbital contribution. To relate the DM interaction to spin susceptibility, we examine the general DM term,

$$H_{DM} = \mathbf{D}_{12} \cdot (\mathbf{S}_1 \times \mathbf{S}_2) = \epsilon_{\gamma\alpha\beta} D_{12,\gamma} S_{1\alpha} S_{2\beta} \tag{4.21}$$

my argument here will be that the DM interaction is related to the susceptibility and resistivity by,

$$\epsilon_{\gamma\alpha\beta} D_{12,\gamma} \sim \chi_{\alpha\beta} \sim \rho_{xy} \tag{4.22}$$

due to the cross product nature this means that the off-diagonal terms of susceptibility correspond to the DM interaction while diagonal terms correspond to Heisenberg exchange, J. The susceptibility tensors are,

$$\chi_{\alpha\beta}^{M^+M^+}(\mathbf{q}, i\omega_m) = \frac{T}{2V} \sum_{\mathbf{k}, i\omega_n} tr[G_0(\mathbf{q}+\mathbf{k}, i\omega_m + i\omega_n)\sigma_\alpha \tau_0 G_0(\mathbf{k}, i\omega_n)\sigma_\beta \tau_0] \tag{4.23}$$

where,

$$G_0(\mathbf{k}, i\omega_n) = \sum_{s,t=\pm} \frac{P_{st\mathbf{k}}}{i\omega_n + \mu - E_{st\mathbf{k}}} \tag{4.24}$$

the projection operator for Surface and QW states are,

$$P^{surf}_{st\mathbf{k}} = \frac{1}{4}(1 + \frac{s}{D_{t\mathbf{k}}}(m_k\sigma_0\tau_z + v_F(k_y\sigma_x - k_x\sigma_y)\tau_x + U\sigma_0\tau_x))(1 + t(\hat{k}_y\sigma_x - \hat{k}_x\sigma_y)) \quad (4.25)$$

$$P^{QW}_{st\mathbf{k}} = \frac{1}{4}(1 + \frac{s}{D_{t\mathbf{k}}}(N_k\sigma_0\tau_z + A(k_y\sigma_x - k_x\sigma_y)\tau_x + \tilde{U}\sigma_0\tau_x))(1 + t(\hat{k}_y\sigma_x - \hat{k}_x\sigma_y)) \quad (4.26)$$

and I have defined $\hat{k}_\nu = \frac{k_\nu}{k}$, $\nu = x, y$, $E_{st\mathbf{k}} = s\sqrt{m_k^2 + (v_F k + tU)^2}$, and $E_{+t\mathbf{k}} = D_{t\mathbf{k}}$. The derivation of the projection operators can be found in appendix C. Thus, the susceptibility becomes,

$$\chi^{M^\pm M^\pm}_{\alpha\beta}(\mathbf{q}, i\omega_m) = \frac{T}{2V}\sum_{\mathbf{k},i\omega_n}\sum_{l,r,s,t}\left(\frac{1}{i\omega_n + i\omega_m + \mu - E_{lr\mathbf{k}+\mathbf{q}}}\frac{1}{i\omega_n + \mu - E_{st\mathbf{k}}}\right) tr[P_{lr\mathbf{k}+\mathbf{q}}\sigma_\alpha\tau_{0/x}P_{st\mathbf{k}}\sigma_\beta\tau_{0/x}] \quad (4.27)$$

to solve the frequency summation I can use the residue theorem. I will define $h(\omega_n)$ to be,

$$h(\omega_n) = T\left(\frac{1}{i\omega_n + i\omega_m + \mu - E_{lr\mathbf{k}+\mathbf{q}}}\frac{1}{i\omega_n + \mu - E_{st\mathbf{k}}}\right) \quad (4.28)$$

to do this sum I choose the function $g(z) = \frac{\beta}{e^{\beta z}+1}$ where $\beta = \frac{1}{T}$ and I find the residues of $g(z)h(-iz)$. So I can write the sum as,

$$\sum_n h(\omega_n) = Res(g(z)h(-iz)) = \frac{n_F(E_{st\mathbf{k}} - \mu) - n_F(E_{lr\mathbf{k}+\mathbf{q}} - \mu)}{i\omega_m + E_{st\mathbf{k}} - E_{lr\mathbf{k}+\mathbf{q}}} \quad (4.29)$$

Transforming the sum over $\mathbf{k}$ to an integral yields,

$$\chi^{M^\pm M^\pm}_{\alpha\beta}(\mathbf{q}, i\omega_m) = \frac{1}{2(2\pi)^2}\int dk_x dk_y \sum_{l,r,s,t}\left(\frac{n_F(E_{st\mathbf{k}} - \mu) - n_F(E_{lr\mathbf{k}+\mathbf{q}} - \mu)}{i\omega_m + E_{st\mathbf{k}} - E_{lr\mathbf{k}+\mathbf{q}}}\right) tr[P_{lr\mathbf{k}+\mathbf{q}}\sigma_\alpha\tau_{0/x}P_{st\mathbf{k}}\sigma_\beta\tau_{0/x}] \quad (4.30)$$

As the system breaks mirror symmetry with respect to the x-y plane, $\chi_{xy} = 0$, and we thus focus on the off-diagonal components χ_{xz} and χ_{yz}. As expected from the Moriya

rule[14], $\chi_{xz}(\chi_{yz})$ is linearly proportional to $q_x(q_y)$(Fig. 4.4). By choosing a non-zero q_x value, I calculated χ_{xz} as a function of energy for the QW and surface states with different asymmetric potential U(Fig. 4.3d,e) and found a non-zero U is, indeed, required to break the inversion symmetry and induce a finite χ_{xz}. I will mention that in real samples, in addition to the chemical potential (μ), U also depends on V_g but, its dependence on V_g is much weaker in the experiment performed[14]. The surface states contribution to χ_{xz} shows a double peak structure around the charge neutral point. For the bulk QW states, χ_{xz} reveals a peak when μ lies between two spin-split(valence) bands and then drops and even changes its sign when μ crosses both spin bands. The bulk conduction band is well above the energy range of interest(-30-40meV) and thus does not contribute.

Figure 4.3f shows the total χ_{xz}, which behaves similarly to the ρ_{yx}^{THE} in the experiment. The large asymmetry between the electron- and hole-doping sides arises because the surface states are close to the valence band, but well below the conduction band. At $V_g < V_g^0$, a large contribution to χ_{xz} from the bulk valence-band top significantly enhances the DM interaction and ρ_{yx}^{THE} in consequence. It should be true that including more bulk QW states in the models can further enhance the DM interaction in the hole-doping regime. However, the surface state contribution prevails in the $V_g > V_g^0$ regime. When μ is well above the charge neutral point, χ_{xz} vanishes, which is consistent with ρ_{yx}^{THE} in the electron doping regime. The parameters used here are, $m_0 = .01, m_2 = 0, v_F = 3, U = .02, C_0 = .16, C_2 = 0, N_0 = -.18, N_2 = 0, \tilde{U} = .02, A = 3$.

4.4 Conclusion

So what was I able to show in this chapter? Well, the experiment realized the Topological Hall Effect in a Magnetic Topological Insulator where we do not expect any Skyrmions to be present due to its structure. However, there should be some chiral domain walls that arise upon the magnetic field sweep that induces a Dzyaloshinskii-Moriya interaction where

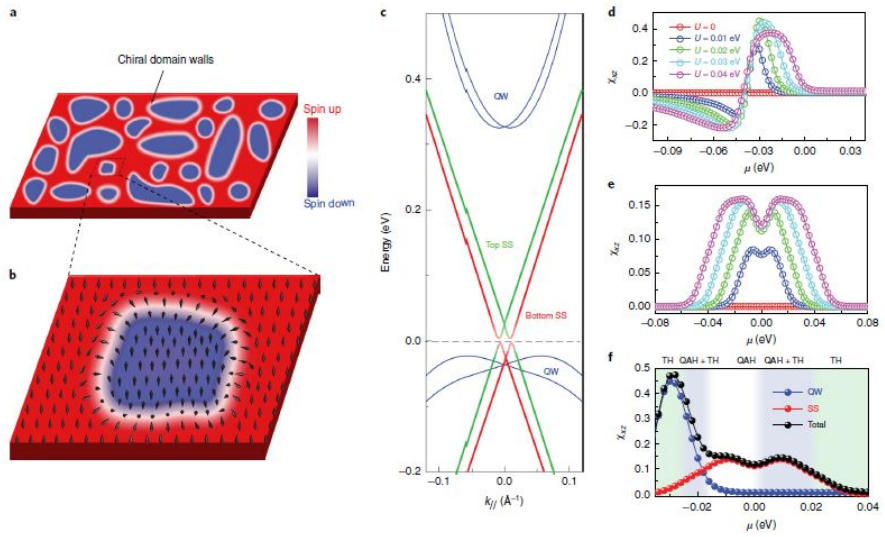

Figure 4.4 Chiral domain walls and theoretical interpretations of the appearance of the TH effect. a, The formation of the chiral domain walls during magnetization reversals. b, A magnified view that depicts the spin distribution of the chiral domain wall. c, The energy dispersions of the SSs and bulk QW bands in magnetic TI. d,e, χ_{xz} as a function of chemical potential for the QW (d) and SS (e) under different asymmetric potentials U. f, The QW contribution to χ_{xz}, Surface State contribution to χ_{xz} and the total χ_{xz} in the magnetic TI sandwich heterostructures when U = 0.02 eV, $q_x = 0.005\mathring{A}$ and q_y =0 in d–f.[14]

a Topological Hall Effect arises. I was able to use a field theory approach to calculate the spin susceptibility tensor, which, physically describes the likelihood of an electrons' spin to align with the magnetization. I argued that this tensor was related to the Dzyaloshinskii-Moriya interaction. It was also found that it showed a strikingly similar appearance to ρ_{yx}^{THE}, the off-diagonal resistivity. I was able to show that the resistivity has contributions from the Surface States as well as the Bulk Quantum Well States. This work is one of two of my works that strive to diverge from conventional meaning of Topological Hall Effect implies Skyrmions. My hope is that these works can be the starting point of a change in thought process of the community. For now, I will continue into the next chapter with another discussion related to the Hall Effect. However, it will not be about the THE nor about Skyrmions. I will discuss second order Hall effects. As I do recognize that this chapter does not align with the rest of my work, I will make this following argument. This next chapter does fall in line with

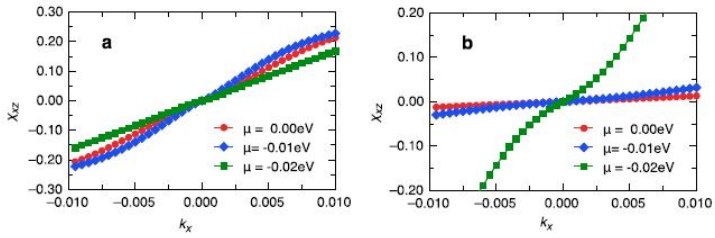

Figure 4.5 Linearity between off-diagonal susceptibility and momentum. The susceptibility χ_{xz} function of momentum k_x at different chemical potentials for (a) topological surface states and (b) bulk QW states. Linear relations are almost respected at small momenta.[14]

the other chapters in the sense that it still discusses transport phenomena and does focus on a Hall effect. Also, I hope this can stand as a future project for another student that finds interest in non-linear Hall effects, which has many applications, one notably being solar panels[14].

Chapter Five

Shift Current

Here I will discuss some of my research into the topic of another type of Hall effect known as the Shift Current. The two main calculations of this chapter will be about how non-linear Hall effects arise from a density matrix formalism and I will show that inversion symmetry breaking alone cannot produce a shift current. This chapter is outlined in the following: Section (1) I will introduce the notion of shift current along with why I was interested in this topic. Specifically, the interest with solar panel efficiency[cite]. In section (2) I will work out the third rank conductivity tensor from a density matrix formalism. This tensor is what produces a shift current. Finally, in section (3) I will show how using a simple Hamiltonian that only involves inversion breaking does not yield a shift current.

5.1 Introduction to Shift Current

Previous studies have shown that the Hall effect generally has three conditions, a non-vanishing Hall conductivity that arises from the momentum-integrate Berry curvature, a Hall voltage that is linearly proportional to the external electric field, and a Hall conductivity that is a fraction of the longitudinal conductivity. The non-vanishing Hall conductivity requires time reversal symmetry breaking and is realized in magnets or by application of a magnetic field[5].

Theoretically, Hall effects beyond these three factors are possible and the shift current is one example. This current highlights a second-order non-linear Hall effect. In particular, even in a non-magnetic material, inversion symmetry breaking may segregate the positive and negative Berry curvatures in different momentum regions leading to a Berry curvature dipole moment, $\Lambda \sim \int_{\mathbf{k}} f_0 \partial\Omega$, where f_0 is the Fermi-Dirac distribution. Such a dipole should give rise to a Hall effect.

The end goal I had in mind for the shift current was because of its rise in the area of solar energy. Specifically, the fact that materials that hosted this shift current were actually found to have high efficiency as a solar panel[26]. However, some fundamental ideas were troubling to me about the shift current. For example most works attribute to just inversion breaking in the material. I will show for just a simple inversion breaking Hamiltonian that I do not obtain a non-zero shift current. First, let me discuss a little about the interest in solar cells.

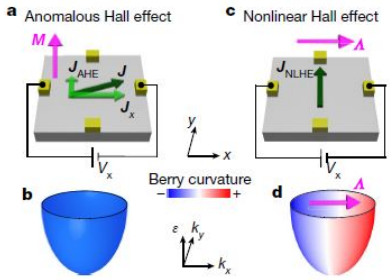

Figure 5.1 (a), Anomalous Hall effect in a magnetic metal. M is the magnetization, J_{AHE} is the anomalous Hall current, J_x and V_x are the current and voltage, respectively, along the x direction. (b), Band structure and Berry curvature of a simple magnetic metal. The anomalous Hall conductivity arises from the momentum-integrated Berry curvature, which requires the breaking of time-reversal symmetry. (c), Demonstration of the nonlinear Hall effect. Because of the in-plane Berrycurvature dipole Λ, leads to a nonlinear Hall current (J_{NLHE}). (d), Band structure and Berry curvature for a wide class of non-magnetic, inversion-symmetry-breaking quantum materials with non-zero Λ. Λ originates from the separation of positive and negative Berry curvature in momentum space, which does not necessarily break TRS.[5]

5.1.1 Shockley Queisser Limit

Solar energy is anticipated to be the most viable source of sustainable green energy[26]. A large challenge facing solar cells is the Shockley Queisser limit, which refers to the theoretical maximum efficiency of a solar cell using a single cell p-n junction to collect power from the cell. A promising new solar cell that seems to be able to overcome this limit is the Perovskite material. Now, the maximum efficiency of a solar cell is dependent on the band gap energy of the material.

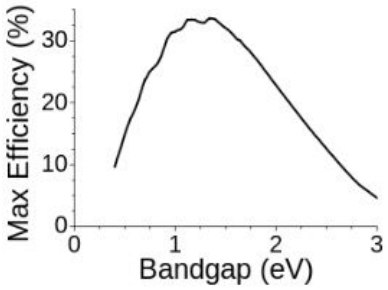

Figure 5.2 Shockley Queisser limit showing the Max efficiency of a solar cell and its dependence on the band gap energy of the material[27]

What was found in a single layer perovskite material was that it had the highest efficiency for a band gap of 3.2eV[26]. It was found to be 4.8 percent[26].

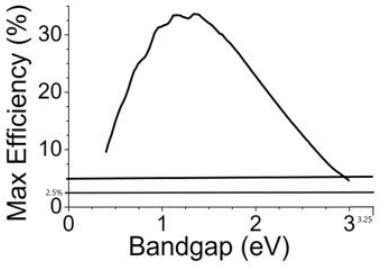

Figure 5.3 Shockley Queisser Limit showing the Perovskite material efficiency for band gap of 3.2eV. The line at 2.5percent is the normal value.[27]

However, this material having a band gap energy of 3.2eV has a low efficiency compared to the most popular solar cells used today. The goal would then be to set out to find materials that have smaller band gaps, around where the limit usually peeks. I would then expect to see the efficiency be much higher than even the most popular solar cells.

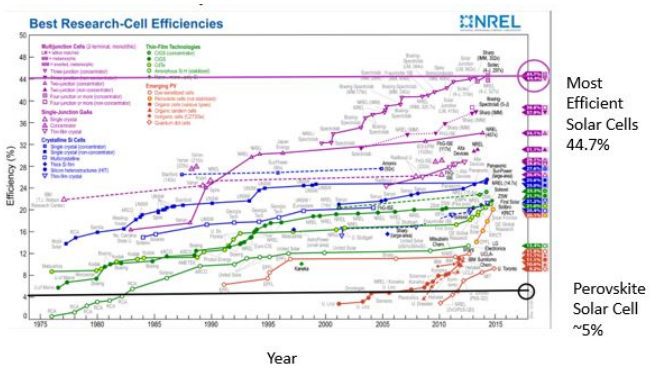

Figure 5.4 Efficiency of Solar Cells since 1975. [28]

So, although there was some promise into this Perovskite material, I do not think much progress will be made until a material with a lower band gap that also hosts the shift current can be found. Let me now move into the theory of the shift current. In the next section I will show how to derive it using a density matrix formalism.

5.2 Density Matrix and Perturbation

I will consider a system of free electrons where at $t = 0$ an electric field is turned on. To begin, note that in thermal equilibrium, the density operator $\rho(t)$ of a system with Hamiltonian H_0 and electron number N is given by,

$$\rho_0 = Z^{-1} \exp\left[-\beta(H_0 - \mu N)\right] = \frac{1}{1 + \exp\left[-\beta(H_0 - \mu N)\right]} \tag{5.1}$$

Once the electric field is turned on, the density operator evolves in time according to,

$$i\hbar\dot{\rho} = [H, \rho(t)] - i\hbar\frac{(\rho(t) - \rho_0)}{\tau} \tag{5.2}$$

where $H = H_0 + V(t)$ is full Hamiltonian of the system and $V(t)$ describes the interaction between the electrons and the electric field. Allowing the scalar potential to be zero, the interaction is written as,

$$V(t) = \mathbf{J} \cdot \mathbf{A}(t) + \frac{e^2}{2m_0 V}\mathbf{A}^2 \tag{5.3}$$

with,

the vector potential, $\mathbf{A}(t)$ and current, $\mathbf{J}$ defined as,

$$\mathbf{A}(t) = \frac{\mathbf{E}}{\omega}\cos(\omega t) \tag{5.4}$$

$$\mathbf{J} = -\frac{e}{m_0 V}\sum_{i=1}^{N}\mathbf{p}_i \tag{5.5}$$

here V denotes the volume of the crystal and m_0 is the mass of the electron. The interaction $V(t)$ comes from the velocity gauge, starting with $H_0 = \frac{1}{2m_0 V}\mathbf{p}^2$ and once the electric field is turned on the momentum becomes, $\mathbf{p} - e\mathbf{A}$. Plugging this new momentum into the Hamiltonian and expanding results in the interaction above. Next, I want to calculate the current density which is induced by the electric field. This performed with the help of the density matrix,

$$j(t) = Tr[\rho(t)\mathbf{J}_A] \tag{5.6}$$

with,

$$\mathbf{J}_A = \mathbf{J} - \frac{e}{m_0}\mathbf{A} \tag{5.7}$$

$\mathbf{J}_A$ is used because I am looking at $t > 0$ when the electric field has been turned on. $\mathbf{J}_A$ is the current density satisfying the commutation relation,

$$\begin{aligned}
\frac{1}{i\hbar}[r,H] &= \frac{1}{i\hbar}[r,\frac{1}{2m_0V}(p-eA)^2] \\
&= \frac{1}{i\hbar}[r,\frac{1}{2m_0V}(p^2-2eAp+e^2A^2)] \\
&= \frac{1}{2m_0Vi\hbar}\left([r,p^2]-2e[r,Ap]+e^2[r,A^2]\right) \\
&= \frac{1}{m_0V}p-\frac{e}{m_0V}A \\
&= J_A
\end{aligned} \tag{5.8}$$

where I have used that the position operator commutes with the magnetic vector potential. With J_A I now need to solve the Heisenberg equation of motion for the density matrix. This is done by transforming it to an integral equation then to solve by iteration[cite],

$$\rho(t) = -\frac{i}{\hbar}\int_0^t ds\left([H_0,\rho(s)]+[V(s),\rho(s)]\right)-\frac{1}{\tau}\int_0^t(\rho(s)-\rho_0 \tag{5.9}$$

and I expand using the ansatz[cite],

$$\rho(t) = \rho_0+\rho_1(t)+\rho_2(t)+\ldots \tag{5.10}$$

$$\rho_{n+1}(t) = -\frac{i}{\hbar}\int_0^t ds\exp[-s/\tau]U^\dagger(s)[V(s),\rho_n(t)]U(s) \tag{5.11}$$

with $U(s) = \exp[-isH_0/\hbar]$. Now, I want to calculate the current to second order in electric field, more specifically I want to find the current of the form $j \sim \sigma_{\nu\alpha\mu}E^\alpha E^\mu$. This form can only be found for the term $Tr[\rho_2(t)\mathbf{J}$. I will note that there is another term that is proportional to E^2 but the conductivity is not a third rank tensor and thus will not yield a shift current. This term is $Tr[\rho_1(t)A^\nu]$, $\rho_1(t)$ is,

$$\rho_1(t) = -\frac{i}{\hbar}\int_0^t \exp[-s/\tau]U^\dagger(s)[V(s),\rho_0]U(s) \tag{5.12}$$

the term that will give an E^2 contribution will only come from the first term of the potential. Therefore, this term is,

$$\begin{aligned} Tr[\rho_1(t)A^\nu] &\sim Tr[[J_\mu(s)A^\mu, \rho_0]]A^\nu \\ &\sim Tr[[J_\mu(s), \rho_0]]E^\mu E^\nu \\ &\sim \sigma_\mu E^\mu E^\nu \end{aligned} \tag{5.13}$$

where, $J_\mu(s) = U^\dagger(s)J_\mu U(s)$, thus this term will not contribute to the shift current. What will be calculated is $Tr[\rho_2(t)\mathbf{J}]$ using only the first term from the potential. With this information the calculation is as follows,

$$\begin{aligned} Tr[\rho_2(t)\mathbf{J}] &= Tr[-(i/\hbar)\int_0^t \exp[-s/\tau]U^\dagger(s)[\mathbf{J}\cdot\mathbf{A}, \rho_1(t)]U(s)\mathbf{J}] \\ &= -\left(\frac{i}{\hbar\omega}\right)^2 \int_0^t\int_0^t dsds' \exp\left[-\frac{s+s'}{\tau}\right] Tr[U^\dagger(s)[J_\mu, U^\dagger(s')[J_\mu, \rho_0]U(s')J_\nu]] \\ &\cos(\omega s)\cos(\omega s')E^\mu E^\nu \\ &= E^\mu E^\nu \int_0^t\int_0^t dsds'\sigma_{\mu\mu\nu}(\omega, s, s')\cos(\omega s)\cos(\omega s') \end{aligned} \tag{5.14}$$

the conductivity is,

$$\sigma_{\mu\mu\nu}(\omega,s,s') = -\left(\frac{i}{\hbar\omega}\right)^2 \exp\left[-\frac{s+s'}{\tau}\right] Tr[U^\dagger(s)[J_\mu, U^\dagger(s')[J_\mu,\rho_0]U(s')J_\nu]]$$

$$= f(\omega,s,s',\tau)Tr[U^\dagger(s)[J_\mu, U^\dagger(s')(J_\mu\rho_0 - \rho_0 J_\mu)U(s')J_\nu]]$$

$$= f(\omega,s,s',\tau)Tr[U^\dagger(s)J_\mu U^\dagger(s')(J_\mu\rho_0 - \rho_0 J_\mu)U(s') - U^\dagger(s')(J_\mu\rho_0 - \rho_0 J_\mu)U(s')J_\mu U(s)J_\nu]]$$

$$= f(\omega,s,s',\tau)Tr[U^\dagger(s)J_\mu U^\dagger(s')J_\mu\rho_0 U(s')U(s)J_\nu] - Tr[U^\dagger(s)J_\mu U^\dagger(s')\rho_0 J_\mu U(s')U(s)J_\nu] -$$

$$Tr[U^\dagger(s)U^\dagger(s')J_\mu\rho_0 U(s')J_\mu U(s)J_\nu] + Tr[U^\dagger(s)U^\dagger(s')\rho_0 J_\mu U(s')J_\mu U(s)J_\nu]$$

$$= f(\omega,s,s',\tau)Tr[\rho_0 J_\nu(s+s')J_\mu(s')J_\mu] - Tr[\rho_0 J_\mu J_\nu(s+s')J_\mu(s')] - Tr[\rho_0 J_\mu(s')J_\nu(s+s')J_\mu]$$

$$+ Tr[\rho_0 J_\mu J_\mu(s')J_\nu(s+s')]$$

$$= f(\omega,s,s',\tau)Tr[\rho_0[J_\mu,[J_\mu(s'),J_\nu(s+s')]]] \quad (5.15)$$

where I have defined $f(\omega,s,s',\tau) = -\left(\frac{i}{\hbar\omega}\right)^2 \exp\left[-\frac{s+s'}{\tau}\right]$. Equation (5.15) is the first result I was able to reproduce from [29]. In its derivation I used the fact that the trace is invariant under cyclic permutation, then I inserted $UU^\dagger$ so that I could write the time dependent current densities, $J_\mu(s')$ and $J_\nu(s+s')$. To simplify this expression, use a single particle approximation, $H_0 = \sum_n E_n C_n^\dagger C_n$ where $C_n^\dagger$, C_n are the creation and annihilation fermion operators. The current density can be written in terms of states of the single particle Hamiltonian, H_0 as,

$$\mathbf{J} = -\frac{e}{m_0 V}\sum_{n,n'} \langle n'|\mathbf{p}|n\rangle C_{n'}^\dagger C_n \quad (5.16)$$

with this I can write the conductivity in terms of momentum and states of the single particle Hamiltonian. To do this, observe the first term in line (4) of (5.15),

$$
\begin{aligned}
Tr[\rho_0 J_\nu(s+s')J_\mu(s')J_\mu] &= \sum_\alpha \left\langle \alpha \left| \rho_0 U^\dagger(s+s') J_(s+s') U^\dagger(s') J_(s') J_\mu \right| \alpha \right\rangle \\
&= -\left(\frac{e}{m_0 V}\right)^3 \sum_\alpha f_\alpha \left\langle \alpha \left| U^\dagger(s+s') C^\dagger_{n'} C_n U(s+s') U^\dagger(s') C^\dagger_{l'} C_l U(s') C^\dagger_{m'} C_m \right| \alpha \right\rangle \times \\
&\qquad \langle n' \left| p_\nu \right| n \rangle \langle l' \left| p_\mu \right| l \rangle \langle m' \left| p_\mu \right| m \rangle \\
&= -\left(\frac{e}{m_0 V}\right)^3 \sum_{\alpha,\beta,\gamma} \sum_{n,n',l,l',m,m'} f_\alpha \exp[iE_\alpha(s+s')/\hbar] \exp[-iE_\beta(s+s')/\hbar] \exp[iE_\beta s'/\hbar] \times \\
&\qquad \exp[-iE_\gamma s'/\hbar] \delta_{n'\alpha}\delta_{n\beta}\delta_{l'\beta}\delta_{l\gamma}\delta_{m'\gamma}\delta_{m\alpha} \langle n' \left| p_\nu \right| n \rangle \langle l' \left| p_\mu \right| l \rangle \langle m' \left| p_\mu \right| m \rangle \\
&= -\left(\frac{e}{m_0 V}\right)^3 \sum_{n,m,l} f_m \exp[-i(E_n - E_m)s/\hbar] \exp[-i(E_l - E_m)s'/\hbar] \langle n' \left| p_\nu \right| n \rangle \langle l' \left| p_\mu \right| l \rangle \langle m' \left| p_\mu \right| m \rangle
\end{aligned}
\tag{5.17}
$$

the other three terms are found similarly, the conductivity can then be written as,

$$
\sigma_{\mu\mu\nu}(s,s',\omega) = -\left(\frac{i}{\hbar\omega}\right)^2 \left(\frac{e}{m_0 V}\right)^3 \exp[-\frac{s+s'}{\tau} \sum_{n,m,l} (f_n - f_l) \exp[-i(E_n - E_m)s'/\hbar] \langle m \left| p_\mu \right| l \rangle \times
$$

$$
\exp[-i(E_l - E_m)s/\hbar] \langle m \left| p_\nu \right| n \rangle \langle n \left| p_\mu \right| l \rangle - \exp[-i(E_n - E_l)s/\hbar] \langle m \left| p_\mu \right| n \rangle \langle n \left| p_\nu \right| l \rangle \tag{5.18}
$$

to obtain the shift current, first examine the second order response,

$$
j_\nu(t) = \sum_{\mu,\lambda} \int_{-\infty}^{t} dt' \int_{-\infty}^{t} {}' dt'' \sigma^{(2)}_{\lambda\mu\nu}(t-t';t'-t'') E_\lambda(t') E_\mu(t'') \tag{5.19}
$$

to simplify this take a monochromatic plane wave that is linearly polarized ($E_\mu = E_\lambda$) parallel to one fo the coordinate axes and define new parameters, $s = t - t'$ and $s' = t' - t''$,

$$
j_\nu(\omega) = E_\mu^2 \int_0^\infty ds \int_0^\infty ds' \sigma^{(2)}_{\mu\mu\nu}(s,s',\omega) \cos(\omega s). \tag{5.20}
$$

Therefore, plugging the conductivity into (5.20) gives,

$$j_\nu(\omega) \sim E_\mu^2 \sum_{n,m,l} \sum_{\Omega=\pm\omega} (f_n - f_l) \frac{\langle m|p_\mu|l\rangle}{E_n - E_m + \hbar\Omega - i\frac{\hbar}{\tau}} \left(\frac{\langle m|p_\nu|n\rangle \langle n|p_\mu|l\rangle}{E_l - E_m - i\frac{\hbar}{\tau}} - \frac{\langle m|p_\mu|n\rangle \langle n|p_\nu|l\rangle}{E_n - E_l - i\frac{\hbar}{\tau}} \right) \tag{5.21}$$

which is the second result I was able to reproduce from[29]. This reveals that the shift current is a three particle interaction and can be represented in a Feynman diagram.

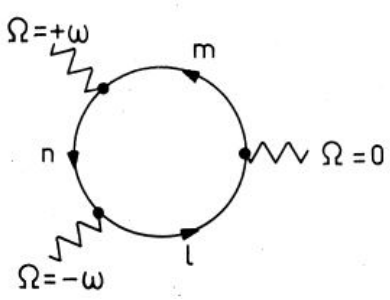

Figure 5.5 Feynman Diagram for the Shift current[29]

Next, I will go into my application of the shift current theory. In the following section I will use a simple Hamiltonian that involves only inversion symmetry breaking. Then I can show how I can calculate the shift current and how it produces the null result. Signifying that other symmetries should be considered when searching for materials that host this non-linear effect.

5.3 Inversion Symmetry Breaking Hamiltonian to Produce a Null Shift Current

In this section I will discuss my calculation of the third rank conductivity tensor σ_{abb} where I use a Hamiltonian with inversion symmetry broken. It is a simple two dimensional(2-D) Hamiltonian that is the sum of the free electron part $k^2/2m$, the Rashba spin orbit term, $(k \times \sigma)$, which breaks the inversion symmetry, and a Zeeman coupling term. I include these

terms for the following reasons; (1) I wanted to write down the simplest Hamiltonian that breaks inversion symmetry to see if this symmetry alone can produce finite shift current, (2) the Zeeman coupling term was necessary to produce a non-zero Berry curvature, and (3) if this produces a zero shift current can I find the simplest Hamiltonian that does produce a non-zero shift current? Related to figure (5.1) I will show that there is indeed no separation in the Berry curvature, which yields the null result. I will give a brief discussion as to what other symmetries should be broken along with how one can break these other symmetries in experiment. Let me begin the set up of the problem.

5.3.1 Shift Current for Minimal Inversion Breaking Hamiltonian

The starting point for this calculation follows from [30]. The shift current is a second-order optical effect with the induced direct current proportional to the square of the optical field, i.e., $J^a = \sigma^{abc}(\omega)E_b(\omega)E_c(-\omega)$[30]. For linearly polarized light, the shift current tensor is given by

$$\sigma^{abb}(\omega) = \frac{2\pi e^3}{\hbar}\int \frac{d^D k}{(2\pi)^D}\sum_{\alpha\beta} f_{\alpha\beta}|r^b_{\alpha\beta}|^2 R^a_{\alpha\beta}\delta(\hbar\omega - E_{\beta\alpha}) \tag{5.22}$$

where D is the dimension and will be set to 2 for the case below, $r^a_{\alpha\beta} = i\langle u_\alpha|\partial_a u_\beta\rangle$ with $\alpha \neq \beta$ is the interband Berry connection; $f_{\alpha\beta} = f_\alpha - f_\beta$ with $f_\alpha = \frac{1}{1+\exp[(E_\alpha(k)-\mu)/k_B T]}$ the Fermi-Dirac distribution function, where μ is the chemical potential, T is the temperature, and k_B is the Boltzmann constant; $E_{\beta\alpha} = E_\beta(k) - E_\alpha(k)$ represents the energy difference between two bands labeled by α and β at momentum k; $R^a_{\alpha\beta} = -\partial_a arg(r^b_{\alpha\beta}) + \xi^a_{\alpha\alpha} - \xi^b_{\beta\beta}$ is known as the shift vector which is related to the electric polarization between bands; $\xi^a_{\alpha\alpha} = i\langle u_\alpha|\partial_a u_\alpha\rangle$ is the intraband Berry connection. The Hamiltonian takes the form,

$$H(k) = \frac{k^2}{2m} + v_F(\sigma_x k_y - \sigma_y k_x) + B\sigma_z = \mathbf{d}(k)\cdot\boldsymbol{\sigma} + \epsilon(k)\sigma_0 \tag{5.23}$$

where, $\mathbf{d}(k) = (d_x(k), d_y(k), d_z(k)) = (v_F k_y, -v_F k_x, B)$, $\boldsymbol{\sigma} = (\sigma_x, \sigma_y, \sigma_z)$, $\epsilon(k) = \frac{k^2}{2m}$, and σ_0 is the 2x2 identity matrix. The energy eigenvalues read

$$E_{\pm}(k) = \epsilon(k) \pm d(k) \tag{5.24}$$

and the eigenvectors are

$$\begin{aligned} |u_+\rangle &= \begin{pmatrix} \cos\frac{\theta}{2} \\ \\ \sin\frac{\theta}{2} e^{i\phi} \end{pmatrix} \\ |u_-\rangle &= \begin{pmatrix} \sin\frac{\theta}{2} e^{-i\phi} \\ \\ -\cos\frac{\theta}{2} \end{pmatrix} \end{aligned} \tag{5.25}$$

where $d(k) = \sqrt{d_x^2(k) + d_y^2(k) + d_z^2(k)}$, $\tan\theta = \frac{\sqrt{d_x^2(k)+d_y^2(k)}}{d_z(k)}$, and $\tan\phi = \frac{d_y(k)}{d_x(k)}$. Now, the inter and intraband Berry connections can be calculated using the eigenvectors given above.

$$\begin{aligned} r^b_{-+} = -\frac{ie^{i\phi}}{2}(\partial_b\theta + i\sin\theta\partial_b\phi) = (r^b_{+-})^* \\ \xi^a_{--} = \sin^2\frac{\theta}{2}\partial_a\phi \\ \xi^a_{++} = -\sin^2\frac{\theta}{2}\partial_a\phi \end{aligned} \tag{5.26}$$

Thus, $|r^b_{-+}|^2 = \frac{1}{4}\left[(\partial_b\theta)^2 + \sin^2\theta(\partial_b\phi)^2\right]$, and the shift vector is,

$$R^a_{-+} = -\cos\theta\partial_a\phi - \partial_a \arctan\frac{\sin\theta\partial_b\phi}{\partial_b\theta} \tag{5.27}$$

With the procedure in [32] one can write the conductivity as,

$$\sigma^{abb} = \sigma^{abb}_I + \sigma^{abb}_{II} \tag{5.28}$$

the first term is,

$$\sigma_I^{abb} = \frac{4\pi e^3}{\hbar^4\omega^3}\int \frac{d^D k}{(2\pi)^D}\mathbf{d}\cdot(\partial_{ab}\mathbf{d}\times\partial_b\mathbf{d})\, f_{-+}\delta(\hbar\omega - 2d) \tag{5.29}$$

and the second,

$$\sigma_{II}^{abb} = \frac{2\pi e^3}{\hbar^2\omega}\int \frac{d^D k}{(2\pi)^D}\Omega_{ab}(\partial_b d) f_{-+}\delta(\hbar\omega - 2d) \tag{5.30}$$

$\Omega_{ab} = -\mathbf{d}\cdot(\partial_a\mathbf{d}\times\partial_b\mathbf{d})/2d^3$ is the Berry curvature of the valence band. With the model given above σ_I^{abb} is trivially 0. The second term vanishes due to the fact that $\partial_b d \sim k_b$ and switching to polar coordinates, one finds the angular part of the integral is 0, along with the fact that the Berry curvature does not change sign in the momentum space. As mentioned in Fig(5.1) with a sign change in Berry curvature, gives rise to the dipole, Λ. This is shown by calculating for example, Ω_{xy},

$$\Omega_{xy} = -\frac{\mathbf{d}\cdot(\partial_x\mathbf{d}\times\partial_y\mathbf{d})}{2d^3} = -\frac{Bv_F^2}{(v_F^2k^2 + B^2)^{3/2}}. \tag{5.31}$$

Thus, it is found that the Berry curvature does not change sign, yielding a zero dipole moment. So it is found for this simple model that inversion symmetry alone does not give rise to shift current. The vanishing of the shift current can be given by the following physical picture. The Hamiltonian used gives rise to a massive Dirac cone which is protected by mirror symmetry. With this protected symmetry the conductivity must vanish[31]. So another requirement for shift current is to break mirror symmetry.

A simple way to do this is to replace $k^2/2m$ with αk_y, which amounts to a tilt in the Dirac cone. The tilt leads to a Berry Curvature which will have the sign change to give rise to a Dipole moment.This tilt is allowed by symmetry and has been observed in ARPES studies [31].

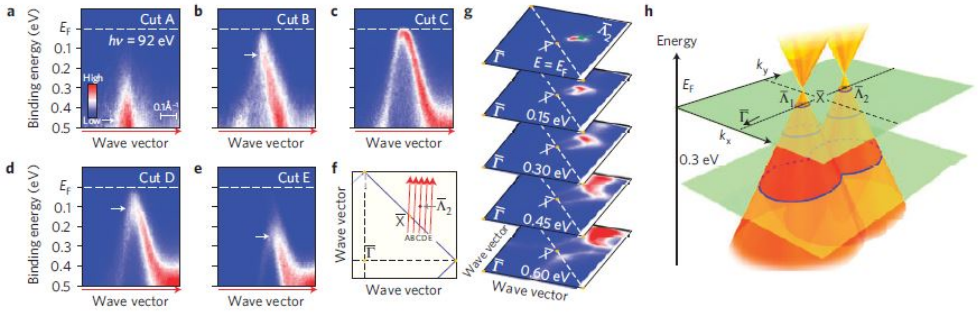

Figure 5.6 2-D band dispersion of SnTe with ARPES measurements of tilted Dirac Cone.[31]

5.4 Conclusion

To reiterate, this chapter was my studies into the non-linear Hall effect known as the shift current. I discussed its potential of being able to find high efficient solar panels, I showed that it is a three particle interaction by way of a density matrix formalism, and showed that inversion symmetry alone is not enough to produce a non-zero shift current. I also understand that this has deviated from the general discussion of this document being focused on the Topological Hall Effect. However, I wanted to highlight this topic because this was the main focus of the proposal along with the fact that this does tie in to the more general topic of quantum transport, which is what this entire document focuses on. Also, this continued the symmetry considerations. It is in non-centrosymmetric materials that the shift current is measured. So, these are the reasons that I wanted to highlight this work. In the sixth and final chapter I will again come back to the discussion of the Topological Hall Effect. This time I will talk about a 3-D version of a Skyrmion known as a Hopfion. This Hopfion actually has no overall magnetic field unlike the Skyrmion. Such a spin structure, one would not expect a Hall effect. However, that is not what is actually found. Thus, chapter six yields more results of a Topological Hall Effect where there is no mention of Skyrmion.

Chapter Six

Scattering Phenomena Related to the Hopfion

In this final chapter I will discuss work that I was part of in a paper that was recently submitted to PRB. It focuses on a similar premise to that in chapter three. However, there a two main distinctions. First, this project deals with a Hopfion, which is the three dimensional counterpart to the Skyrmion. Second, although the Hopfion is essentially a three dimensional Skyrmion, it's average magnetic field is zero and thus one would suspect no Topological Hall Effect. However, this will be another example of when there still is this THE but no Skyrmion. Unlike chapter four though, there is no experimental evidence of this. I will discuss later in this chapter how we expect one can find this signature in the case of a Hopfion. My contributions to this work are two-fold. Firstly, from my work in chapter 4 it was quite straight forward as to how we would know if there would be any THE for an electron scattering off a Hopfion. Recall from chapter four that one can examine the cross terms between the first and second Born approximation of the scattering amplitude. If it is non-zero then there should be a THE. Secondly, I help work out an interesting discovery for the case of a Hopfion in the first Born approximation; that the scattering amplitude is related to the first moment defined by,

$$B_{\alpha,\beta} = \int d^3 r B_\alpha(r) r_\beta. \tag{6.1}$$

The final chapter will be laid out as follows, in section one I will introduce our motivation to this topic of Hopfion scattering events. Then I will introduce how the Hopfion is considered. Followed, by my calculation of the first Born approximation relating to the first order moments. Finally I will discuss that the cross terms between first and second Born approximations is non-zero along with where we expect in experiment to find it, followed by a conclusion of all these works.

6.1 Introduction

In the celebrated paper [32], Aharonov and Bohm considered scattering of electrons off a solenoid carrying magnetic flux Φ and showed that the differential cross-section is a periodic function of Φ. That work laid the foundation for the discussion of the topological effects in quantum mechanics. In many respects, the recent investigation on the topological Hall effect [33, 34] in non-collinear magnetic textures is the most recent incarnation of the Aharonov-Bohm physics. In the appropriate transport regime [12], the non-colinear spin configuration generates a (fictitious magnetic) field[35] $B_\gamma(r) \equiv \epsilon_{\alpha\beta\gamma}\, S \cdot (\nabla_\alpha S \times \nabla_\beta S)/4 \neq 0$, which produces a skew-scattering deflection of carriers. For example, a magnetic Skyrmion, observed in two-dimensional magnetic films [36, 37, 38], generates a fictitious magnetic flux equivalent to the flux quantum. Therefore, electronic scattering off such structures closely resembles the Aharonov-Bohm set up. Owing to a small size (large density) of Skyrmions, the fictitious magnetic field B produced in such structures may be an order of magnitude larger (~ 500 T) than that attainable in conventional magnetic experiments (~ 50 T). That magnetic field may produce a large topological Hall effect [39]. We note that the topological Hall effect was also predicted in systems without Skyrmions [40, 41].

In recent past, there has also been a significant push to extend the research of non-colinear magnetic structures to three dimensions (3D). Magnetic simulations [33, 34] reveal that, under appropriate conditions, three-dimensional magnets may host a zoo of exotic magnetic textures and quasiparticles interesting from both fundamental and practical standpoints. New experimental imaging tools [42] are becoming available, which may facilitate the search and identification of such objects. In this paper, we focus on one such paradigmatic topological object - a magnetic Hopfion. Conceived originally in the context of field theory [43, 44], Hopfions are now discussed in the realm of magnetic systems [45, 46, 47, 48, 49]. Various recipes have been proposed how to stabilize Hopfions in specific materials [48] and finite geometries [45, 46, 47]. [50] reported a first observation of a Hopfion in a magnetic nano-disk. Hopfions were also discussed in the context of superconducting [51] and ferroelectric systems[52].

It is an appropriate point to mention that a Hopfion has a non-trivial profile of the emergent magnetic field $B(r)$ [see Fig. 6.1(b)]. It is characterized by a non-vanishing Hopf number

$$Q = \frac{1}{(2\pi)^2} \int d^3r \, B(r) \cdot A(r), \tag{6.2}$$

where $A(r)$ is the associated vector potential, i.e. $B(r) = \nabla \times A(r)$. Another notable feature is that the average emergent magnetic field vanishes

$$\langle B(r) \rangle \equiv \int d^3r \, B(r) = 0. \tag{6.3}$$

Nevertheless, as we show in this work, a Hopfion configuration does lead to skew-scattering and the Hall effect within the *Hopfion plane*. Now, let me discuss how one defines a Hopfion, mathematically.

6.2 Magnetic Hopfion

To set the stage, I will discuss details of a Hopfion texture in this section. We consider a 3D ferromagnet described by a magnetization vector $S(r)$ normalized to unity $|S(r)| = 1$. A hopfion is a localized topological soliton of the field $S(r)$. We use the following parametrization of the Hopfion [49]

$$S(r) = \hat{z} + \delta S(r), \tag{6.4}$$
$$\delta S(r) = \frac{\sin 2\eta(r)}{r} \begin{pmatrix} x \\ y \\ 0 \end{pmatrix} - \frac{2\sin^2 \eta(r)}{r^2} \begin{pmatrix} -yz \\ xz \\ x^2+y^2 \end{pmatrix}.$$

Here, $\hat{z}$ describes a uniform magnetization at $r \to \infty$, whereas $\delta S(r)$ encapsulates the localized hopfion texture. The phase $\eta(r)$ is an arbitrary monotonic function of $r = \sqrt{x^2+y^2+z^2}$ with constraints $\eta(0) = 0$ and $\eta(\infty) = \pi$. It controls the extent of the hopfion in the radial direction. The texture (6.4) has cylindrical symmetry around $\hat{z}$ axis. For that reason, $\hat{z}$ axis is referred to as the *hopfion axis*, and $z = 0$ - the *hopfion plane*. A hopfion occupies finite space, as illustrated in Fig. 6.1(a), and may be thought of as a localized magnetic quasiparticle. Its dynamics under the applied electric current was studied in Ref. [Zang2020].

A complementary description of a hopfion may be obtained by evaluating an emergent field $B_\gamma(r) = \epsilon_{\alpha\beta\gamma}\, S \cdot (\nabla_\alpha S \times \nabla_\beta S)/4$. We evaluate both the field

$$B = \frac{2\cos\theta \sin^2 \eta(r)}{r^2}\, e_r - \frac{\sin\theta\, \sin 2\eta(r)\, \eta'(r)}{r}\, e_\theta + \frac{2\sin\theta \sin^2 \eta(r)\, \eta'(r)}{r}\, e_\phi \tag{6.5}$$

and the associated vector potential

$$A = 2\cos\theta \sin^2 \eta(r)\, \eta'(r)\, e_r + \frac{\sin\theta\, \sin^2 \eta(r)}{r}\, e_\phi \tag{6.6}$$

satisfying the conventional relation $B = \nabla \times A$. In writing Eqs. (6.5) and (6.6), we used spherical coordinates, where $\cos\theta = z/r$ and e_r, e_θ, e_ϕ denote the orthogonal unit vectors in the radial, polar and azimuthal directions with respect to the *hopfion axis* $\hat{z}$.

The topological character of a hopfion may be illustrated in two complementary ways: either directly from the spin-configuration $S(r)$ or using the Hopf number Q. To illustrate the former, let us pick arbitrary two vectors on the unit sphere S_1 and S_2, i.e. $|S_1| = |S_2| = 1$. Then, the two contours, determined by the solutions of the equations $S(r) = S_1$ and $S(r) = S_2$, are linked. A specific example, corresponding to $S_1 = \hat{x}$ and $S_2 = \hat{y}$, is shown in Fig. 6.1(a). On the other hand, the linking number between these contours equals [53] the topological Hopf number Q defined in Eq. (6.2). We substitute Eqs. (6.5) and (6.6) in Eq. (6.2) and verify the value $Q = 1$.

We note that the average emergent magnetic field vanishes according to Eq. (6.3). The profile of the field in the $y = 0$ and $z = 0$ planes is shown in the left and right panels of Fig. 6.1(b). The field in the $y = 0$ plane has a skyrmion-antiskyrmion structure. The field in the hopfion plane $z = 0$ has a structure reminiscent of a target skyrmion[54]. As usual in electrodynamics, a non-uniform distribution of the field $B(r)$ may be characterized by moments. Evaluating the first-order moment $B_{\alpha,\beta} \equiv \int d^3r\, B_\alpha(r) r_\beta$ for the field (6.5), we find

$$\begin{aligned} B_{\alpha,\beta} &= \epsilon_{\alpha\beta\gamma} L_\gamma, \\ L &= \frac{1}{2}\int d^3r\, [r \times B(r)] = L\,\hat{z}, \end{aligned} \tag{6.7}$$

where $L = \frac{2}{3}\int d^3r\, \sin^2[\eta(r)]\,\eta'(r)$. Vector L is referred to as the toroidal moment [55] and originates from the azimuthal component ($\propto e_\phi$) of the field $B(r)$ winding along a torus. A slice of that torus is shown in the left panel of Fig. 6.1(b).

The two representations of a hopfion either via a magnetic texture (6.4) or the emergent fields (6.5)-(6.6) are complementary.

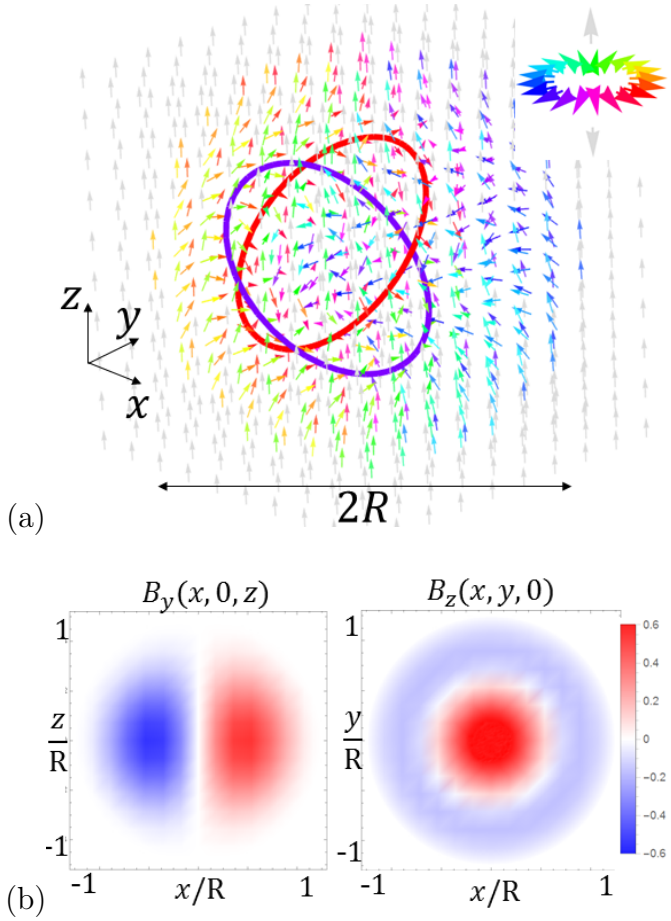

Figure 6.1 Hopfion texture. (a) Magnetic vector $S(r)$ in 3D. Coloring scheme is shown in the top-right color: the vectors with components in the $z = 0$ plane are shown in colors, whereas vectors with $S(r) \parallel \hat{z}$ are shown in gray. The two linked contours are the solutions of equations $S(r) = \hat{x}$ (red) and $S(r) = -\hat{y}$ (blue). (b) Profile of the emergent magnetic field $B(r)$ in the $y = 0$ plane (left) and $z = 0$ plane (right). Average field vanishes, see Eq. (6.3). [17]

In the next section I will show how one can relate the scattering amplitude to the toroidal moment.

6.3 Scattering Amplitude and Toroidal Moment

To start, take the following Hamiltonian,

$$H = \frac{1}{2m}(\mathbf{k} - \mathbf{A}(\mathbf{r}))^2 \tag{6.8}$$

where $\mathbf{A}$ is the vector potential due to the Hopfion discussed in the last section. Now, expanding this to first order in the vector potential only I am able to write an unperturbed and perturbed part to the Hamiltonian,

$$H = H_0 + V(\mathbf{r}) = \frac{\mathbf{k}^2}{2m} - \frac{1}{2m}(\mathbf{k}\cdot\mathbf{A}(\mathbf{r}) + \mathbf{A}(\mathbf{r})\cdot\mathbf{k}). \tag{6.9}$$

With the perturbation it is simple to write down the scattering amplitude as I discussed in Chapter 3.

$$f_{\mathbf{k},\mathbf{k}'} = \frac{1}{4\pi}(\mathbf{k}+\mathbf{k}')\cdot\mathbf{A}(\mathbf{k}'-\mathbf{k}) \tag{6.10}$$

$\mathbf{k}$, $\mathbf{k}'$ are the initial and final scattering momenta, respectively. Also, I have taken the Fourier transform of the vector potential. Since I am looking for the moment which is related to the magnetic field I can re-write the vector potential as,

$$\mathbf{B}(\mathbf{r}) = \nabla\times\mathbf{A}(\mathbf{r}) \tag{6.11}$$

to solve this the vector potential in terms of the magnetic field is simply done by first observing what happens when I take the curl of each side of (6.11),

$$\nabla\times\mathbf{B}(\mathbf{r}) = \nabla\times(\nabla\times\mathbf{A}(\mathbf{r})) = \nabla(\nabla\cdot\mathbf{A}(\mathbf{r})) - \nabla^2\mathbf{A}(\mathbf{r}) \tag{6.12}$$

by taking the Coulomb gauge, $\nabla\cdot\mathbf{A}(\mathbf{r}) = 0$ and transforming to momentum space, one finds that,

$$\mathbf{A}(\mathbf{q}) = i\frac{\mathbf{q}\times\mathbf{B}(\mathbf{q})}{q^2}. \tag{6.13}$$

With this, the scattering amplitude becomes,

$$f_{\mathbf{k},\mathbf{k}'} = \frac{i}{4\pi}(\mathbf{k}+\mathbf{k}')\cdot\left(\frac{\mathbf{q}\times\mathbf{B}(\mathbf{q})}{q^2}\right) \tag{6.14}$$

$$= \frac{i}{4\pi}(2\mathbf{k}+\mathbf{q})\cdot\left(\frac{\mathbf{q}\times\mathbf{B}(\mathbf{q})}{q^2}\right) \tag{6.15}$$

$$= \frac{i}{4\pi}\left(2\mathbf{k}\cdot\left(\frac{\mathbf{q}\times\mathbf{B}(\mathbf{q})}{q^2}\right)+\mathbf{q}\cdot\left(\frac{\mathbf{q}\times\mathbf{B}(\mathbf{q})}{q^2}\right)\right) \tag{6.16}$$

$$= \frac{i}{4\pi}\left(2\mathbf{B}(\mathbf{q})\cdot\left(\frac{\mathbf{k}\times\mathbf{q}}{q^2}\right)+\mathbf{B}(\mathbf{q})\cdot\left(\frac{\mathbf{q}\times\mathbf{q}}{q^2}\right)\right) \tag{6.17}$$

$$= \frac{i}{2\pi q^2}\left(\mathbf{B}(\mathbf{q})\cdot(\mathbf{k}\times\mathbf{q})\right) \tag{6.18}$$

where I have defined $\mathbf{q} = \mathbf{k}' - \mathbf{k}$. Now, writing out the definition of $\mathbf{q}$ I am able to write the amplitude as,

$$f_{\mathbf{k},\mathbf{k}'} = \frac{i}{2\pi}\mathbf{B}(\mathbf{k}'-\mathbf{k})\cdot\frac{\hat{n}\times\hat{n}}{|\hat{n}'-\hat{n}|^2} \tag{6.19}$$

defining $\hat{n} = \frac{\mathbf{k}}{k}$ and $\hat{n}' = \frac{\mathbf{k}'}{k}$. The Fourier transform of the magnetic field is,

$$\mathbf{B}(\mathbf{k}'-\mathbf{k}) = \int d^3r \exp -ik(\hat{n}'-\hat{n})\cdot\mathbf{r}\mathbf{B}(\mathbf{r}) \tag{6.20}$$

where I will write the exponential as a series and look at the zeroth order and first order in kr since I am assuming a long wavelength limit $kr << 1$. The magnetic field is,

$$B_a(\mathbf{k},\mathbf{k}') = \int d^3r \exp -ik(\hat{n}'-\hat{n})\cdot\mathbf{r}B_a(\mathbf{r}) \tag{6.21}$$

$$\sim \int d^3r\,(1-ik(\hat{n}'-\hat{n})\cdot\mathbf{r})\,B_a(\mathbf{r}) \tag{6.22}$$

$$= -ik(\hat{n}'-\hat{n})_\alpha \int d^3r r_\alpha B_a(\mathbf{r}) \tag{6.23}$$

with this the amplitude becomes,

$$f_{\mathbf{k}',\mathbf{k}} \propto B_{a,\alpha} \propto \epsilon_{a\alpha\gamma} L_\gamma \tag{6.24}$$

so I have been able to show that the first Born approximation is related to the first moment of the Hopfion magnetic field. So, how could one find this in experiment? As an example let $\alpha = z$, along the Hopfion axis. Therefore the scattering amplitude will be odd under time reversal and inversion due to the term, $(k'_z - k_z)$. Even upon taking the square of the amplitude, when considering the second Born approximation(see discussion below) this term will still be odd under both symmetries. Specifically, the differential cross-section for electrons propagating in $\hat{z}$ and $-\hat{z}$ directions is distinct. It is conceivable[19, 56] that a device containing a hopfion could exhibit a diode-type behavior along the *hopfion axis* $\hat{z}$. In other words, the I-V curve could be asymmetrical in the applied bias voltage V_z, i.e. $I_z(V_z) \approx G_0 V_z + G_1 V_z^2 + \mathcal{O}(V_z^3)$. Here, the second-order conductance G_1 is induced by the toroidal moment L. To show that the THE in this case is non-zero recall from chapter three that it was the mixing between the first and second Born approximations. Again, this what is examined in this work and that we reveal a non-zero THE. Firstly, a quick discussion on the actual applicability of Born approximation in two and three dimensions.

6.4 Scattering Off a Hopfion

6.4.1 Applicability in 3-D

Here, we define the Hamiltonian and discuss the applicability of approximations used in the following sections. We assume that the magnetic system, described by vector $S(r)$, is embedded in a metallic host, so the total Hamiltonian is

$$\begin{aligned} &H = H_0 + V, \\ &H_0 = \frac{p^2}{2m} - \sigma_z \Delta - \mu, \quad V = -\Delta\, \delta S(r) \cdot \sigma, \end{aligned} \tag{6.25}$$

where p is a 3D momentum of itinerant electrons. The terms proportional to Δ describe the exchange coupling between the spin σ of itinerant electrons and the static magnetization vector $S(r)$. The Hamiltonian (6.25) is split into the bare H_0 and the perturbation V part induced by the hopfion. We use units $\hbar = 1$ throughout this work.

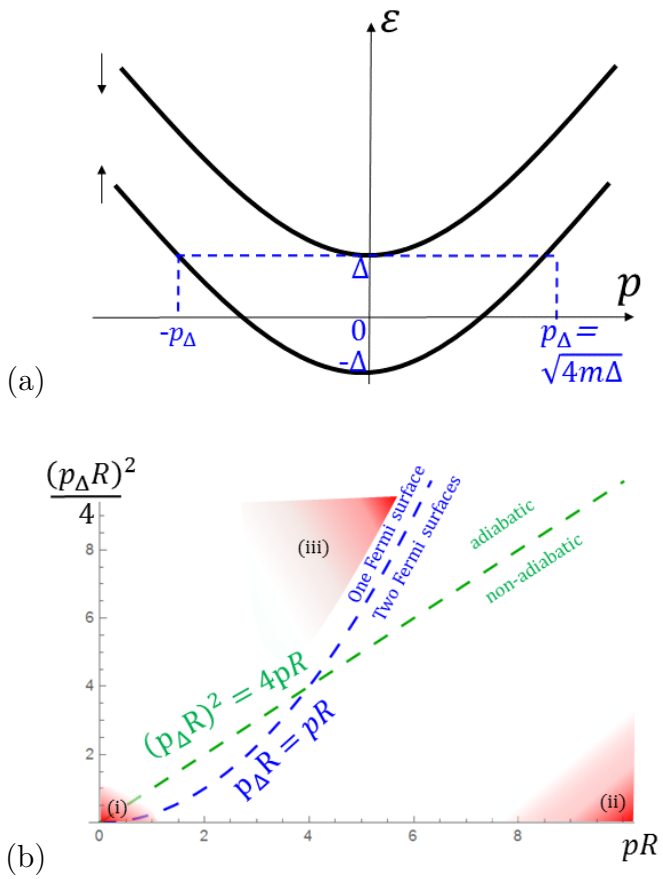

Figure 6.2 (a) Energy spectrum of a two-band model given by Hamiltonian (6.25). For simplicity, we assume that only the lower band is occupied, i.e. $p < p_\Delta$. (b) Diagram of applicability of the Born and eikonal approximations. The Born approximation is applicable in the domains (i) and (ii). The eikonal approximation is evaluated in the case of one Fermi surface in the adiabatic limit. The shaded area (iii) indicates the domain where it is applicable. [17]

Following [12], we examine basic parameters that determine different scattering regimes in this subsection. The electronic energy spectrum of the bare Hamiltonian H_0 consists of two branches $\varepsilon_{1,2} = \frac{p^2}{2m} \pm \Delta$ shifted by the energy gap 2Δ, as shown in Fig. 6.2(a). The electrons with energy in the interval $-\Delta < \varepsilon < \Delta$ occupy only the bottom band, whereas

the electrons with higher energy $\varepsilon > \Delta$ may occupy both bands. In momentum variables p, the boundary between the two domains is determined by the equation $p = p_\Delta$, where $p_\Delta = \sqrt{4m\Delta}$ is the momentum associated with energy 2Δ. That boundary is illustrated with a dashed blue line in Fig. 6.2(b). For simplicity, we restrict the discussion throughout this work to the case with a single Fermi surface, i.e. $p < p_\Delta$.

The dynamics of the electronic spin is determined by the adiabaticity parameter $\lambda = \tau\Delta$. Here, $\tau = Rm/p$ is the time it takes to traverse the hopfion, and Δ is spin precession frequency. If $\lambda \gg 1$, the electronic spin adjusts to the local magnetic direction $S(r)$ as an electron travels through the magnetic texture. In the opposite regime $\lambda \ll 1$, the spin does not keep up with a fast motion of the electron. The former regime is referred to as an adiabatic and the latter as non-adiabatic. It is convenient to re-write these conditions in dimensionless variables pR and $(p_\Delta R)^2$ as follows $pR \ll (p_\Delta R)^2/4$ and $pR \gg (p_\Delta R)^2/4$ for the adiabatic and non-adiabatic regimes, respectively. The line separating these domains $pR = (p_\Delta R)^2/4$ is shown in green in Fig. 6.2(b).

In our work, we evaluate the scattering amplitude using the Born and eikonal approximations. Let us comment on their applicability conditions. The applicability of Born approximation[57] in the long-wavelength $pR \ll 1$ and short-wavelength $pR \gg 1$ limits are $mR^2\Delta \equiv (p_\Delta^2 R)/4 \ll 1$ and $mR^2\Delta \equiv (p_\Delta^2 R)/4 \ll pR$, respectively. Both domains are shown schematically as shaded regions (i) and (ii) in Fig. 6.2(b). In Sec. **??**, we evaluate the scattering amplitude in the long-wavelength region (i).

Note that Born approximation is incorrectly applied in some modern literature on two-dimensional (2D) skyrmions in the limit $pR \to 0$. The scattering amplitude has a logarithmic non-analiticity in 2D in that limit [57], so the Born approximation is not applicable. .

The eikonal approximation relies on two assumptions: that semiclassical approximation is applicable and that semiclassical trajectories may be approximated as straight lines. The semiclassical approximation is applicable when the momenta associated with the two bands are large, i.e. at $pR \gg 1$ and $|(p_\Delta R)^2 - (pR)^2| \gg 1$. The straight-line approxima-

tion assumes that the momentum change due to the Lorentz force is much smaller than the magnitude of the initial momentum p. For a hopfion, that condition amounts to $pR \gg 1$ and coincides with the condition on semiclassics. As stated above, we focus on the case where only the bottom band is occupied, i.e. $p < p_\Delta$. The domain, where all these inequalities are satisfied, is shown as a shaded area (iii) in Fig. 6.2(b). To note, since the eikonal approximation is not related to the THE the reader is encouraged to investigate[17].

6.4.2 THE in the Case of a Hopfion

In this Section, we examine scattering amplitude in the long-wavelength $pR \ll 1$ and weak-coupling $p_\Delta R \ll 1$ limit. To simplify the discussion, we focus on the case of a single Fermi surface, i.e. we further assume that the Fermi momentum is low $pR < p_\Delta R$. The combination of these conditions defines a shaded domain (i) in the space of parameters shown in Fig. 6.2(b). Then scattering may be analyzed using the Born series in $V = -\Delta\, \sigma \cdot \delta S(r)$, see Eq. (6.25). Below, we discuss results of Born series evaluated to second order. The details of the calculation are presented in Appendix D.

To simplify calculation in this section, we rely on the hopfion profile (6.4) with a Gaussian-type hopfion profile (see Appendix D for details). In the long-wavelength limit $pR \ll 1$ electrons do not resolve the fine spatial structure of the perturbation. As in electrodynamics, it is natural to analyze scattering in terms of moments. Therefore instead of the exact hopfion configuration (6.4), we may use an approximate one

$$\delta S(r) = \left[\frac{a_1}{R} \begin{pmatrix} x \\ y \\ 0 \end{pmatrix} - \frac{a_2}{R^2} \begin{pmatrix} -yz \\ xz \\ x^2+y^2 \end{pmatrix} \right] e^{-r^2/R^2}, \tag{6.26}$$

where the dimensionless numerical coefficients $a_1, a_2 \sim 1$ play the role of moments.

Anticipating the Born series, let us evaluate the diagonal $V_{\uparrow\uparrow}(q) = -\Delta\, \delta S_z(q)$ as well

as the off-diagonal $V_{\downarrow\uparrow}(q) = -\Delta\,[\delta S_x(q) + i\,\delta S_y(q)]$ and $V_{\uparrow\downarrow}(q) = -\Delta\,[\delta S_x(q) - i\,\delta S_y(q)]$ matrix elements of the perturbation V with respect to the plane-wave eigenstates of Hamiltonian (6.25). To that end, we evaluate the Fourier transform of the Gaussian-type configuration (6.26) and obtain

$$\begin{aligned} V_{\uparrow\uparrow}(q) &= -\pi^{3/2}\Delta\, R\,(\partial_{qx}^2 + \partial_{qy}^2)\, e^{-q^2R^2/4} \\ V_{\downarrow\uparrow}(q) &= -i\pi^{3/2}\Delta\, R\,(\partial_{q_x} + i\partial_{q_y})(R\,a_1 + a_2\,\partial_{q_z})\, e^{-q^2R^2/4} \\ V_{\uparrow\downarrow}(q) &= -i\pi^{3/2}\Delta\, R\,(\partial_{q_x} - i\partial_{q_y})(R\,a_1 - a_2\,\partial_{q_z})\, e^{-q^2R^2/4} \end{aligned} \tag{6.27}$$

Here the derivatives $\partial_{q_x} \equiv \partial/\partial q_x$ and $\partial q_y \equiv \partial/\partial q_y$ originate from the terms x and y in the real space [see Eq. (6.26)]. We commence with the first-order Born approximation, which is related to the Fourier transform $f^{(1)}(n', n) = -\frac{m}{2\pi} V_{\uparrow\uparrow}[p(n' - n)]$ (we use units $\hbar = 1$), where $n = p/p$ and $n' = p'/p'$ are the unit vectors in the direction of propagation of an incident and scattered electron. Within this section, it is practical to use a following notation for the scattering amplitude $f(n', n)$, where n and n' denote the unit vectors aligned with the direction of propagation of incident and scattered electrons. Expressing $\Delta = p_\Delta^2/4m$ and using Eq. (6.27), we obtain

$$\begin{aligned} &f^{(1)}_{\uparrow\uparrow}(n', n) = \\ &\frac{\sqrt{\pi} a_2 p_\Delta^2 R^3}{8} \left\{ -1 + (pR)^2 \left[1 - n' \cdot n - \frac{1}{4}(n'_z - n_z)^2 \right] \right\} \\ &\qquad\qquad + \mathcal{O}(R^7), \end{aligned} \tag{6.28}$$

where we also expanded in powers of R. Note that anisotropy of the hopfion configuration along the *hopfion axis* $\hat{z}$ carries over to the anisotropy of scattering amplitude in that direction. In the second-order approximation, the scattering amplitude contains the no-spin-flip

and spin-flip contributions

$$
\begin{aligned}
f^{(2)}(n',n) &= f^{(2)}_{\uparrow\uparrow\uparrow}(n',n) + f^{(2)}_{\uparrow\downarrow\uparrow}(n',n) \\
&= \frac{m^2}{\pi}\int \frac{d^3k}{(2\pi)^3}\,\frac{V_{\uparrow\uparrow}(p'-k)V_{\uparrow\uparrow}(k-p)}{k^2-p^2-i\delta} \\
&\quad + \frac{m^2}{\pi}\int \frac{d^3k}{(2\pi)^3}\,\frac{V_{\uparrow\downarrow}(p'-k)V_{\downarrow\uparrow}(k-p)}{k^2+p_\Delta^2-p^2-i\delta}.
\end{aligned}
\tag{6.29}
$$

The sign of the infinitesimal imaginary part in the denominators accounts for causality in the scattering theory [57]. It may be dropped in the spin-flip term $f^{(2)}_{\uparrow\downarrow\uparrow}(p',p)$ due to the assumed condition $p_\Delta > p$. We evaluate the integrals above in [17] and expand in powers of R:

$$
\begin{aligned}
f^{(2)}_{\uparrow\uparrow\uparrow}(n',n) &= \frac{\sqrt{\pi}\,p_\Delta^4\,R^5}{4!\,8\sqrt{2}}\Big\{c_1 + 3\,i\,(pR)\sqrt{2\pi} \\
&\quad +(pR)^2\left[-c_2 + c_3 n'\cdot n - c_4 n'_z n_z + c_5(n'^2_z + n_z^2)\right]\Big\} + O(R^8),
\end{aligned}
\tag{6.30}
$$

$$
\begin{aligned}
f^{(2)}_{\uparrow\downarrow\uparrow}(n',n) &= \frac{\sqrt{\pi}p_\Delta^4 R^5}{4!\,8\sqrt{2}}\left\{c_6 + c_7\,(pR)\,(n'_z+n_z) - c_8(p_\Delta R)^2\right. \\
&\quad \left.+(pR)^2\left[-c_9 + c_{10}\,n'\cdot n + c_{11}\,n'_z n_z + c_{12}\,(n'^2_z+n_z^2) + i\,c_{13}\,(n'\times n)_z\right]\right\} + O(R^8)
\end{aligned}
\tag{6.31}
$$

The second-order Born correction (6.30)-(6.31) has a rich angular structure. A few comments are in order. (i) The dimensionless coefficients c_1 - c_{13} are numbers of order 1 and depend on the details of the hopfion structure at short-range scale. Their specific values are listed in Appendix D. (ii) The imaginary part of $f^{(2)}_{\uparrow\uparrow\uparrow}$ is universal (i.e. independent of short-scale geometry of the hopfion) and originates from the on-shell processes in the denominator in Eq. (6.28). It satisfies the optical theorem and together with the first-order Born result (6.28) serves as an additional verification of Eqs. (6.30)-(6.31). (iii) The scattering amplitude is anisotropic due to the anisotropy of the hopfion profile. (iv) The lowest order $\propto R^5$ terms are scalars, which produce s-wave scattering. The first term with non-trivial angular dependence $c_7(n'_z+n_z)$ appears in the order $\propto R^6$ in $f^{(2)}_{\uparrow\downarrow\uparrow}$. It is odd both under inversion and time-reversal

transformations. We interpret it as a scattering due to the *toroidal moment* of the hopfion (see the discussion above). (v) Observe that the skew-scattering term $\propto ic_{13}(n' \times n)_z$ is generated in $f_{\uparrow\downarrow\uparrow}$. Its interference with the imaginary term in Eq. (6.30) produces a skew-scattering term in the differential cross-section $|f(n', n)|^2$, which results in the non-zero Hall effect.

6.5 Conclusion

To recap this chapter, it is indeed found that yet another example of the Topological Hall Effect is produced without the Skyrmion. Although this work, unlike in chapter four where there was experimental data, we are still looking for some experimental back-up for the Hopfion. If one can find the voltage bias does indeed break from linearity for a device that can host a Hopfion then the calculation in section (6.3) will be of good use. Now, let me end this thesis with what my hopes are for these works.

Chapter Seven

Conclusion

From Inversion and time reversal symmetry to the Topological Hall Effect. It has been discussed throughout this thesis the importance of transport phenomena and why understanding the fundamental physics is important to new developments in this field. Also, the fact that we would like to open up the community to this discussion and really make sure that everyone understands the Topological Hall Effect. My work can hopefully construct a path to a more complete understanding of Scattering processes off of non-trivial spin structures.

REFERENCES

[1] Lars Onsager. "Reciprocal Relations in Irreversible Processes. II." In: *Phys. Rev.* 38 (12 Dec. 1931), pp. 2265–2279. DOI: 10.1103/PhysRev.38.2265. URL: https://link.aps.org/doi/10.1103/PhysRev.38.2265.

[2] Nagaosa Tokura. "Nonreciprocal responses from non-centrosymmetric quantum materials". In: *Nature Communications* 9 (1 Sept. 2018), p. 3740. DOI: 10.1038/s41467-018-05759-4. URL: https://doi.org/10.1038/s41467-018-05759-4.

[3] Christophe Caloz et al. "Electromagnetic Nonreciprocity". In: *Physical Review Applied* 10.4 (Oct. 2018). ISSN: 2331-7019. DOI: 10.1103/physrevapplied.10.047001. URL: http://dx.doi.org/10.1103/PhysRevApplied.10.047001.

[4] Richa Pandey et al. "Mutual Insight on Ferroelectrics and Hybrid Halide Perovskites: A Platform for Future Multifunctional Energy Conversion". In: *Advanced Materials* 31.43 (Aug. 2019), p. 1807376. ISSN: 1521-4095. DOI: 10.1002/adma.201807376. URL: http://dx.doi.org/10.1002/adma.201807376.

[5] Qiong Ma et al. "Observation of the nonlinear Hall effect under time-reversal-symmetric conditions". In: *Nature* 565.7739 (Dec. 2018), pp. 337–342. ISSN: 1476-4687. DOI: 10.1038/s41586-018-0807-6. URL: http://dx.doi.org/10.1038/s41586-018-0807-6.

[6] Xiao-Liang Qi, Yong-Shi Wu, and Shou-Cheng Zhang. "Topological quantization of the spin Hall effect in two-dimensional paramagnetic semiconductors". In: *Phys. Rev. B* 74 (8 Aug. 2006), p. 085308. DOI: 10.1103/PhysRevB.74.085308. URL: https://link.aps.org/doi/10.1103/PhysRevB.74.085308.

[7] Kitagawa. *Quantum Information Processing*. 2012.

[8] Karin Everschor-Sitte and Matthias Sitte. "Real-space Berry phases: Skyrmion soccer (invited)". In: *Journal of Applied Physics* 115 (Apr. 2014). DOI: 10.1063/1.4870695.

[9] N. Kanazawa et al. "Discretized topological Hall effect emerging from skyrmions in constricted geometry". In: *Phys. Rev. B* 91 (4 Jan. 2015), p. 041122. DOI: 10.1103/PhysRevB.91.041122. URL: https://link.aps.org/doi/10.1103/PhysRevB.91.041122.

[10] A. Neubauer et al. "Topological Hall Effect in the *A* Phase of MnSi". In: *Phys. Rev. Lett.* 102 (18 May 2009), p. 186602. DOI: 10.1103/PhysRevLett.102.186602. URL: https://link.aps.org/doi/10.1103/PhysRevLett.102.186602.

[11] URL: https://www.slideserve.com/cianna/german-physical-society-meeting-march-26-th-2012-berlin-germany.

[12] K. S. Denisov. "Theory of an electron asymmetric scattering on skyrmion textures in two-dimensional systems". In: *J. Phys.: Condens. Matter* 32 (2020), p. 415302. DOI: 10.1088/1361-648X/ab966e. URL: https://iopscience.iop.org/article/10.1088/1361-648X/ab966e.

[13] J. C. Gallagher et al. "Robust Zero-Field Skyrmion Formation in FeGe Epitaxial Thin Films". In: *Phys. Rev. Lett.* 118 (2 Jan. 2017), p. 027201. DOI: 10.1103/PhysRevLett.118.027201. URL: https://link.aps.org/doi/10.1103/PhysRevLett.118.027201.

[14] Jue Jiang et al. "Concurrence of quantum anomalous Hall and topological Hall effects in magnetic topological insulator sandwich heterostructures". In: *Nature Materials* 19.7 (Feb. 2020), pp. 732–737. ISSN: 1476-4660. DOI: 10.1038/s41563-020-0605-z. URL: http://dx.doi.org/10.1038/s41563-020-0605-z.

[15] URL: https://link.aps.org/doi/10.1103/PhysRevLett.93.096806.

[16] URL: https://newatlas.com/ibm-researchers-bring-racetrack-memory-another-step-closer-to-reality/17414/.

[17] Sergey S. Pershoguba, Domenico Andreoli, and Jiadong Zang. *Electronic scattering off a magnetic hopfion*. 2021. arXiv: 2104.09584 [cond-mat.mes-hall].

[18] URL: https://www.space.com/skyrmions.html.

[19] Y. Tokura and N. Nagaosa. "Nonreciprocal responses from non-centrosymmetric quantum materials". In: *Nat. Commun.* 9 (2018), p. 3740. DOI: 10.1038/s41467-018-05759-4. URL: https://www.nature.com/articles/s41467-018-05759-4.

[20] URL: https://www1.physik.uni-hamburg.de/en/inf/ag-wiesendanger/forschung/noncollinear-spins.html.

[21] URL: https://en.wikipedia.org/wiki/Hall_effectl.

[22] URL: https://www.slideserve.com/daniel_millan/intro-anomalous-hall-effect-berry-phase-and-karplus-luttinger-theory-anomalous-nernst-effect-in-cucr2se4-nernst-effect-f.

[23] N. Kanazawa et al. "Large Topological Hall Effect in a Short-Period Helimagnet MnGe". In: *Phys. Rev. Lett.* 106 (15 Apr. 2011), p. 156603. DOI: 10.1103/PhysRevLett.106.156603. URL: https://link.aps.org/doi/10.1103/PhysRevLett.106.156603.

[24] Jian-Xiao Zhang et al. *Topological Hall Effect in Magnetic Topological Insulator Films*. 2018. arXiv: 1809.02210 [cond-mat.mes-hall].

[25] P. Bruno, V. K. Dugaev, and M. Taillefumier. "Topological Hall Effect and Berry Phase in Magnetic Nanostructures". In: *Phys. Rev. Lett.* 93 (9 Aug. 2004), p. 096806. DOI: 10.1103/PhysRevLett.93.096806. URL: https://link.aps.org/doi/10.1103/PhysRevLett.93.096806.

[26] Jonathan E. Spanier. "Power conversion efficiency exceeding the Shockley–Queisser limit in a ferroelectric insulator". In: *Nature Photonics* 10 (9 Sept. 2016), pp. 611–616. DOI: 10.1038/nphoton.2016.143. URL: http://www.nature.com/articles/nphoton.2016.143.

[27] Hans J. Queisser William Shockley. "Detailed Balance Limit of Efficiency of p-n Junction Solar Cells". In: 32 (3 Oct. 1961). DOI: https://doi.org/10.1063/1.1736034. URL: https://aip.scitation.org/doi/pdf/10.1063/1.1736034.

[28] URL: https://en.wikipedia.org/wiki/Solar_cell_efficiency.

[29] Ralph von Baltz and Wolfgang Kraut. "Theory of the bulk photovoltaic effect in pure crystals". In: *Phys. Rev. B* 23 (10 May 1981), pp. 5590–5596. DOI: 10.1103/PhysRevB.23.5590. URL: https://link.aps.org/doi/10.1103/PhysRevB.23.5590.

[30] Zhongbo Yan. *Precise determination of critical points of topological phase transitions via shift current in two-dimensional inversion asymmetric insulators*. 2018. arXiv: 1812.02191 [cond-mat.mes-hall].

[31] Y. Tanaka et al. "Experimental realization of a topological crystalline insulator in SnTe". In: *Nature Physics* 8.11 (Sept. 2012), pp. 800–803. ISSN: 1745-2481. DOI: 10.1038/nphys2442. URL: http://dx.doi.org/10.1038/nphys2442.

[32] Y. Aharonov and D. Bohm. "Significance of Electromagnetic Potentials in the Quantum Theory". In: *Phys. Rev.* 115 (3 Aug. 1959), pp. 485–491. DOI: 10.1103/PhysRev.115.485. URL: https://link.aps.org/doi/10.1103/PhysRev.115.485.

[33] C. Back et al. "The 2020 skyrmionics roadmap". In: *J. Phys. D: Appl. Phys.* 53.36 (June 2020), p. 363001. DOI: 10.1088/1361-6463/ab8418. URL: https://doi.org/10.1088/1361-6463/ab8418.

[34] B. Göbel, I. Mertig, and O. A. Tretiakov. "Beyond skyrmions: Review and perspectives of alternative magnetic quasiparticles". In: *Phys. Rep.* 895 (2021), pp. 1–28. ISSN: 0370-1573. DOI: https://doi.org/10.1016/j.physrep.2020.10.001. URL: https://www.sciencedirect.com/science/article/pii/S0370157320303525.

[35] Jinwu Ye et al. "Berry Phase Theory of the Anomalous Hall Effect: Application to Colossal Magnetoresistance Manganites". In: *Phys. Rev. Lett.* 83 (18 Nov. 1999),

p. 3737. DOI: 10.1103/PhysRevLett.83.3737. URL: https://link.aps.org/doi/10.1103/PhysRevLett.83.3737.

[36] S. Mühlbauer et al. "Skyrmion Lattice in a Chiral Magnet". In: *Science* 323.5916 (2009), p. 915. DOI: 10.1126/science.1166767. URL: https://science.sciencemag.org/content/323/5916/915.

[37] X. Z. Yu et al. "Real-space observation of a two-dimensional skyrmion crystal". In: *Nature* 465 (2010), p. 901. DOI: 10.1038/nature09124. URL: https://www.nature.com/articles/nature09124.

[38] S. Heinze et al. "Spontaneous atomic-scale magnetic skyrmion lattice in two dimensions". In: *Nat. Phys.* 7 (2011), p. 713. DOI: 10.1038/nphys2045. URL: https://www.nature.com/articles/nphys2045.

[39] T. Kurumaji et al. "Skyrmion lattice with a giant topological Hall effect in a frustrated triangular-lattice magnet". In: *Science* 365.6456 (2019), p. 914. DOI: 10.1126/science.aau0968. URL: https://science.sciencemag.org/content/365/6456/914.

[40] W.-T. Hou et al. "Thermally driven topology in chiral magnets". In: *Phys. Rev. B* 96 (14 Oct. 2017), p. 140403. DOI: 10.1103/PhysRevB.96.140403. URL: https://link.aps.org/doi/10.1103/PhysRevB.96.140403.

[41] H. Ishizuka and N. Nagaosa. "Spin chirality induced skew scattering and anomalous Hall effect in chiral magnets". In: *Science Advances* 4.2 (2018). DOI: 10.1126/sciadv.aap9962. URL: https://advances.sciencemag.org/content/4/2/eaap9962.

[42] C. Donnelly et al. "Three-dimensional magnetization structures revealed with X-ray vector nanotomography". In: *Nature* 547 (2017), p. 328. DOI: 10.1038/nature23006. URL: https://www.nature.com/articles/nature23006.

[43] F. Wilczek and A. Zee. "Linking Numbers, Spin, and Statistics of Solitons". In: *Phys. Rev. Lett.* 51 (25 Dec. 1983), p. 2250. DOI: 10.1103/PhysRevLett.51.2250. URL: https://link.aps.org/doi/10.1103/PhysRevLett.51.2250.

[44] L. Faddeev and A. J. Niemi. "Stable knot-like structures in classical field theory". In: *Nature* 387 (1997), p. 58. DOI: 10.1038/387058a0. URL: https://www.nature.com/articles/387058a0.

[45] Y. Liu, R. K. Lake, and J. Zang. "Binding a hopfion in a chiral magnet nanodisk". In: *Phys. Rev. B* 98 (17 Nov. 2018), p. 174437. DOI: 10.1103/PhysRevB.98.174437. URL: https://link.aps.org/doi/10.1103/PhysRevB.98.174437.

[46] P. Sutcliffe. "Hopfions in chiral magnets". In: *J. Phys. A* 51 (2018), p. 375401. DOI: 10.1088/1751-8121/aad521. URL: https://iopscience.iop.org/article/10.1088/1751-8121/aad521.

[47] J.-S. B. Tai and I. I. Smalyukh. "Static Hopf Solitons and Knotted Emergent Fields in Solid-State Noncentrosymmetric Magnetic Nanostructures". In: *Phys. Rev. Lett.* 121 (18 Oct. 2018), p. 187201. DOI: 10.1103/PhysRevLett.121.187201. URL: https://link.aps.org/doi/10.1103/PhysRevLett.121.187201.

[48] F. N. Rybakov et al. *Magnetic hopfions in solids*. 2019. eprint: arXiv:1904.00250.

[49] Y. Liu et al. "Three-Dimensional Dynamics of a Magnetic Hopfion Driven by Spin Transfer Torque". In: *Phys. Rev. Lett.* 124 (12 Mar. 2020), p. 127204. DOI: 10.1103/PhysRevLett.124.127204. URL: https://link.aps.org/doi/10.1103/PhysRevLett.124.127204.

[50] N. Kent et al. "Creation and confirmation of Hopfions in magnetic multilayer systems". In: *Nat. Commun.* 12 (2021), p. 1562. DOI: 10.1038/s41467-021-21846-5. URL: https://www.nature.com/articles/s41467-021-21846-5.

[51] E. Babaev, L. D. Faddeev, and A. J. Niemi. "Hidden symmetry and knot solitons in a charged two-condensate Bose system". In: *Phys. Rev. B* 65 (10 Feb. 2002), p. 100512. DOI: 10.1103/PhysRevB.65.100512. URL: https://link.aps.org/doi/10.1103/PhysRevB.65.100512.

[52] I. Luk'yanchuk et al. "Hopfions emerge in ferroelectrics". In: *Nat. Comm.* 11 (2020), p. 2433. DOI: 10.1038/s41467-020-16258-w. URL: https://www.nature.com/articles/s41467-020-16258-w.

[53] D. A. Nicole. "Solitons with non-vanishing Hopf index". In: *Journal of Physics G: Nuclear Physics* 4.9 (Sept. 1978), p. 1363. DOI: 10.1088/0305-4616/4/9/008. URL: https://doi.org/10.1088/0305-4616/4/9/008.

[54] F. Zheng et al. "Direct Imaging of a Zero-Field Target Skyrmion and Its Polarity Switch in a Chiral Magnetic Nanodisk". In: *Phys. Rev. Lett.* 119 (19 Nov. 2017), p. 197205. DOI: 10.1103/PhysRevLett.119.197205. URL: https://link.aps.org/doi/10.1103/PhysRevLett.119.197205.

[55] V.M. Dubovik and V.V. Tugushev. "Toroid moments in electrodynamics and solid-state physics". In: *Phys. Rep.* 187.4 (1990), p. 145. ISSN: 0370-1573. DOI: https://doi.org/10.1016/0370-1573(90)90042-Z. URL: https://www.sciencedirect.com/science/article/pii/037015739090042Z.

[56] J. Mannhart. "Non-reciprocal Interferometers for Matter Waves". In: *J. Supercond. Nov. Magn.* 31 (2018), p. 1649. DOI: 10.1007/s10948-018-4637-4. URL: https://link.springer.com/article/10.1007/s10948-018-4637-4.

[57] L. D. Landau and E. M. Lifshitz. *Quantum Mechanics – Non-relativistic theory*. 3rd ed. Vol. 3. Pergamon Press, 1991.

Appendix A

Deriving Total Energy

A.1 Magnetization Vector

From chapter two I wrote the magnetization vector for the Skyrmion as,

$$\mathbf{M} = \cos\psi \sin\theta \hat{x} + \sin\psi \sin\theta \hat{y} + \cos\theta \hat{z} \tag{A.1}$$

to show how to get from (2.2) to (2.3) using the magnetization vector I will analyze each term in (2.2) separately. The first term is $J(\nabla \mathbf{M})^2$ this can be written as,

$$J(\nabla \mathbf{M})^2 = J[(\nabla m_x)^2 + (\nabla m_y)^2 + (\nabla m_z)^2] \tag{A.2}$$

however, in Cartesian coordinates this calculation becomes complicated since the gradients will be in cartesian coordinates while the functions (ρ) and $\psi(\rho)$ depend on the cylindrical coordinate, $\rho = \sqrt{x^2 + y^2}$. Therefore to simplify this problem I will re-write the magnetization vector in cylindrical coordinates. To do this note that the unit vectors $\hat{x}$ and $\hat{y}$ can be written in terms of $\hat{\rho}$ and $\hat{\phi}$,

$$\hat{x} = \cos\phi\hat{\rho} - \sin\phi\hat{\phi} \tag{A.3}$$

$$\hat{y} = \sin\phi\hat{\rho} + \cos\phi\hat{\phi} \tag{A.4}$$

the vector now becomes,

$$\mathbf{M} = (\cos\psi\sin\theta\cos\phi + \sin\psi\sin\theta\sin\phi)\hat{\rho} + (-\cos\psi\sin\theta\sin\phi + \sin\psi\sin\theta\cos\phi)\hat{\phi} + \cos\theta\hat{z}. \tag{A.5}$$

Now, with the vector in cylindrical coordinates, the Heisenberg term $(\nabla\mathbf{M})^2$ is written as,

$$(\nabla\mathbf{M})^2 = (\nabla m_\rho)^2 + (\nabla m_\phi)^2 + (\nabla m_z)^2 \tag{A.6}$$

then just using the gradient in cylindrical coordinates, $\nabla = \hat{\rho}\partial_\rho + \frac{\hat{\phi}}{\rho}\partial_\phi + \hat{z}\partial_z$ one can solve (A.6) and you get the first term in (2.3). The same goes for the DM term in (2.2). Calculate $\nabla \times \mathbf{M}$ in cylindrical coordinates, taking the dot product with $\mathbf{M}$ will yield the second term in (2.3).

Appendix B

Coefficient for Differential Cross Section

B.1 Born Approximation

Here the scattering amplitude in 2-d will be calculated using a 4-band Hamiltonian where the correct coefficient for the amplitude will be found by examining the Born approximation. The scattered wave takes the form in 2-d,

$$\psi_{sc}(r) \sim e^{ikx} + \frac{1}{\sqrt{r}} f e^{ikr} \tag{B.1}$$

f is the scatttering amplitude and will be determined by Lippmann-Schwinger equation.

$$|\psi\rangle = |\phi\rangle + G_0^R V |\phi\rangle \tag{B.2}$$

where V is the scattering potential, $|\phi\rangle$, $|\psi\rangle$ are the incident and scattered waves, respectively and G_0^R is the retarded Green's function corresponding to the unperturbed 4 band Hamiltonian,

$$H_0 = M(k)\sigma_0\tau_z + \alpha(k_x\sigma_x + k_y\sigma_y)\tau_x \tag{B.3}$$

$M(k) = Bk^2 + M$. Projecting into a position basis gives,

$$\psi(r) = e^{ikx} + \int d^2r' \langle r|G_0^R|r'\rangle V(r') e^{i\mathbf{k}\cdot\mathbf{r}'} \tag{B.4}$$

Since the Green's function is a 4x4 matrix due to the fact that the Hamiltonian is a 4

band model it is written as,

$$G_0^R = \sum_\lambda \frac{|\lambda\rangle\langle|\lambda|}{E - E_\lambda + i\epsilon} \tag{B.5}$$

the states $|\lambda\rangle$ are eigenstates of the Hamiltonian. In the position basis this is and inserting a momentum and spin basis,

$$G_0^R(r,r') = \sum_{\lambda\alpha\beta} \int \frac{d^2k}{(2\pi\hbar)^2} \frac{d^2k'}{(2\pi\hbar)^2} e^{i\mathbf{k}\cdot\mathbf{r}} |\alpha\rangle \frac{\langle k|k'\rangle\langle\alpha|\lambda\rangle\langle\lambda|\beta\rangle}{E - E_\lambda + i\epsilon} e^{-i\mathbf{k}'\cdot\mathbf{r}'} \langle\beta| \tag{B.6}$$

The α, β, and λ states are all orthogonal, yielding,

$$= \sum_\lambda \int \frac{d^2k}{(2\pi\hbar)^2} \frac{e^{i\mathbf{k}\cdot(\mathbf{r}-\mathbf{r}')}}{E - E_\lambda + i\epsilon} |\lambda\rangle\langle|\lambda| \tag{B.7}$$

Using the identity $\frac{1}{x\pm i\epsilon} = P(1/x) \mp i\pi\delta(x)$ and changing to an energy integral gives the integral

$$G_0^R(r,r') = -i\pi \sum_\lambda \int D(E_\lambda) dE_\lambda d\phi e^{ik|r-r'|\cos\phi} \delta(E - E_\lambda) |\lambda\rangle\langle\lambda| \tag{B.8}$$

where $D(E_\lambda)$ is the density of states given by $D(E) = \frac{1}{2B^2} \frac{E}{\sqrt{\frac{E^2-M^2}{B^2} + \frac{\Gamma^2}{4B^4}}}$ and $\Gamma = 2BM + \alpha^2$. Performing the angular and energy integrals,

$$G_0^R(r,r') = \frac{-i\pi}{(2\pi\hbar)^2} 2\pi J_0(k(E)|r - r'|) D(E) \sum_\lambda |\lambda\rangle\langle\lambda| \tag{B.9}$$

k(E) solves the equation $E_\lambda(k) = E$ and E is the incident energy of the electron. Taking the limit $r \to \infty$ and $r' \to 0$ the Bessel's function is,

$$G_0^R(r) = \frac{-iD(E)}{2\hbar^2} \frac{1}{\sqrt{2\pi kr}} e^{ikr - i\frac{\pi}{4}} \tag{B.10}$$

So, the scattered wave function reads,

$$\psi(r) = e^{ikx} + f\frac{e^{ikr}}{\sqrt{r}} \tag{B.11}$$

with $f = \frac{-iD(E)e^{-i\pi/4}}{2\hbar^2}\frac{1}{\sqrt{2\pi k}}\int d^2r' V(r')e^{i\mathbf{k}\cdot\mathbf{r}'}$.

Therefore the cross section is,

$$\frac{d\sigma}{d\phi} = |f|^2 = \frac{D^2}{8\pi\hbar^4 k}\left|\int d^2r' V(r')e^{i\mathbf{k}\cdot\mathbf{r}'}\right|^2 \tag{B.12}$$

To get a sense of the coefficient examine the simple case of $M = \alpha = 0$ and let $B \to \frac{1}{2m}$ therefore the coefficient is $\frac{m^2}{2\pi\hbar^4 k}$. There is another way to find the coefficient to the scattering amplitude. This time using Fermi Golden rule.

B.2 Fermi-Golden Rule

According to Fermi Golden rule the transition rate is,

$$w = \frac{2\pi}{\hbar}\left|\langle p_f|V|p_i\rangle\right|^2 \delta(E - E_i) \tag{B.13}$$

The cross section can be written in terms of the transition rate and incident current density,

$$\frac{d\sigma}{d\phi} = \frac{1}{j_{in}}\int w\frac{kdk}{(2\pi\hbar)^2} \tag{B.14}$$

where we integrate over the final momentum. The incident current is given by $j_{in} = \langle\lambda|\frac{\partial H}{\partial k}|\lambda\rangle$ where λ is the initial state. This also shows why the Hall effect diverges near the top of the valence band. This is because near the top of the band the velocity is zero and since the current is proportional to the velocity the current is zero and hence the cross section diverges. Conversion to an integral over energy gives the cross section,

$$\frac{d\sigma}{d\phi} = \frac{D(E)}{j_{in}}w = |f|^2 \tag{B.15}$$

The incident current can be determined by finding it's x and y components, adding them

together and taking the expectation value. The unperturbed Hamiltonian is,

$$H_0 = (M + Bk^2)\sigma_0\tau_z + \alpha(k_x\sigma_x + k_y\sigma_y)\tau_x \tag{B.16}$$

the x-component of the current density is,

$$j_x = \frac{\partial H}{\partial k_x} = 2Bk_x\sigma_0\tau_z + \alpha\sigma_x\tau_x \tag{B.17}$$

similarly for the y-component,

$$j_y = \frac{\partial H}{\partial k_y} = 2Bk_y\sigma_0\tau_z + \alpha\sigma_y\tau_x. \tag{B.18}$$

Assuming the incident electron is along the x-direction, we take $p_x = p$, $p_y = 0$. The initial state is $|1\rangle$ which is determined in section 3.2 on the differential cross section calculation. The incident current is,

$$\langle 1|(j_x + j_y)|1\rangle = \frac{2Bk(Bk^2 + M) + \alpha^2 k}{\sqrt{(Bk^2 + M)^2 + (\alpha k)^2}} \tag{B.19}$$

We can see that the coefficient is the same as calculating the Green's function by taking $M = \alpha = 0$ and $B \to \frac{1}{2m}$ I find $D(E)/j_{in} \sim m^2/k$.

Appendix C

Projection Operators for Surface and Quantum Well States

C.1 Energy Eigenvalues

First, I will discuss how to derive the energy eigenvalues for the Hamiltonian in Chapter four. Consider,

$$H_0 = \epsilon_k + m_k\tau_3 + A_0(k_y\sigma_1 - k_x\sigma_2)\tau_1 + V_0\tau_1 \tag{C.1}$$

the eigenvalues can easily be obtained by using the properties of the Pauli matrices and the τ matrices since they also behave similarly to the Pauli matrices.

$$(H_0 - \epsilon_k)^2 = m_k^2 + A_0^2k^2 + 2A_0V_0(k_y\sigma_1 - k_x\sigma_2)$$

$$((H_0 - \epsilon_k)^2 - m_k^2 - A_0^2k^2 - V_0^2)^2 = 4A_0^2V_0^2k^2$$

$$(H_0 - \epsilon_k^2)^2 = m_k^2 + A_0^2k^2 + V_0^2 \pm 2A_0V_0k$$

$$= m_k^2 + (A_0k \pm V_0)^2 \tag{C.2}$$

therefore the eigenvalues are,

$$E_k = \epsilon_k \pm \sqrt{m_k^2 + (A_0 k \pm V_0)^2} \tag{C.3}$$

here I introduce two parameters to label the the states,

$$E_{stk} = \epsilon_k + s\sqrt{m_k^2 + (A_0 k + tV_0)^2} \tag{C.4}$$

where $s, t = \pm$ and sometimes for shorthand notation will use $\lambda = (s, t)$.

C.2 Projection Operators

To obtain the operators consider first the Green's function,

$$G_0(k, i\omega_n) = \frac{1}{i\omega_n - H_0 + \mu} \tag{C.5}$$

$$= \frac{1}{i\omega_n + \mu - \epsilon_k - m_k\tau_3 - A_0(k_y\sigma_1 - k_x\sigma_2)\tau_1 - V_0\tau_1} \tag{C.6}$$

$$= \frac{i\omega_n + \mu - \epsilon_k - m_k\tau_3 - A_0(k_y\sigma_1 - k_x\sigma_2)\tau_1 - V_0\tau_1}{(i\omega_n + \mu - \epsilon_k)^2 - (m_k^2 + A_0^2k^2 + V_0^2 + 2A_0V_0(k_y\sigma_1 - k_x\sigma_2))} \tag{C.7}$$

$$= \frac{i\omega_n + \mu - \epsilon_k - m_k\tau_3 - A_0(k_y\sigma_1 - k_x\sigma_2)\tau_1 - V_0\tau_1}{((i\omega_n + \mu - \epsilon_k)^2 - m_k^2 - A_0^2k^2 - V_0^2)^2 - 4A_0^2V_0^2k^2} \times \tag{C.8}$$

$$((i\omega_n + \mu - \epsilon_k)^2 - m_k^2 - A_0^2k^2 - V_0^2 + 2A_0V_0(k_y\sigma_1 - k_x\sigma_2)) \tag{C.9}$$

note that I can write the denominator as,

$$((i\omega_n+\mu-\epsilon_k)^2-m_k^2-A_0^2k^2-V_0^2)^2-4A_0^2V_0^2k^2 = ((i\omega_n+\mu-\epsilon_k)^2-m_k^2-A_0^2k^2-V_0^2-2A_0V_0k)\times$$
$$((i\omega_n + \mu - \epsilon_k)^2 - m_k^2 - A_0^2k^2 - V_0^2 + 2A_0V_0k) \tag{C.10}$$

let me define,

$$F_1 = (i\omega_n + \mu - \epsilon_k)^2 - m_k^2 - A_0^2k^2 - V_0^2. \tag{C.11}$$

Therefore,

$$\frac{(i\omega_n+\mu-\epsilon_k^2)^2-m_k^2-A_0^2k^2-V_0^2+2A_0V_0(k_y\sigma_1-k_x\sigma_2)}{((i\omega_n+\mu-\epsilon_k)^2-m_k^2-A_0^{k2}-V_0^2)^2-4A_0^2V_0^2k^2} \tag{C.12}$$

$$=\frac{F_1+2A_0V_0(k_y\sigma_1-k_x\sigma_2)}{(F_1-2A_0V_0k)(F_1+2A_0V_0k)} \tag{C.13}$$

$$=\frac{1}{2}\left(\frac{1}{F_1-2A_0V_0k}+\frac{1}{F_1+2A_0V_0k}\right)+ \tag{C.14}$$

$$\frac{1}{2}\left(\frac{1}{F_1-2A_0V_0k}-\frac{1}{F_1+2A_0V_0k}\right)\frac{2A_0V_0(k_y\sigma_1-k_x\sigma_2)}{2A_0V_0k} \tag{C.15}$$

which becomes,

$$\frac{1}{2}\frac{1+\hat{k_y}\sigma_1-\hat{k}_x\sigma_2}{F_1-2A_0V_0k}+\frac{1}{2}\frac{1-(\hat{k_y}\sigma_1-\hat{k}_x\sigma_2)}{F_1+2A_0V_0k} \tag{C.16}$$

here I have defined $\hat{k}_{x/y}=\frac{k_{x/y}}{k}$. With this the Green's function becomes,

$$G_0(k,i\omega_n)=(i\omega_n+\mu-\epsilon_k+m_k\tau_3+A_0(k_y\sigma_1-k_x\sigma_2)\tau_1+V_0\tau_1)\frac{1}{2}\sum_{t=\pm}\frac{1=t(\hat{k}_y\sigma_1-\hat{k}_x\sigma_2}{F_1-2tA_0V_0k} \tag{C.17}$$

the denominator will be,

$$F_1-2tA_0V_0k=(i\omega_n+\mu-\epsilon_k)^2-m_k^2-A_0^2k^2-V_0^2-2tA_0V_0k \tag{C.18}$$

$$=(i\omega_n+\mu-\epsilon_k)^2-m_k^2-(A_0k+tV_0)^2 \tag{C.19}$$

$$=(i\omega_n+\mu-\epsilon_k-\sqrt{m_k^2+(A_0k+tV_0)^2})(i\omega_n+\mu-\epsilon_k+\sqrt{m_k^2+(A_0k+tV_0)^2} \tag{C.20}$$

here I will define $F_2 = i\omega_n + \mu - \epsilon_k$ and $D_{tk} = \sqrt{m_k^2 + (A_0 k + tV_0)^2}$. Then,

$$\frac{i\omega_n + \mu - \epsilon_k + m_k\tau_3 + A_0(k_y\sigma_1 - k_x\sigma_2)\tau_1 + V_0\tau_1}{F_1 - 2tA_0V - 0k} \tag{C.21}$$

$$= \frac{F_2 + m_k\tau_3 + A_0(k_y\sigma_1 - k_x\sigma_2)\tau_1 + V_0\tau_1}{(F_2 - D_{tk})(F_2 + D_{tk}} \tag{C.22}$$

$$= \frac{1}{2}\left(\frac{1}{F_2 - D_{tk}} + \frac{1}{F_2 + D_{tk}}\right) + \frac{1}{2}\left(\frac{1}{F_2 - D_{tk}} - \frac{1}{F_2 + D_{tk}}\right) \times \tag{C.23}$$

$$\frac{m_k\tau_3 + A_0(k_y\sigma_1 - k_x\sigma_2)\tau_1 + V_0\tau_1}{D_{tk}} \tag{C.24}$$

$$= \frac{1}{2}\left(1 + \frac{1}{D_{tk}}\left(m_k\tau_3 + A_0(k_y\sigma_1 - k_x\sigma_2)\tau_1 + V_0\tau_1\right)\right)\frac{1}{F_2 - D_{tk}} \tag{C.25}$$

$$+\frac{1}{2}\left(1 - \frac{1}{D_{tk}}\left(m_k\tau_3 + A_0(k_y\sigma_1 - k_x\sigma_2)\tau_1 + V_0\tau_1\right)\right)\frac{1}{F_2 + D_{tk}} \tag{C.26}$$

now the Green's function can be written in terms of the projection operator,

$$G_0(k, i\omega_n) = \frac{1}{4}\sum_{s,t=\pm}\frac{(1 + \frac{s}{D_{tk}}(m_K\tau_3 + A_0(k_y\sigma_1 - k_x\sigma_2)\tau_1 + V_0\tau_1))(1 + t(\hat{k}_y\sigma_1 - \hat{k}_x\sigma_2))}{i_n + \mu - \epsilon_k - sD_{tk}} \tag{C.27}$$

which is written more compactly as,

$$G_0(k, i\omega_n) = \sum_{s,t=\pm}\frac{P_{stk}}{i_n + \mu - E_{stk}} \tag{C.28}$$

where,

$$E_{stk} = \epsilon_k + sD_{tk} = \epsilon_k + s\sqrt{m_k^2 + (A_0 k + tV_0)^2} \tag{C.29}$$

and,

$$P_{stk} = \frac{1}{4}(1 + \frac{s}{D_{tk}}(m_K\tau_3 + A_0(k_y\sigma_1 - k_x\sigma_2)\tau_1 + V_0\tau_1))(1 + t(\hat{k}_y\sigma_1 - \hat{k}_x\sigma_2)) \tag{C.30}$$

are the eigenvalues and projection operator, respectively.

Appendix D

Details of Second Born Approximation

In this appendix, the details of evaluating the second-order Born approximation in perturbation V (see Eq. (6.25)) for a hopfion configuration (6.4).

(i) The strategy is to reduce hopfion spatial configuration (6.4) to a gaussian-type profile, for which integrals (6.29) may be evaluated carefully. We write the hopfion configuration as

$$\delta S(r) = \begin{pmatrix} x \\ y \\ 0 \end{pmatrix} \frac{\sin 2\eta(r)}{r} - \begin{pmatrix} -yz \\ xz \\ x^2+y^2 \end{pmatrix} \frac{2\sin^2\eta(r)}{r^2}. \tag{D.1}$$

Let us choose a specific form for the trigonemetric functions appearing in Eq. (D.1)

$$\begin{aligned} \sin\eta(r) &= \frac{r}{R}\, e^{\frac{1}{2}\left(1-\frac{r^2}{R^2}\right)}, \\ \cos\eta(r) &= \mathrm{sign}(R-r)\sqrt{1-\left(\frac{r}{R}\right)^2 e^{\left(1-\frac{r^2}{R^2}\right)}}. \end{aligned} \tag{D.2}$$

The two functions $\sin\eta(r)$ and $\sin 2\eta(r)$, which appear in Eq. (D.1), are plotted in Fig. D.1. As intended, they correspond to a monotonic $\eta(r)$ ranging from 0 to π as r goes from 0 to ∞. Observe that $\sin\eta$ is a product of r and a Gaussian function $e^{-r^2/2R^2}$, which renders it convenient for integration (performed below). In contrast, $\cos\eta(r)$, which ranges from 1 to -1 as r goes from 0 to ∞, is not easily reduced to a Gaussian. Nevertheless, observe that $\cos\eta(r)$ enters Eq. (D.1) via $\sin 2\eta(r) = 2\sin\eta(r)\cos\eta(r)$. Due to that and to the fact that $\sin\eta(r)$ is exponentially-localized (see Fig. D.1), we do not need a uniform approximation of

$\cos\eta(r)$. We may approximate $\cos\eta(r)$ as a product of a Gaussian and polynomial of r^2

$$\cos\eta(r) \approx e^{-\frac{r^2}{2R^2}} \sum_{n=0}^{N} c_n \left(\frac{r}{R}\right)^{2n}. \tag{D.3}$$

For example, setting $N = 4$ and evaluating coefficients c_n produces a very good approximation for $\sin 2\eta(r)$ shown with a dashed line in Fig. D.1. Further increase of N produces an approximation for $\sin 2\eta$ indistinguishable from the exact result. To simplify analytical calculations, we truncate the polynomial in Eq. (D.3) to $N = 0$ and set the only coefficient $c_0 = 1$. It yields $\sin 2\eta(r)$ plotted with a dash-dotted line in Fig. D.1. A significant disparity between that approximation and the exact dependence (solid dashed line) is not essential since we are interested in evaluating the long-wavelength behavior $pR \ll 1$. To conclude this paragraph, setting $\cos\eta(r) = e^{-r^2/2R^2}$ and using $\sin\eta(r)$ from Eq. (D.2) allows to write Eq. (D.1) as

$$\delta S(r) = \left[\frac{a_1}{R}\begin{pmatrix} x \\ y \\ 0 \end{pmatrix} - \frac{a_2}{R^2}\begin{pmatrix} -yz \\ xz \\ x^2+y^2 \end{pmatrix}\right] e^{-r^2/R^2}, \tag{D.4}$$

where the dimensionless coefficients $a_1 = 2\sqrt{e}$ and $a_2 = 2e$ are introduced to keep track the contribution of the distinct terms in the calculations below. Observe that equation (D.4) is a product of a Gaussian and simple polynomials of coordinates (x, y, z). As such it is amenable for the analytical calculation performed below.

(ii) Anticipating the Born approximation, we evaluate the Fourier transform of Eq. (D.4)

$$\delta S(q) \tag{D.5}$$
$$= \pi^{3/2} R^3 \left[\frac{a_1}{R} \begin{pmatrix} i\partial_{q_x} \\ i\partial_{q_y} \\ 0 \end{pmatrix} + \frac{a_2}{R^2} \begin{pmatrix} -\partial_{q_y}\partial_{q_z} \\ \partial_{q_x}\partial_{q_z} \\ \partial^2_{q_x} + \partial^2_{q_z} \end{pmatrix} \right] e^{-\frac{(qR)^2}{4}}$$

where we retain the momentum derivatives $\partial_q = \left(\frac{\partial}{\partial q_x}, \frac{\partial}{\partial q_y}, \frac{\partial}{\partial q_z}\right)$. Using Eq. (D.5), we may also explicitly write the matrix elements of the perturbation

$$V_{\uparrow\uparrow}(q) \equiv -\Delta \delta S_z(q) \tag{D.6}$$
$$= -\pi^{3/2} \Delta\, R\, (\partial^2_{q_x} + \partial^2_{q_y})\, e^{-q^2R^2/4}$$
$$V_{\downarrow\uparrow}(q) \equiv -\Delta\, [\delta S_x(q) + i S_y(q)] \tag{D.7}$$
$$= -i\pi^{3/2} \Delta\, R\, (\partial_{q_x} + i\partial_{q_y})(R\, a_1 + a_2\, \partial_{q_z})\, e^{-q^2R^2/4}$$
$$V_{\uparrow\downarrow}(q) \equiv -\Delta\, [\delta S_x(q) - i S_y(q)] \tag{D.8}$$
$$= -i\pi^{3/2} \Delta\, R\, (\partial_{q_x} - i\partial_{q_y})(R\, a_1 - a_2\, \partial_{q_z})\, e^{-q^2R^2/4}$$

(iii) *First-order Born approximation.* The scattering amplitude in the first-order Born approximation may be evaluated (in units $\hbar = 1$)

$$f^{(1)}_{\uparrow\uparrow} = -\frac{m}{2\pi} V_{\uparrow\uparrow}(q)$$
$$= \frac{\sqrt{\pi}\, a_2\, p^2_\Delta\, R}{8} \left(\partial^2_{q_x} + \partial^2_{q_y}\right) e^{-q^2R^2/4}$$

where $q = p' - p$ is the momentum transfer; p and p' are the momenta of the initial and finite state. Further, we denote $p' = p\, n'$ and $p = p\, n$ and expand the equation above in powers of

R

$$f^{(1)}_{\uparrow\uparrow}(n',n) = \frac{\sqrt{\pi}a_2 p_\Delta^2 R^3}{8}\left\{-1+(pR)^2\left[1-n'\cdot n-\frac{1}{4}(n'_z-n_z)^2\right]\right\} + \mathcal{O}(R^7). \tag{D.9}$$

(iv) *Second-order Born approximation: the no-spin-flip contribution.* Now, let us evaluate the no-spin-flip part of the second-order Born approximation

$$\begin{aligned} f^{(2)}_{\uparrow\uparrow\uparrow}(p',p) &= \frac{m^2}{\pi}\int\frac{d^3k}{(2\pi)^3}\,\frac{V_{\uparrow\uparrow}(p'-k)V_{\uparrow\uparrow}(k-p)}{k^2-p_E^2-i\delta} \\ &= \frac{\pi^2 a_2^2 p_\Delta^4 R^2}{16}(\partial^2_{p'_x}+\partial^2_{p'_y})(\partial^2_{p_x}+\partial^2_{p_y})I(p',p), \\ \text{where } I(p',p) &= \int\frac{d^3k}{(2\pi)^3}\,\frac{e^{-[(p'-k)^2+(k-p)^2]R^2/4}}{k^2-p_E^2-i\delta}. \end{aligned} \tag{D.10}$$

Here, we substitute the matrix element (D.6) and pulled the derivatives over the "external" momenta outside the integral sign. In the denominator of the integrand, we used a distinct notation $p_E=\sqrt{2mE}$ to distinguish it from the variables p and p', over which the derivatives are taken. We set $p_E\to p$ at the end of the calculation. The integral $I(p',p)$ is evaluated in Appendix **??**. In principle, Eq. (D.10) contains complete information about the second-order scattering amplitude $f^{(2)}_{\uparrow\uparrow\uparrow}$. However, we are interested in the small-R expansion

$$\begin{aligned} f^{(2)}_{\uparrow\uparrow\uparrow}(n',n) = \frac{\sqrt{\pi}\,p_\Delta^4\,R^5}{192\sqrt{2}}\Big\{&c_1+3\,i\,(pR)\sqrt{2\pi} \\ &+(pR)^2\left[-c_2+c_3 n'\cdot n-c_4 n'_z n_z+c_5(n'^2_z+n_z^2)\right]\Big\} \\ &+\mathcal{O}(R^8), \end{aligned} \tag{D.11}$$

where $c_1=23a_2^2/5$, $c_2=1677a_2^2/140$, $c_3=157a_2^2/140$, $c_4=-114a_2^2/140$ and $c_5=153a_2^2/140$ are the numerical coefficients. Observe that, to the lowest order in R, the imaginary

part of the second-order amplitude satisfies the optical theorem, i.e. $\sigma_{\propto R^6} = \frac{4\pi}{p}\mathrm{Im} f^{(2)}_{\uparrow\uparrow\uparrow} = 4\pi \left| f^{(1)}_{\uparrow\uparrow\ \propto R^3} \right|^2$. It serves as an independent verification of the numerical coefficients.

(v) Similarly, we may evaluate the *spin-flip cotribution* to the second-order scattering amplitude

$$
\begin{aligned}
f^{(2)}_{\uparrow\downarrow\uparrow}(p',p) &= \frac{m^2}{\pi}\int \frac{d^3k}{(2\pi)^3}\,\frac{V_{\uparrow\downarrow}(p'-k)V_{\downarrow\uparrow}(k-p)}{k^2-p_E^2-i\delta} \\
&= \frac{\pi^2 a_2^2 p_\Delta^4 R^2}{16}(\partial_{p'_x}-i\partial_{p'_y})(Ra_1-a_2\partial_{p'_z}) \\
&\qquad\qquad \times(\partial_{p_x}+i\partial_{p_y})(Ra_1-a_2\partial_{p_z})\tilde{I}(p',p), \\
\tilde{I}(p',p) &= \int \frac{d^3k}{(2\pi)^3}\,\frac{e^{-[(p'-k)^2+(k-p)^2]R^2/4}}{k^2+p_\Delta^2-p_E^2},
\end{aligned}
$$

where we substitute the matrix-elements (D.7)-(D.8), pulled the derivatives outside of the integral $\tilde{I}$. The latter integral may be obtained from the integral I, given by Eq. (**??**), by the substitution

$$
p_E \to i\kappa, \quad \kappa = \sqrt{p_\Delta^2 - p_E^2}.
$$

So, we may obtain an expansion of the amplitude in powers of R

$$
\begin{aligned}
f^{(2)}_{\uparrow\downarrow\uparrow}(n',n) = \frac{\sqrt{\pi}p_\Delta^4 R^5}{192\sqrt{2}}\big\{ & c_6 + c_7\,(pR)\,(n'_z+n_z) - c_8(\kappa R)^2 \\
& + (pR)^2\left[-c_9 + c_{10}\,n'\cdot n + c_{11}\,n'_z n_z + c_{12}\,(n'^2_z+n_z^2) + ic_{13}\,(n'\times n)_z\right]
\end{aligned}
$$

where $c_6 = a_1^2 + 3a_2^2/20$, $c_7 = a_1a_5/5$, $c_8 = a_1^2 + a_2^2/20$, $c_9 = 7a_1^2/10 + 27a_2^2/280$, $c_{10} = 13a_1^2/10 + 29a_2^2/280$, $c_{12} = 7a_1^2/40 - 27a_2^2/1120$ and $c_{13} = a_1^2/28 + a_2^2/20$ are numerical coefficients of order 1.

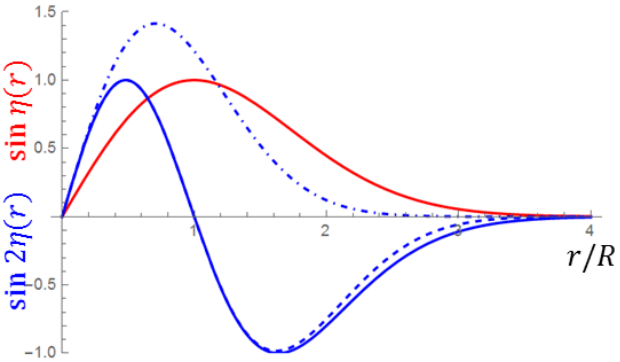

Figure D.1 Dependence of $\sin\eta(r)$ and $\sin 2\eta(r)$, which specifies a hopfion profile (D.1). Solid lines correspond to the exact Eq. (D.2), whereas dashed and dashed-dotted lines correspond to different approximations of $\cos\eta(r)$. [17]